In presenting the dissertation as a partial fulfillment of the requirements for an advanced degree from the Georgia Institute of Technology, I agree that the Library of the Institute shall make it available for inspection and circulation in accordance with its regulations governing materials of this type. I agree that permission to copy from, or to publish from, this dissertation may be granted by the professor under whose direction it was written, or, in his absence, by the Dean of the Graduate Division when such copying or publication is solely for scholarly purposes and does not involve potential financial gain. It is understood that any copying from, or publication of, this dissertation which involves potential financial gain will not be allowed without written permission.

3/17/65
b

HEAT AND MASS TRANSFER IN SEMI-POROUS CHANNELS

A THESIS

Presented to

The Faculty of the Graduate Division

by

William Moore Massey, Jr.

In Partial Fulfillment

of the Requirements for the Degree

Doctor of Philosophy in the School of Mechanical Engineering

Georgia Institute of Technology

August, 1968

HEAT AND MASS TRANSFER IN SEMI-POROUS CHANNELS

Approved:

Chairman

Date approved by Chairman: Aug. 15, 1968

ACKNOWLEDGMENTS

The author would like to thank Dr. J. E. Sunderland, his thesis advisor, whose advice and encouragement have been willingly given throughout his graduate career. Thanks are also due to Dr. G. T. Colwell and Dr. W. W. Graham for their service on the reading committee. Also, the author must express his appreciation to the administration and staff of the department of mechanical and aerospace engineering at the North Carolina State University for their assistance during his stay at that institution for the last year of his graduate study.

The author would like to express his gratitude for the Public Health Service Research Grants EF 00102-03 and EF 00102-04 from the Division of Environmental Engineering and Food Protection, and UI 00093-04 and UI 00712-01 from the National Center for Urban and Industrial Health, which provided full support for this investigation.

Finally, the author would like to express his deep gratitude to his wife, Nita, his children, Michelle and Gregory, and his parents, Mr. and Mrs. W. M. Massey, Sr. The completion of this work and the author's educational goals would not have been possible without their continual encouragement and devotion to him.

TABLE OF CONTENTS

TABLE OF CONTENTS (Continued)

LIST OF TABLES

LIST OF ILLUSTRATIONS

LIST OF ILLUSTRATIONS (Continued)

LIST OF ILLUSTRATIONS (Continued)

NOMENCLATURE

Symbol		Units
a	coefficient in velocity distribution (Eq. (3-3))	fps
a_1	coefficient in temperature distribution (Eq. (4-3))	$^{\circ}R$
a_2	coefficient in concentration distribution (Eq. (5-2))	$\frac{\text{lbm } H_2O}{\text{lbm mixture}}$
A	surface area	ft^2
b	coefficient in velocity distribution (Eq. (3-3))	ft/sec ft
b_1	coefficient in temperature distribution (Eq. (4-3))	$^{\circ}R/ft$
b_2	coefficient in concentration distribution (Eq. (5-2))	$\frac{\text{lbm } H_2O}{\text{lbm mixture ft}}$
B	radiosity	Btu/hr ft^2
c	coefficient in velocity distribution (Eq. (3-3))	ft/sec ft^2
c_1	coefficient in temperature distribution (Eq. (4-3))	$^{\circ}R/ft^2$
c_2	coefficient in concentration distribution (Eq. (5-2))	$\frac{\text{lbm } H_2O}{\text{lbm mixture ft}^2}$
c_p	constant pressure specific heat	Btu/lbm $^{\circ}R$
C_1	integration constant in momentum solution (Eq. (3-14))	ft^2/sec
C_2	coefficient defined by Eq. (3-26)	ft^{13}/lbm^2
C_3	coefficient defined by Eq. (3-27)	$ft^{10}/lbm\ sec^2$
C_4	coefficient defined by Eq. (3-28)	ft^7/sec^2

Symbol		Units
C_5	coefficient defined by Eq. (3-29)	ft^7/sec^4
C_6	coefficient defined by Eq. (4-11)	dimensionless
C_7	coefficient defined by Eq. (4-12)	dimensionless
C_8	coefficient defined by Eq. (4-13)	dimensionless
C_9	integration constant in energy solution (Eq. (4-18))	$^oR/ft^2$
C_{10}	coefficient defined by Eq. (5-23)	dimensionless
C_{11}	integration constant in concentration solution (Eq. (5-27))	$\frac{\text{lbm } H_2O}{\text{lbm mixture ft}^5}$
C_{12}	integration constant in concentration solution (Eq. (5-31))	$\frac{\text{lbm } H_2O}{\text{lbm mixture ft}^4}$
C_{13}	parameter defined by Eq. (5-39)	dimensionless
d	coefficient in velocity distribution (Eq. (3-3))	$ft/sec\ ft^3$
d_1	coefficient in temperature distribution (Eq. (4-3))	$^oR/ft^3$
d_2	coefficient in concentration distribution (Eq. (5-2))	$\frac{\text{lbm } H_2O}{\text{lbm mixture ft}^3}$
D	diffusion coefficient	ft^2/sec
e_2	coefficient in concentration distribution (Eq. (5-2))	$\frac{\text{lbm } H_2O}{\text{lbm mixture ft}^4}$
f	velocity ratio	dimensionless
f_1	pressure parameter defined by Eq. (3-41)	dimensionless
f_2	pressure parameter defined by Eq. (3-42)	dimensionless
f_3	parameter in concentration solution (Eq. (5-32))	ft^4
F	radiation geometric view factor	dimensionless

Symbol		Units
g	polynomial function (Eq. (6-11))	dimensionless
g_0, g_1, g_2, g_3	coefficients in pressure distribution (Eq. (3-31))	-
h_c	local convection heat transfer coefficient	Btu/hr ft^2 $^\circ$F
$\bar{h}_c$	average convection heat transfer coefficient	Btu/hr ft^2 $^\circ$F
h_r	local radiation heat transfer coefficient	Btu/hr ft^2 $^\circ$F
$\bar{h}_r$	average radiation heat transfer coefficient	Btu/hr ft^2 $^\circ$F
h_{cr}	local combined convection and radiation coefficient	Btu/hr ft^2 $^\circ$F
$\bar{h}_{cr}$	average combined convection and radiation coefficient	Btu/hr ft^2 $^\circ$F
H	channel width	ft
ΔH	heat of sublimation	Btu/lbm
I	integrated function	-
I.F.	integration factor	-
k	thermal conductivity of water-vapor	Btu/hr ft $^\circ$F
k_d	thermal conductivity of dried region	Btu/hr ft $^\circ$F
Kn	Knudsen number	dimensionless
L	channel half length	ft
m	per cent moisture	-
N	mass flow rate	lbm/ft^2 sec
Nu	local Nusselt number	dimensionless
$\overline{Nu}$	average Nusselt number	dimensionless
p	pressure	lbf/ft^2
Δp_x	x-direction pressure change	lbf/ft^2

Symbol		Units
Δp_y	y-direction pressure change	lbf/ft^2
Pr	Prandtl number	dimensionless
q	heat flux	Btu/hr ft^2
q_c	convection heat flux	Btu/hr ft^2
q_r	radiant heat flux	Btu/hr ft^2
q_d	conduction heat flux	Btu/hr ft^2
r	distance coordinate	ft
R	wall or injection Reynolds number defined by Eq. (2-8)	dimensionless
R_g	gas constant	ft lbf/lbm ^oR
Sc	Schmidt number	dimensionless
T	temperature	^oR
u	velocity in the x-direction	fps
$\bar{u}(x)$	velocity function defined by Eq. (6-4)	fps
$\bar{U}(0)$	average velocity at entrance to porous section of channel	fps
$\bar{U}$	overall coefficient of heat transfer	Btu/hr ft^2 ^oF
v	velocity in y-direction	fps
x	distance coordinate measured from center of channel	ft
X	distance coordinate defined by Eq. (6-9)	dimensionless
X_1	integration variable	dimensionless
X_2	integration variable	dimensionless
X_d	dried layer thickness	ft
X_f	frozen region thickness	ft

Symbol		Units
X_t	total product thickness	ft
y	distance coordinate measured from porous surface	ft
z	distance coordinate	ft
Z	parameter in concentration solution defined by Eq. (5-30)	dimensionless

Greek Letter Symbols

α	thermal diffusivity	ft^2/hr
β	pressure derivative defined by Eq. (3-20)	lbf/ft^3
β_1	pressure parameter defined by Eq. (3-19)	dimensionless
γ	parameter in energy solution defined by Eq. (4-15)	dimensionless
δ	porosity	dimensionless
ϵ	thermal emissivity	dimensionless
η	parameter in concentration solution defined by Eq. (5-22)	dimensionless
θ	temperature ratio defined by Eq. (4-23)	dimensionless
λ	mean free path	ft
μ	viscosity	lbm/ft sec
ν	kinematic viscosity	ft^2/sec
ξ	coordinate defined by Eq. (3-1)	dimensionless
ρ	density	lbm/ft^3
ρ_i	reflectivity of i-th surface	dimensionless
σ	Stefan-Boltzmann constant	$Btu/ft^2\ hr(^oR)^4$
τ	time	hrs

Symbol		Units
τ_w	wall shear stress	lbf/ft^2
ϕ	angle	radians
Ψ	stream function	dimensionless
ω	mass concentration	$\frac{lbm\ H_2O}{lbm\ mixture}$
$\bar{\omega}$	average mass concentration	$\frac{lbm\ H_2O}{lbm\ mixture}$
ω_c	chamber concentration	$\frac{lbm\ H_2O}{lbm\ mixture}$

Subscripts

a	air
d	interface position
e	channel exit
f	frozen region
H	solid wall
i	surface in radiation enclosure
j	surface in radiation enclosure
LH	position on solid wall
m	mean value
n	integer
w	water-vapor
0	porous wall position
1	solid wall position
2	channel exit
3	channel exit

SUMMARY

An analytical investigation is made to determine the heat and mass transfer mechanisms of a binary mixture of gases flowing in a parallel plate channel where mass injection occurs at one wall. The walls of this "semi-porous channel" are at different temperatures. Applications of this investigation to freeze-drying of foods are presented.

The analysis uses the integral continuity, momentum, energy, and diffusion equations to establish the velocity and pressure distributions, the temperature profiles, and the mass concentration profiles in the channel. The flow in the channel is assumed to be steady, laminar, and incompressible. Closed form solutions are obtained for the velocity, temperature, and concentration distributions. The accuracy of the approximate hydrodynamic solution is established by comparison with existing solutions of the differential equations.

The region between the heater platen and the porous product surface in a typical freeze-drying installation is typical of a semi-porous channel. The heater surface is impermeable, and the dried product surface may be assumed uniformly porous. The dimensions of the platens and food trays are large compared with the distance between them, which is usually about 0.5 inch. Hence, the analytical results of this thesis are applied to the external transport mechanisms of freeze-drying between the heater and the product. Previous theoretical analyses have been concerned only with the internal transport mechanisms inside the product itself.

Two typical methods of freeze-drying are examined. First, the

mean heater surface temperature is assumed to be constant with respect to time. The variation of the product surface temperature during drying is examined theoretically, and the results are compared with published experimental data which serves to establish the accuracy of the energy solution. Second, the product surface temperature is assumed to be constant with respect to time, and the variation of the mean heater surface temperature during drying is examined.

Radiation heat transfer is included in the calculation of the overall energy exchange between the heater and product. The relative amounts of radiation and convection heat transfer to the product surface are calculated. Average heat transfer coefficients at the product surface and the overall heat transfer coefficient from the heater surface to the frozen region of the drying product are defined, and typical values are presented. The external conditions in the channel are related to successive stages of drying by means of existing internal drying rate solutions.

The semi-porous channel analysis when applied to freeze-drying yields some important results. The role of radiation heat transfer to the product surface is established as the dominant mode of heat transfer. Radiation may range from 60 to 95 per cent of the total heat transfer. Heat transfer by convection and conduction increases as the channel width decreases. It is shown theoretically that decreasing the channel width results in an increased overall heat transfer coefficient and slightly increased drying rates. For the long narrow channel usually encountered in commercial use, the fluid in the channel is almost pure water-vapor and only hydrodynamic flow exists. Any residual air is swept away from the surface of the product at the start of drying, and hence diffusional

flow is negligible in the channel.

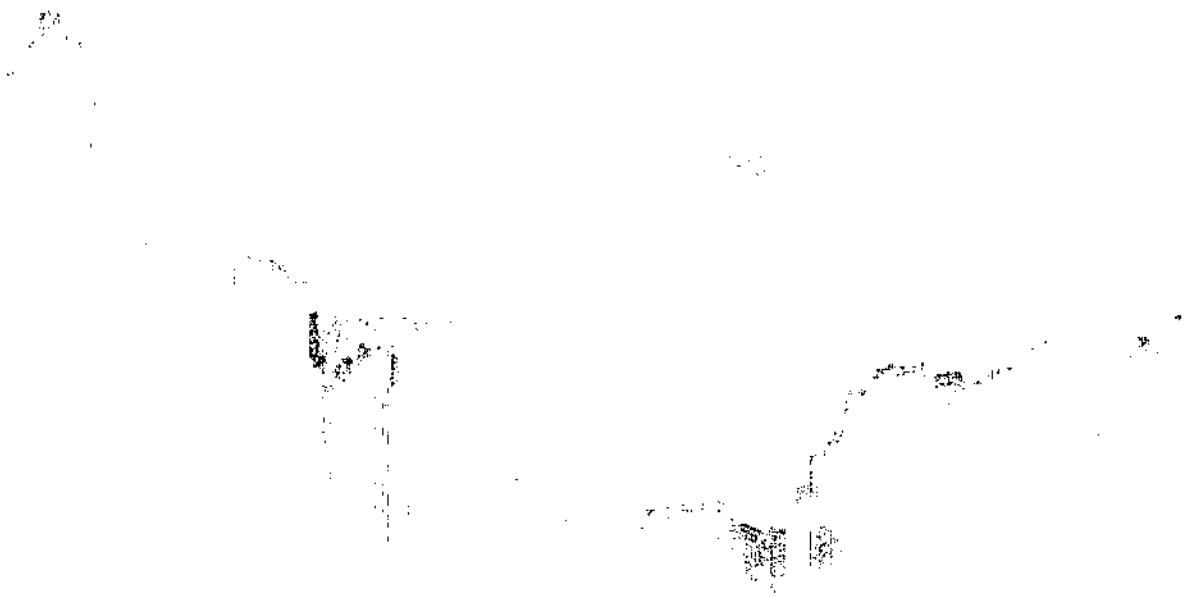

CHAPTER I

INTRODUCTION

General

Sublimation dehydration, commonly called freeze-drying, is a food preservation technique wherein a food product is first frozen and subsequently dried in low vacuum surroundings. There are several different methods for supplying the heat of sublimation for freeze-drying foods. The methods vary according to the requirements of the individual process. The ultimate objective of each is, however, the same and that is to remove the moisture from the food product until it is virtually dry. Since the triple point of water is 4.65 torr (mm Hg), the product must remain under low vacuum conditions so that no melting takes place. Further, a path must be provided for the escaping water-vapor to leave the immediate surroundings of the product. Finally, care must be exercised to insure that the resulting dried product is not overheated as the frozen interface recedes into the product. If the product is properly dried, a lightweight easily stored food item is obtained which upon reconstitution possesses nearly the same flavor qualities as the fresh item.

Some of the common methods of supplying heat for sublimation are hot shelf drying, spiked plate heating, radiant heating, infrared heating, and dielectric heating.

Hot shelf drying is the simplest method but perhaps the least efficient. The frozen product is simply placed on a heated shelf where-

upon heat is supplied to the bottom surface by conduction. In this method, the contact resistance between shelf and product is high, and since the maximum temperature is quite limited, radiation from the shelf above the product is ineffective. Spiked plate heaters are used to pierce the product with a number of spikes which provide heat directly to the internally frozen region. However, the resulting product suffers in basic appearance, and this method, although providing rapid drying, is not widely accepted. Radiant heating plates are successfully employed when the product is placed on trays which are subsequently suspended between the heaters, thus leaving open spaces between the top and bottom of the product for radiation heat transfer. The temperature of the heated plates may be controlled over a wide range of temperature to provide the maximum heat transfer to the surface without scorching it. Further, since the product is on separate trays, this facilitates handling during loading and unloading a large vacuum chamber which consists of stacks of alternating heaters and trays. Some work has been done using infrared heaters and dielectric heaters, but certain basic problems have prevented wide use of these methods on a commercial scale.

In Europe, the contact-plate heating method has gained wide acceptance. In this method, expandable metal grids are placed between the heating platens and food product. These facilitate vapor removal and yet maintain direct contact under pressure with the product throughout the drying cycle. This method provides improved drying rates, but the equipment is expensive and irregularly shaped pieces present difficulties.

The majority of analytical studies involving freeze-drying have dealt primarily with the internal drying mechanisms. This has been due

to the fact that the dried layer offers the greatest resistance to heat and mass transfer during the greatest part of the process. Recently interest has revived in improving the external heat transfer to the product surface and in studying the mechanisms involved with the ultimate objective of improving equipment design and drying rates.

The most widely used but least understood method is the radiant heating method. The physical description of this method may be represented by a channel infinite in depth but finite in length with one wall impermeable (the heater) and the other porous (the product). This type of channel is termed a semi-porous channel (see Figure 1). Much related work has been performed in the field of porous and semi-porous channels in the literature. Thus, using the semi-porous channel to describe the typical freeze-drying arrangement for radiant heating provides an excellent opportunity to study analytically the external fluid flow patterns and heat transfer mechanisms.

Literature

General

Much of the literature written in connection with freeze-drying deals with the general aspects of the process. The majority of the work involving the transport processes has been confined to the internal mechanism. A brief summary of the literature on this problem is presented here.

Harper and Tappel (1) present analytical investigations of the internal heat and mass transfer. However, they neglect to combine the diffusional and hydrodynamic flow. Bannister (3) and Koumoutsos and

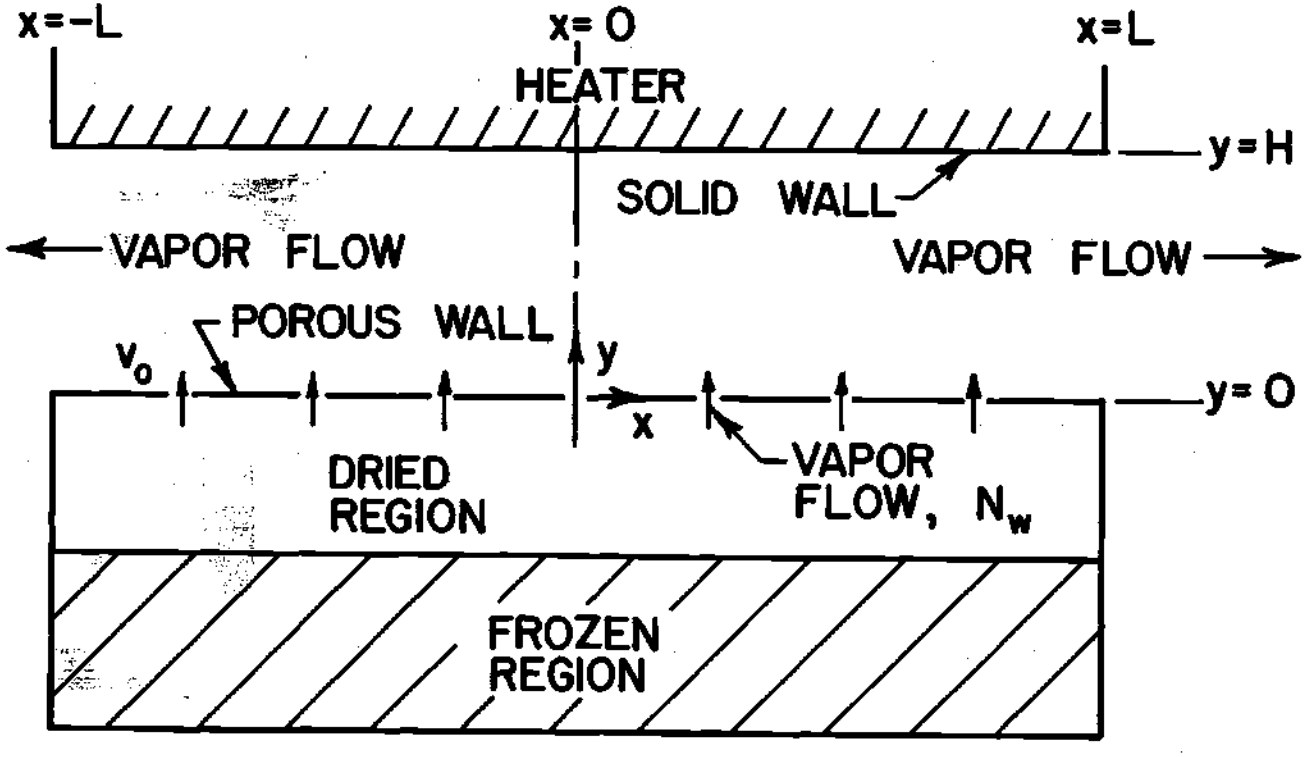

Figure 1. Semi-Porous Channel Arrangement of Heater Platen and Food Product in Freeze-Drying

Sunderland (4) present similar analyses on the basis of hydrodynamic and diffusional flow through a bundle of capillaries.

Hardin (2) and Dyer and Sunderland (5) present improved solutions for drying rates and drying times considering the internal flow to be in the transitional flow regime. Hill (7) presents approximate solutions for drying rates and times in all the molecular flow regimes.

In considering the problems associated with the heat transfer between the heater and the product surface, it is desirable to consider the physical arrangement of equipment commonly used in commercial installations.

The industrial method of freeze-drying large batches of food products in general consists of a stack of alternating trays and heaters in a large vacuum chamber. A space of 0.25 inch to 1 inch is left between each heater and the top and bottom surfaces of the product to allow the vapor to escape to the condenser (see Figure 2). The physical system thus resembles a series of parallel plate channels which are semi-porous. That is, one wall is solid, the heater, and the other wall is porous, the product. The vapor is injected through the porous wall and moves down the channel under the influence of total and partial pressure gradients. The heater wall is of course at a higher temperature and heat transfer occurs by the modes of radiation and combined convection and conduction.

External Heat and Mass Transfer

The published literature dealing with the external transport processes is conspicuous by its absence. A few references mentioned here have considered the problem but little substantial analytical work has been done.

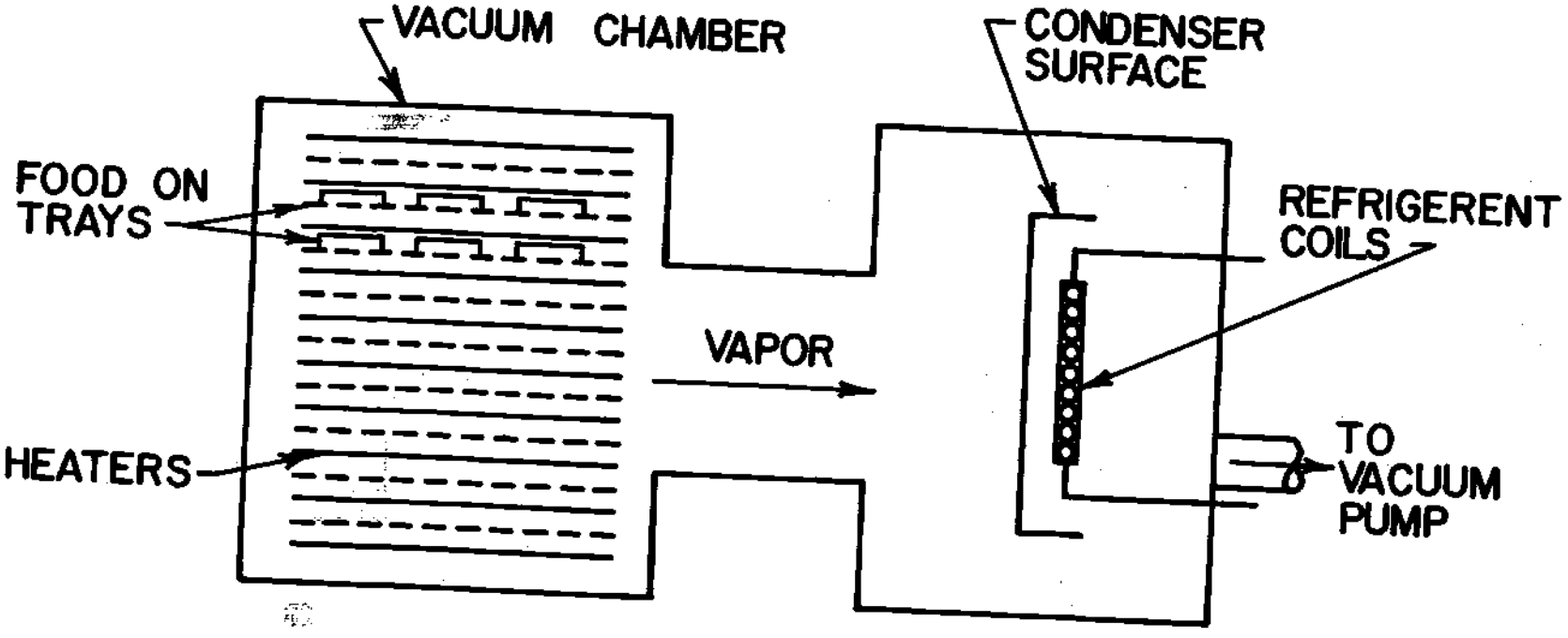

Figure 2. Typical Freeze-Drying Apparatus

Lambert (8) has studied analytically and experimentally the heat and mass transfer internal and external to the food product. However, the model treated does not resemble the industrial method for freeze-drying. The heat transfer occurs by conduction only between a heated plate and the product resting on it. The vapor issues into an unrestricted region above the product and hence to a refrigerated condenser. Thus, the flow is described by diffusion equations, and the hydrodynamic equations are not applicable.

Peck and Morraine (10) also have studied the heat and mass transfer external to the product. Again the model used does not resemble typical industrial methods. Experimentally a block of ice was suspended between heaters that are 3 feet apart. Their conclusion is that the mode of heat transfer is entirely by radiation which in this case is probably correct.

Kan and deWinter (9) present a simplified analysis of the heat and mass transfer internal and external to the product. They assume that the heat transfer between the heater and product surface is by radiation and conduction with no convection. They further assume that there is no total pressure drop through the dried layer or down the channel separating the heater and product. Their analysis more closely represents the industrial process. However, the assumptions mentioned above are somewhat questionable.

Burke and Decareau (6) discuss the relative effects of radiation, conduction, and convection between the heater and product. They conclude from experimental results that the main mode of heat transmission is conduction-convection in nature. However, their conclusions are based mostly on speculation and are not rigorously supported. They conclude

their discussion by mentioning that considerable work must be done in this area to establish the exact mechanisms involved.

Zamzow and Marshall (51) and Abelow and Flosdorf (52) made some early experimental studies on improved uses of radiant energy in freeze-drying. These studies illustrate the relative advantages radiant heating has over methods employing pure conduction heating. The work of Zamzow and Marshall (51) centered around freeze-drying of organic dyes. The method of supplying radiant heat to the product was through a transparent retaining medium to the frozen solid. The energy penetrates the frozen solid and sublimation occurs from the opposite or exposed surface. This procedure is not readily adaptable to large scale commercial food freeze-drying. Abelow and Flosdorf (52) made some studies which showed the advantages of using blackened heaters and trays in connection with conventional freeze-drying, but they did not fully attempt to arrive at optimum drying conditions.

Smithies and Blakley (46) made some extensive experimental studies involving radiant heating in freeze-drying food products. They were able to show that radiant heating could be used to operate a moderately fast freeze-drying process.

Lusk, et al. (53) more recently have made some experimental studies on the effect of heater temperature, freezing temperature, and chamber pressure on the rates of freeze-drying shrimp. They clearly demonstrated the improved drying rates obtainable with higher heater temperatures.

As can be seen, most of the work to present points to radiant heating as the best all around method for freeze-drying. However, no attempt has been made to substantiate any experimental findings with analytical

studies of the transport mechanisms involved between heater and product.

Flow in Porous Channels

An extensive amount of work has been done in the field of porous channels, tubes, annuli, and flat plates. The suction or injection of fluid through the walls bounding a confined flow field find several useful applications. Withdrawing fluid from the flow field serves to reduce the pressure drop required to maintain flow. Also, suction at the walls may serve to maintain laminar flow at higher Reynolds numbers. Injection of a cooling fluid at the walls will serve to effectively cool channel walls along which hot gases are flowing. For external flow over flat plates or other arbitrary surfaces, both suction and injection at the surface serve to retard boundary layer separation although for different physical reasons.

Aside from the practical aspects of flow in porous channels, there exists an interesting problem in solving the Navier-Stokes equations and further confirming their validity. Under certain conditions for porous tube flow, there exist closed form solutions of the Navier-Stokes equations.

Berman (11) appears to be among the first to investigate the problem of the fully porous channel where both walls are porous. He defined a stream function with which the Navier-Stokes equations for two-dimensional porous channel flow could be reduced to a single parametric, total differential equation. He then obtained a first-order perturbation solution in terms of the wall Reynolds number, a parameter based on the normal injection or suction velocity at the wall and the width of the channel. His solution is valid for suction or injection at low wall Reynolds number,

$|R| \leq 1$. It should be noted that a change in sign of R indicates a change from injection to suction. In effect, he reduced two partial differential equations to an ordinary differential equation by means of a similarity transformation in an analogous manner to the way boundary layer flow is treated. Berman's technique has been the basis for much of the later work in this field.

Berman (12) has also investigated the laminar flow in an annulus with porous walls. By considering injection at one wall and suction at the other at constant and equal rates, he was able to obtain an exact solution valid for all values of the cross flow.

Sellers (13) has presented a solution which is valid for large values of suction at the channel walls.

Yuan (14) presented a solution which covered a wider range of wall Reynolds numbers, $|R| \leq 10$, for the fully porous channel than those of Berman mentioned above. However, in a later paper Berman (15) showed that Yuan's solution was inaccurate for large suction.

Donoughe (16) was apparently the first to obtain solutions for the flow in a semi-porous channel. His approach was similar to that of Berman, but he obtained greater accuracy by considering a higher order perturbation solution. He considered his results to be very accurate for $|R| \leq 4$. Eckert, Donoughe, and Moore (17) extended this work to include fully porous channels, tubes, and boundary layer flow. They did extensive numerical solutions to cover all ranges of wall Reynolds numbers.

White, Barfield, and Goglia (18) presented a unique solution for the fully porous channel. They employed the same function used by Berman to reduce the Navier-Stokes equations. Then with another transformation,

they were able to eliminate the parameter R from the differential equation. This allowed them to solve the equation by a series solution which, when transformed back is absolutely convergent for all values of R. However, the series converges slowly especially for injection. White (19) employed this technique further to the case of tubes and semi-porous channels.

Recently, Terrill (20) has considered the problem of porous wall channel flow. He has further extended the work of Berman in fully porous channels to obtain more accurate solutions over wider ranges of R. Comparisons are made with numerical results. The solution for large R was for suction only. In another paper, Terrill (21) considers the solution for very large injection R.

Terrill and Shrestha (22) were the first to consider the solution for flow in a porous channel where the opposing walls have different permeability. That is, the injection rates at the two walls may differ from one another. The application ranges from the semi-porous to the fully porous channel where both walls have equal permeability. The results are considered to be accurate for $-9 < R < 8$. The solutions are of the perturbation type with numerical results presented for comparison.

Horton and Yuan (24) consider the problem of laminar flow in the entrance region of a porous wall channel. In this case, the solution is similar in some respects to a flat plate analysis since the potential core must be considered, thus requiring a boundary layer analysis. They employ the Karman-Pohlhausen integral method to obtain approximate solutions.

Knight and McInteer (23) present solutions for the case of vanishing viscosity valid for small injection.

Morduchow (50) presents a perturbation solution for large suction for a fully porous channel calculated by the method of averages.

Smith (55) presents an analytical study of wall suction and injection upon steady laminar flow in closed slender channels. A detailed discussion is given to show that the full Navier-Stokes momentum equations may be reduced to a form identical to the Prandtl boundary layer equation. Numerical solutions are presented for two-dimensional and axisymmetric Poiseuille flow and for flow in a conical diffuser. His solutions are valid for small suction and injection rates.

Ishizawa and Hori (56) study the flow of a viscous fluid through a porous wall into a narrow gap. The flow pattern is considered to be axisymmetric, and all the fluid flowing in the gap originates at the wall. Their analysis is unique in that the flow inside the wall is also considered in the solution, and the internal and external boundary conditions are mated with each other. The internal and external equations are solved under the generalized condition that the fluid may flow radially in the porous medium resulting in a velocity slip at the external porous surface. It is shown that for large values of the wall Reynolds number, the effect of a slip at the porous wall must be included. This refinement in porous channel analysis is apparently the first of its kind.

A number of investigators have considered the problem of injection or suction in boundary layers on flat plates or arbitrary surfaces. These workers have considered momentum, heat, and mass transfer in the boundary layers. References (37-42) deal specifically with this problem.

In the area of porous pipe flow, Yuan and Finkelstein (25,26) have considered the hydrodynamic problem of fully developed laminar flow with

injection or suction and the corresponding heat transfer problem where the injected fluid acts as a coolant. Weissberg (27) and Hornbeck, et al. (28) have treated the problem of laminar flow in the entrance region of a porous pipe by various approximate methods. White (29) presents a power series solution for the fully developed laminar flow in a porous tube.

A number of authors have considered the heat transfer problem for both developing and fully developed laminar flow between parallel, impermeable flat plates. The boundary conditions employed are equal wall temperatures, unequal wall temperatures, equal heat fluxes, and unequal heat fluxes at the walls. All of these investigators employ either series or numerical solutions of the differential equations. A partial list of these works is found in the cited literature.

Terrill (30) has considered the problem of heat transfer in a fully porous channel where the wall temperatures are prescribed and equal. A solution is obtained by separation of variables and the superposition of an infinite number of solutions. The solution is considered to be accurate for a range of $|RPr| \leq 3$ where Pr is the Prandtl number. Terrill finds that increasing injection decreases the Nusselt number, whereas increasing suction increases the Nusselt number.

Carter and Gill (31) present solutions for combined free and forced convection in vertical and horizontal channels with uniform injection or suction. Again the wall temperatures are considered to be equal. Lee and Gill (32) present solutions for heat transfer in laminar and turbulent flow in a channel where the injection at one wall equals the suction at the other wall, which is called transverse flow. The wall temperatures

are equal.

Inman (33) solves the heat transfer problem for a porous annulus with unequal temperatures at the walls where transverse flow is superimposed on the main flow.

Purpose and Scope

Much debate is found in the literature on freeze-drying over the relative effects of radiation heat transfer and conduction-convection heat transfer between the heater and product where an open space separates the two. With this in mind, one of the primary objectives of this thesis is to effectively establish the relative contributions of each mode of heat transfer in this region.

Another aim of this work is to consider the relative effects of hydrodynamic and diffusional flow of the air, water-vapor mixture in the channel separating heater and product. The internal aspects of this problem have been dealt with extensively, but the results have hinged on the requirement of maintaining a fixed concentration of water-vapor above the product surface with respect to the total mixture. It is obvious then that the problem must be considered in the confined space above the product to complete the physical picture.

The analysis of this problem requires the consideration of the flow behavior and heat transfer in a semi-porous channel. Thus, another objective of this work is to add to the store of knowledge in the field of porous channels.

The scope of this work encompasses a solution to the Navier-Stokes momentum equations for the flow in a semi-porous channel. Further, the

temperature profiles in the channel must be derived from the energy equation. Finally, the concentration profiles of water-vapor must be derived from the equation of continuity for the water-vapor species. To include the effects of radiation heat transfer between heater and product, an overall energy balance must be performed on the channel.

The extent of this work and the complexity of the problem necessitate the use of approximate integral techniques to effect solutions of the differential equations. A number of simplifying assumptions are required which will not destroy the usefulness of the results but will allow a solution to be attained. The integral techniques of Karman-Pohlhausen have been widely used in boundary layer work with excellent results. Their employment in channel flow hence offers a novel approach to this problem.

CHAPTER II

GOVERNING EQUATIONS

General

The physical model used to describe the typical freeze-drying equipment arrangement is illustrated in Figure 1. The channel extends infinitely into the page hence enabling a two-dimensional treatment of the problem. Fluid flow and heat transfer in the channel is asymmetric with respect to the vertical y-coordinate, therefore its origin was chosen at the product surface as a matter of convenience. In freeze-drying, all fluid flow originates at the porous surface where $y = 0$. The water-vapor turns and flows down the channel to one of the exits. The flow is assumed to be symmetrical about the vertical centerline of the channel, and hence the longitudinal x-coordinate was chosen to originate at this location. The channel width H is constant with respect to the x-direction, and the length 2L is usually much greater than H.

The porous wall at $y = 0$, representing the food surface, must be maintained at or under a prescribed maximum temperature to prevent scorching of the surface. The solid or impermeable wall at $y = H$, which corresponds to the heater surface, must be regulated to a higher temperature level which will maintain the lower surface at the prescribed level.

This model basically describes the typical industrial method for freeze-drying large batches of food. The product is placed on trays which slide between heaters stacked on top of each other, as illustrated

in Figure 2. A space of from 0.25 to 1 inch is required between the heater and product to allow the vapor to escape. In some instances, the product is heated by radiation and convection from the top and direct contact on the bottom. Or using screens as trays, the product may be arranged to employ radiation and convection heating on top and bottom.

All of the analyses reviewed in the literature consider an infinitely long channel divided into a section with no porous walls followed by a section with either one or both walls porous. The main flow proceeds fully developed from the impermeable walled section into the porous walled section where mass is added to or removed from the main flow at the walls. However, as mentioned above, the analysis in this work considers all the mass to originate at the porous wall and hence move down the channel to one of the exits, depending on the location of injection.

The effects of a developing region near $x = 0$ are considered negligible. There is no potential core flow in this situation that is normally encountered in the entrance region of a channel, and hence the boundary layer will grow very quickly reaching the upper surface at $y = H$ within a very few hydraulic diameters of the channel. Also, any exit effects at $x = L$ are neglected for the sake of simplicity. In ordinary channel or pipe flow, Knudsen and Katz (57) show that at low Reynolds numbers an assumption of fully developed flow in entrance regions results in not too serious errors in heat transfer calculations. Ultimately, it will be shown that the greatest part of the heat transfer from the hot surface to the porous surface in freeze-drying is by radiation. Thus it appears reasonable to assume that neglecting certain irregular flow phenomena, under the particular flow situation described here, will have only a very

small effect on the final results. A somewhat similar analysis has been done by Ishizawa and Hori (56) for the case of injection into an axisymmetric channel. They too neglected any effects at the center of the channel and at the exits.

Part of the objectives of this thesis are to theoretically analyze the heat transfer mechanisms between heater and product and to investigate the relative effects of hydrodynamic and diffusional flow in this region. Initially, the continuity and momentum equations must be solved for the velocity and pressure distributions. The results of this solution are used in conjunction with the energy and diffusion equations to obtain solutions for the temperature and water-vapor mass concentration profiles within the confines of the channel. With the proper selection of boundary conditions, the convection and radiation heat transfer modes are uncoupled, and the energy equation is solved independent of the radiation effect. However, in determining the overall heat exchange between the surface, the radiation exchange equations must be applied.

In obtaining a solution to the transport equations, all properties including density, viscosity, and thermal conductivity are assumed constant. In obtaining numerical results, temperature corrections are applied to these properties for greater accuracy.

The flow is assumed to be in the continuum flow regime and to be laminar. The particular type of flow depends on the ratio of the mean free path of the vapor molecules to a characteristic dimension which in this case would be the channel width. This ratio is the Knudsen number,

$$Kn = \frac{\lambda}{H} \quad . \tag{2-1}$$

The type of flow for different ranges of the Knudsen number is given by the following:

$$2 < Kn \quad \text{Free - molecule flow}$$

$$.01 \leq Kn \leq 2 \quad \text{Transition flow}$$

$$Kn \leq .01 \quad \text{Continuum flow}$$

Under certain conditions in freeze-drying, flow in the channel borders on transitional flow, but in general it is in the continuum regime. Due to the very low density of the water-vapor, the channel Reynolds number based on the average channel flow velocity and the channel width lies well within the laminar regime, and hence the assumption of laminer flow is made.

In calculating the radiation heat transfer, the heater surface and the regions surrounding the exits of the channel are assumed to be black bodies. The porous surface is assumed to be grey. Also, the water-vapor flowing in the channel is considered to be transparent to thermal radiation. Reference to any standard heat transfer text shows that at the temperature levels encountered in freeze-drying, coupled with the low densities and short distances involved, the water-vapor absorptivity is practically zero.

Although the freeze-drying process is time-dependent, it is assumed that for short time intervals the flow rate and properties may be assumed constant with respect to time. This type of treatment is called a quasi-steady solution. It has been successfully employed by Dyer, et al. (5) and Hill (7) in determining solutions for flow rates and drying times in freeze-drying.

Differential Equations

The complete set of differential equations which describe the combined momentum, mass, and energy transport in two-dimensional, steady, incompressible, laminar semi-porous channel flow are

$$\frac{\partial u}{\partial x} + \frac{\partial v}{\partial y} = 0 \tag{2-2}$$

$$u \frac{\partial u}{\partial x} + v \frac{\partial u}{\partial y} = - \frac{1}{\rho} \frac{\partial p}{\partial x} + \nu \frac{\partial^2 u}{\partial x^2} + \nu \frac{\partial^2 u}{\partial y^2} \tag{2-3}$$

$$u \frac{\partial v}{\partial x} + v \frac{\partial v}{\partial y} = - \frac{1}{\rho} \frac{\partial p}{\partial y} + \nu \frac{\partial^2 v}{\partial x^2} + \nu \frac{\partial^2 v}{\partial y^2} \tag{2-4}$$

$$u \frac{\partial T}{\partial x} + v \frac{\partial T}{\partial y} = \alpha \frac{\partial^2 T}{\partial x^2} + \alpha \frac{\partial^2 T}{\partial y^2} \tag{2-5}$$

$$u \frac{\partial \omega}{\partial x} + v \frac{\partial \omega}{\partial y} = D \frac{\partial^2 \omega}{\partial x^2} + D \frac{\partial^2 \omega}{\partial y^2} \quad . \tag{2-6}$$

Equation (2-2) is the continuity equation satisfying the conservation of mass in the channel. Equations (2-3) and (2-4) are, respectively, the momentum equations in the x and y directions. Equation (2-5) represents the conservation of energy, and Equation (2-6) the diffusion equation, represents the conservation of the water-vapor species in a two-component flow system. The assumption of constant properties renders these quantities independent of the energy solution and, from this standpoint, uncouples the energy equation from the momentum equation. The effect of the choice of boundary conditions on the uncoupling of the momentum and

energy equations will be discussed later.

The momentum Equations (2-3) and (2-4) have been solved by several investigators (16,19,22) for the case of a semi-porous channel where the injection velocity v_0 at y = 0 is constant for all x. At the upper wall, of course, v is zero. At x = 0 these investigators treat the flow entering the porous region of the channel as fully developed. By defining a stream function

$$\Psi = \left[H\bar{U}(0) - v_0 x\right] f(y/H) \quad , \tag{2-7}$$

where $\bar{U}(0)$ is the average flow velocity at x = 0, and by defining a wall Reynolds number

$$R = \frac{v_0 H}{\nu} \tag{2-8}$$

the differential Equations (2-3) and (2-4) may be reduced to a single ordinary differential equation. Perturbation type solutions are then obtained through a series expansion in terms of R. That is, the injection or suction disturbance at a wall is represented as a small perturbation acting on the main flow field. The length of the series depends on the range of accuracy desired for R. The results, although very accurate, yield quite complicated expressions for u and v, especially when one considers using them in the energy and diffusion equations. These investigators have supported their results by presenting numerically exact solutions of the same equations.

The well known approximate integral techniques are accepted for obtaining accurate solutions to complicated flow situations involving

boundary layers. The method consists of transforming the differential equations for boundary layer flow into integral equations in which the integrals are carried from the surface of the plate to the outer edge of the boundary layer. A polynomial approximation representing the velocity profile is then made to satisfy certain conditions at the surface of the plate and at the edge of the boundary layer. Using the approximate velocity profile in conjunction with the integral equation, one may solve for the thickness of the boundary layer at any position along the plate.

In the same manner, the differential equations governing flow in the semi-porous channel may be transformed into integral equations with integration occurring in the y-direction from the porous surface to the solid surface. In this situation, the boundary layer is essentially the entire flow field, and an unknown pressure distribution must be found. Hence, it is proposed to assume a velocity distribution in the channel subject to conditions at the walls and use this profile in integral equations to solve for the pressure distribution. In an analogous manner, approximate solutions may also be obtained for the temperature distributions and the concentration distribution of water-vapor.

Integral Equations

Continuity and Momentum Equations

Equation (2-2), the continuity expression, may be rearranged as follows:

$$\frac{\partial v}{\partial y} = - \frac{\partial u}{\partial x} \tag{2-9}$$

and integrated from y = 0 where $v = v_0$ to y = H where v = 0 to give

$$v_0 = \int_0^H \frac{\partial u}{\partial x}\, dy \quad . \tag{2-10}$$

It is convenient to consider the y-direction momentum Equation (2-4) first. The velocity v may be calculated from the stream function using the fact that

$$v = - \frac{\partial \psi}{\partial x} \quad . \tag{2-11}$$

Hence, introducing Equation (2-7) into Equation (2-11) gives

$$v = v_0 f(y/H) \quad . \tag{2-12}$$

By requiring that the injection velocity at the porous surface be constant with respect to the x-coordinate, the v component of velocity is necessarily independent of x at all points in the channel. As a result, Equation (2-4) reduces to

$$v \frac{\partial v}{\partial y} = - \frac{1}{\rho} \frac{\partial p}{\partial y} + \nu \frac{\partial^2 v}{\partial y^2} \quad . \tag{2-13}$$

It is convenient here to consider the behavior of the pressure distribution. Since v depends only on y, differentiating Equation (2-13) with respect to x gives

$$\frac{\partial^2 p}{\partial x \partial y} = 0 \quad , \tag{2-14}$$

which implies that $\frac{\partial p}{\partial y}$ is independent of x. Further, since the second order mixed partial differentials are equal,

$$\frac{\partial^2 p}{\partial y \partial x} = 0 \quad , \tag{2-15}$$

which implies that $\frac{\partial p}{\partial x}$ is independent of y. Thus, the following total differential expression for pressure

$$dp = \frac{\partial p}{\partial x} dx + \frac{\partial p}{\partial y} dy \tag{2-16}$$

may be integrated directly to give

$$p = \text{fcn}(x) + \text{fcn}(y) \quad . \tag{2-17}$$

This result has also been observed by Donoughe (16).

Now considering Equation (2-3) and adding the continuity Equation (2-2), multiplied by u, to the left side of Equation (2-3) gives

$$u \frac{\partial u}{\partial x} + v \frac{\partial u}{\partial y} + u \frac{\partial u}{\partial x} + u \frac{\partial v}{\partial y} = - \frac{1}{\rho} \frac{\partial p}{\partial x} + \nu \frac{\partial^2 u}{\partial x^2} + \nu \frac{\partial^2 u}{\partial y^2} \tag{2-18}$$

or by combining derivatives on the left side

$$2u \frac{\partial u}{\partial x} + \frac{\partial uv}{\partial y} = - \frac{1}{\rho} \frac{\partial p}{\partial x} + \nu \frac{\partial^2 u}{\partial x^2} + \nu \frac{\partial^2 u}{\partial y^2} \quad . \tag{2-19}$$

Notice that the left side of Equation (2-2) equals zero, and hence adding it to the left side of Equation (2-3) does not change the equality. Integrating Equation (2-19) with respect to y from zero to H, noting that u = 0 at both walls and $\frac{\partial p}{\partial x}$ is independent of y yields

$$\int_0^H 2u \frac{\partial u}{\partial x} dy = - \frac{H}{\rho} \frac{\partial p}{\partial x} + \nu \int_0^H \frac{\partial^2 u}{\partial x^2} dy + \nu \left.\frac{\partial u}{\partial y}\right|_H - \nu \left.\frac{\partial u}{\partial y}\right|_0 \quad , \tag{2-20}$$

which may be used in conjunction with an assumed velocity profile to calculate $\frac{\partial p}{\partial x}$ or the pressure distribution in the x-direction. Then Equation (2-13) may be used to calculate $\frac{\partial p}{\partial y}$, and finally Equation (2-16) may be used to calculate the complete pressure distribution.

Energy Equation

Equation (2-5), which expresses the conservation of energy in the channel, may also be written in integral notation. Multiplying Equation (2-2) by T and, as before, adding the result to the left side of Equation (2-5) gives, upon combining derivatives,

$$\frac{\partial uT}{\partial x} + \frac{\partial vT}{\partial y} = \alpha \frac{\partial^2 T}{\partial x^2} + \alpha \frac{\partial^2 T}{\partial y^2} \quad . \tag{2-21}$$

Equation (2-21) must be integrated with respect to y from the porous wall at y = 0 where $v = v_0$ to the impermeable wall at y = H where v = 0. The result is

$$\int_0^H \frac{\partial uT}{\partial x}\, dy - v_0 T_0 = \alpha \int_0^H \frac{\partial^2 T}{\partial x^2}\, dy + \alpha \left.\frac{\partial T}{\partial y}\right|_H - \alpha \left.\frac{\partial T}{\partial y}\right|_0 \tag{2-22}$$

for the integral energy equation. Equation (2-22) will be very useful in determining the unknown coefficients of an assumed polynomial temperature profile.

Diffusion Equation

Equation(2-6), which expresses the conservation of the water-vapor component in a two-component system in the channel, may also be written in integral form. The procedure is exactly the same as used to arrive at the integral energy equation. The result is

$$\int_0^H \frac{\partial u\omega}{\partial x}\,dy - v_o\omega_o = D\int_0^H \frac{\partial^2\omega}{\partial x^2}\,dy + D\left.\frac{\partial\omega}{\partial y}\right|_H - D\left.\frac{\partial\omega}{\partial y}\right|_0 \qquad (2\text{-}23)$$

for the integral diffusion equation. As with the integral energy equation, the above is useful in determining the unknown coefficients of the assumed mass concentration distribution of water-vapor.

Boundary Conditions

Momentum Equation

The boundary conditions associated with the momentum equations are:

$$\begin{aligned} &\text{at } y = 0 : \quad u = 0 , \quad v = v_o \\ &\text{at } y = H : \quad u = 0 , \quad v = 0 \\ &\text{at } x = 0 : \quad u = 0 , \quad \frac{\partial p}{\partial x} = 0 . \end{aligned} \qquad (2\text{-}24)$$

The conditions that $u = 0$ at each wall are a result of the no slip condition at the walls. This assumption is of course contingent upon the flow remaining in the continuum regime in the channel which it does under normal drying conditions. Ishizawa and Hori (56) show that under conditions of a large value of R, there may be a certain amount of slip at the porous wall which should not be neglected in the analysis even though continuum flow exists. However, it will be seen in Chapter VI that the values of R encountered in freeze-drying are ordinarily less than one, and hence the effect of slip at the wall is probably negligible. At $x = 0$, there is no flow in the x-direction since otherwise this location would have to be a line source, hence $u = 0$. Further, due to symmetry of

the flow about x = 0, it is necessary that $\frac{\partial p}{\partial x} = 0$ at this location. The injection velocity at y = 0 is taken to be constant with respect to the x-direction, and of course at y = H the impermeable wall implies that v = 0.

Here, it is desirable to comment on the value of v_0. In most practical situations, v_0 will be some unknown function of x which must be solved. The boundary conditions must be so arranged and formulated that this additional unknown can be handled. In this thesis, it is convenient in the application to freeze-drying to require that the surface temperature at y = 0 be constant with respect to x in order to simplify the solution to the energy equation. However, the injection flow rate along the surface and hence the injection velocity are a direct function of the local heat flux and will vary as the heat flux varies. Hence, the momentum equation should be coupled with the energy equation and the two solved simultaneously. It should also be apparent that the concentration equation would be coupled to the energy equation, hence requiring a simultaneous solution of three differential equations. Such a problem would be very difficult to analyze and would require a complete numerical solution. However, all of these difficulties are eliminated by requiring v_0 to be constant with respect to x. This device neatly uncouples the momentum and diffusion equations from the energy equation and considerably simplifies the solutions. As will be seen in Chapter VI, the effects of this simplification are negligible when applied to freeze-drying due to the low range of R. The choice of a constant v_0 also serves to uncouple the momentum equation from the diffusion equation. This will be discussed in more detail in a later section.

In freeze-drying, the flow rate and consequently v_0 decrease with increasing drying time. However, flow conditions may be safely assumed constant for short periods of time. The wall Reynolds number, defined in Equation (2-8), may be altered to establish the flow conditions corresponding to a particular time during the drying cycle. The depth of the porous layer and the drying time are obtained from the solutions of Dyer, et al. (5).

Energy Equation

The boundary conditions imposed on the energy equation are:

$$\text{at } y = 0 \quad : \quad T = T_0$$

$$\text{at } y = H \quad : \quad T = T_H(x) \ , \ T_H > T_0 \tag{2-25}$$

$$\text{at } x = 0 \quad : \quad \frac{\partial T}{\partial x} = 0 \quad .$$

By assuming the temperature or at least the temperature distribution to be known at the walls, the energy equation becomes independent of the radiation heat transfer, and the convection and radiation may be treated separately. However, if one assumes a known amount of heat transfer at the walls, the radiation terms must be included directly in the boundary conditions. Since temperature raised to the fourth power appears, the boundary conditions become non-linear and hence the solution considerably more difficult to obtain. Further, the assumption of a constant temperature, or for that matter a constant heat flux, uncouples the energy equation from the diffusion equation though for a constant heat flux the reverse is not necessarily true. More general boundary conditions which

couple the energy and diffusion equations would not serve any useful purpose here.

The assumption of a constant surface temperature at y = 0 with respect to the x-direction corresponds to the actual process where it is desired to maintain the product surface within a prescribed temperature range. Also, this allows use of the internal drying solutions of Dyer, et al. (5) where a constant surface temperature was assumed. The heater surface temperature distribution will be allowed to assume a profile which will maintain the porous surface temperature constant.

Diffusion Equation

The boundary conditions associated with the diffusion equation are:

$$\begin{aligned} &\text{at } y = 0 \quad : \quad \omega = \omega_0(x) \\ &\text{at } y = H \quad : \quad \omega = \omega_H(x) \\ &\text{at } x = 0 \quad : \quad \frac{\partial \omega}{\partial x} = 0 \\ &\text{at } x = L \quad : \quad \omega = \bar{\omega}(L) = \omega_c \quad . \end{aligned} \tag{2-26}$$

The conditions at y = 0 and at y = H are based on the water-vapor mass concentrations at these boundaries. Generally, these conditions are not known, but as will be seen in Chapter V, they can be related to the v-component of velocity at each wall.

The assumption of a constant injection velocity at y = 0 with respect to x necessarily suppresses any dependence v_0 has on the variation of water-vapor concentration ω_0 along the surface. In freeze-drying, the

surface concentration ω_0 influences the frozen region temperature which subsequently affects the flow rate N_w through the dry layer and hence the injection velocity. However, sample calculations from the results of Dyer, et al. (5) show that a variation in mass concentration of water-vapor of 45 per cent from x = 0 to x = L would have only a 6.5 per cent effect on the injection velocity along the surface. Hence, the assumption of a constant injection velocity for the momentum solution appears justified and is desirable by reducing the complexity of the problem in uncoupling the momentum equation from the diffusion equation.

The conditions at x = 0 and x = L are, respectively, due to the symmetry of the channel and the average concentration of water-vapor in the chamber outside the channel.

The choice of boundary conditions described here for the momentum, energy, and diffusion equations are in part dictated by the relative ease of obtaining a solution to the equations. Part of the objective of this thesis is to obtain solutions which are in closed form and relatively easy to duplicate and use in the future. The boundary conditions chosen allow the equations to be solved independently and, by using approximate techniques, closed form solutions are obtained.

Porous Surface Energy Balance

In freeze-drying, the temperature of the two walls are not independently controlled. The sublimating ice within the food product requires energy which is supplied by the heater. The temperature level of the heater which is, of course, higher than that of the porous surface will then dictate the rate at which drying occurs. If the heater surface temperature is predetermined at a fixed value, then the porous surface

temperature is a function of the heater temperature, and it varies during the drying cycle from a low initial value to finally approaching the temperature of the heater. If the product surface temperature is to be constant during the cycle, then the heater temperature must be so adjusted during the cycle to maintain the product surface at the prescribed level. As the drying cycle proceeds, the rate of drying decreases due to the formation of a continually thickening dried layer surrounding the frozen region. Hence, the rate of heat transfer through the dried layer decreases, and the heater temperature must be continually adjusted to lower levels in order that overheating does not occur. However, this is a very slow process and, as mentioned before, can be treated as a quasi-steady-state process.

Since the two temperatures are not independent, only one of them can be considered known and the other determined by performing a heat balance on the porous surface. With reference to Figure 1, an energy balance at y = 0 yields

$$q_r + q_c = q_d \quad . \tag{2-27}$$

The first term in Equation (2-27) represents the net amount of radiation heat transfer to the porous surface. Radiant exchange exists between the porous surface and the heater surface and each of the channel exits. The second term represents the amount of heat energy which reaches the porous surface as a result of convection and conduction across the channel. The third term represents the heat energy conducted away from the porous surface toward the frozen region which is of course equal to

the heat transfer to the external side of the surface. The majority of the heat conducted away from the porous surface supplies the required heat of sublimation. The remaining portion is used to heat the water-vapor as it flows through the dried layer from the temperature of the ice region to the surface temperature.

The radiation contribution in Equation (2-27) can become a very complex function of geometry and the temperature of the participating surfaces. The convection term is primarily a function of the two wall temperatures, and the amount of heat conducted away from the porous surface is a function of the porous surface temperature and the temperature of the frozen region. The temperature of the frozen region may be determined from internal solutions. If the temperature of either the heater or the product surface is chosen, then the other may be calculated using Equation (2-27).

After the unknown temperature is determined, it is possible to calculate heat transfer coefficients and to determine how much heat transfer occurs by radiation and by convection. The effects of other primary variables such as channel width and length on the temperature levels may also be investigated. Further, by using the internal drying rate solution of Dyer, et al. (5), it is possible to relate the changing heater surface temperature to time.

The solution to the momentum equations are presented in Chapter III, and comparisons are made with more accurate solutions of previous investigators in Chapter VI. The energy solution is presented in Chapter IV along with the energy balance on the porous surface. In Chapter V the diffusion equation is solved for the water-vapor concentration profiles.

Numerical results for freeze-drying are presented in Chapter VI. Also, comparison of the analytical results of this thesis is made with the experimental work of Lusk, et al. (54) on freeze-drying of Haddock fish.

CHAPTER III

MOMENTUM SOLUTION

General

The more general momentum solution for the velocity and pressure distributions in a semi-porous channel considered by previous investigators has been discussed in Chapter II. In this chapter, a special case for the semi-porous channel applicable to freeze-drying will be considered. The important boundary condition that distinguishes this application is that $u(x,y) = 0$ at $x = 0$. Thus, all mass flowing in the channel originates at the porous wall. Basically the solution involves assuming a polynomial velocity profile, finding the coefficients based on conditions at the walls, and using the integral momentum equation to establish the pressure distribution.

Velocity Distribution

It is convenient to non-dimensionalize the vertical coordinate of the channel system as follows:

$$\xi = \frac{y}{H} \quad . \tag{3-1}$$

Substituting for y in Equation (2-20) of Chapter II yields for the x-direction integral equation

$$2 \int_0^1 u \frac{\partial u}{\partial x} \, d\xi = - \frac{1}{\rho} \frac{\partial p}{\partial x} + \nu \int_0^1 \frac{\partial^2 u}{\partial x^2} \, d\xi + \frac{\nu}{H^2} \frac{\partial u}{\partial \xi}\bigg|_1 - \frac{\nu}{H^2} \frac{\partial u}{\partial \xi}\bigg|_0 \quad . \tag{3-2}$$

At this point, a polynomial profile for the x-direction velocity distribution in the following form is assumed.

$$u(x,y) = a(x) + b(x)y + c(x)y^2 + d(x)y^3 \quad . \qquad (3\text{-}3)$$

The polynomial is in terms of powers of the y-coordinate, and the coefficients are assumed to be functions of x. Introducing Equation (3-1) for y gives

$$u(x,\xi) = a(x) + b(x)H\xi + c(x)H^2\xi^2 + d(x)H^3\xi^3 \quad . \qquad (3\text{-}4)$$

The general shape of such a profile is illustrated in Figure 3. The unknown coefficients in Equation (3-4) must be calculated subject to certain conditions at the boundaries. The conditions used here are

$$\text{at } \xi = 0 \ : \qquad u(x,0) = 0 \qquad (3\text{-}5)$$

$$\frac{v_0}{H}\frac{\partial u}{\partial \xi}\bigg|_0 = -\frac{1}{\rho}\frac{\partial p}{\partial x} + \frac{\nu}{H^2}\frac{\partial^2 u}{\partial \xi^2}\bigg|_0 \qquad (3\text{-}6)$$

$$\text{at } \xi = 1 \ : \qquad u(x,1) = 0 \quad . \qquad (3\text{-}7)$$

Equation (3-6) is a result of evaluating the differential Equation (2-3) at the porous surface and using Equation (3-1). Equations (3-5) and (3-7) express the no-slip conditions at the walls.

Since there are four unknown coefficients to determine, a fourth condition is required, and for this the integral continuity Equation (2-10) may be used. Equation (2-10) is repeated here in terms of ξ.

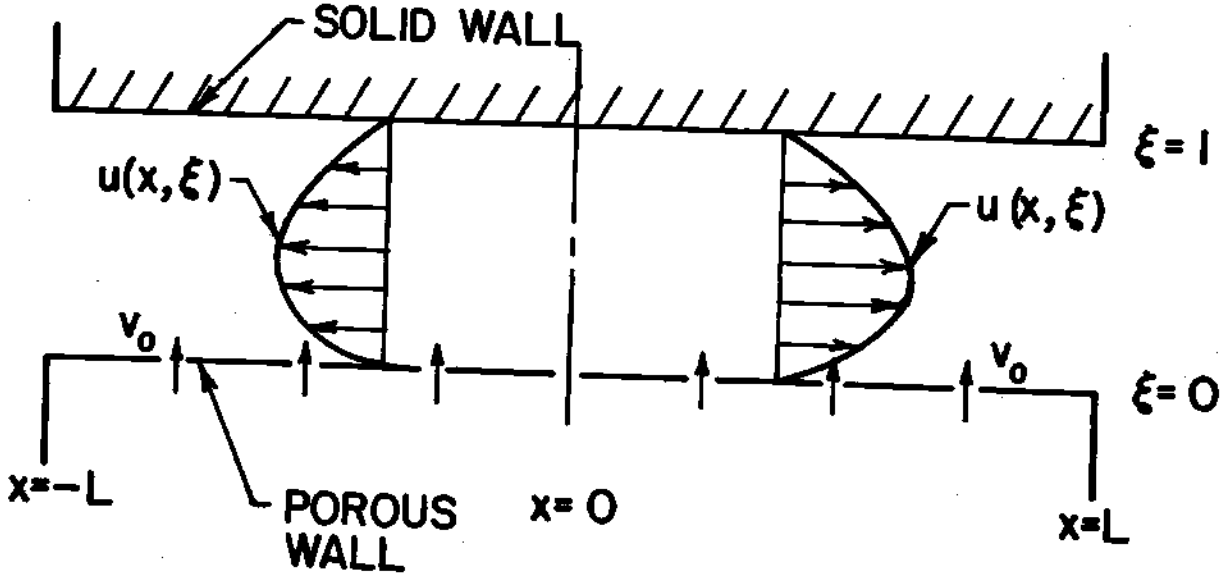

Figure 3. Typical Semi-Porous Channel Velocity Distributions

$$v_0 = H \frac{\partial}{\partial x} \int_0^1 u(x,\xi)\, d\xi \quad . \tag{3-8}$$

Note that the order for differentiation and integration is reversed in Equation (3-8). This can be done because the limits of integration are not dependent on x.

Application of the boundary conditions (Equations (3-5), (3-6) and (3-7)) to Equation (3-4) results in the following set of equations:

$$a = 0 \tag{3-9}$$

$$v_0 b = - \frac{1}{\rho} \frac{\partial p}{\partial x} + 2 \nu c \tag{3-10}$$

$$bH + cH^2 + dH^3 = 0 \quad . \tag{3-11}$$

The coefficients a, b, c, and d are dependent on x. Substituting Equation (3-4) into Equation (3-8) yields

$$v_0 = H \frac{\partial}{\partial x} \int_0^1 (bH\xi + cH^2\xi^2 + dH^3\xi^3)\, d\xi \quad . \tag{3-12}$$

Integration with respect to ξ gives

$$v_0 = \frac{\partial}{\partial x} \left(\frac{bH^2}{2} + \frac{cH^3}{3} + \frac{dH^4}{4} \right) \quad . \tag{3-13}$$

Equation (3-13) may be integrated with respect to x to give

$$v_0 x = \frac{bH^2}{2} + \frac{cH^3}{3} + \frac{dH^4}{4} + C_1(\xi) \quad , \tag{3-14}$$

where $C_1(\xi)$ is an arbitrary constant of integration and may be a function of ξ. The fact that a = 0 has already been taken into account.

Solving Equations (3-10), (3-11), and (3-14) simultaneously for b, c, and d yields the following results.

$$b = \frac{v_0 x}{H}\left(\frac{24 - \frac{H^3}{\rho\nu v_0 x}\frac{\partial p}{\partial x} - \frac{24\, C_1 H}{\nu\, Rx}}{R + 6}\right)\frac{1}{H} \tag{3-15}$$

$$c = \frac{v_0 x}{H}\left(\frac{12\, R + \frac{3H^3}{\rho\nu v_0 x}\frac{\partial p}{\partial x} - \frac{12\, C_1 H}{\nu\, x}}{R + 6}\right)\frac{1}{H^2} \tag{3-16}$$

$$d = \frac{v_0 x}{H}\left(\frac{-12\, R - 24 - \frac{2H^3}{\rho\nu v_0 x}\frac{\partial p}{\partial x} + \frac{24\, C_1 H}{\nu\, Rx} + \frac{12\, C_1 H}{\nu\, x}}{R + 6}\right)\frac{1}{H^3} \quad . \tag{3-17}$$

The various physical quantities involved have been arranged so as to introduce the wall Reynolds number R defined by Equation (2-8).

Substituting b, c, and d into Equation (3-4), noting that at x = 0 where u = 0 and $\frac{\partial p}{\partial x} = 0$ implies that $C_1 = 0$, gives for $u(x,\xi)$

$$u(x,\xi) = \frac{v_0 x}{H}\left\{\left(\frac{24 - \beta_1}{R + 6}\right)\xi + \left(\frac{12\, R + 3\, \beta_1}{R + 6}\right)\xi^2 + \left(\frac{-12\, R - 24 - 2\, \beta_1}{R + 6}\right)\xi^3\right\} \tag{3-18}$$

where the quantity β_1 is defined as

$$\beta_1 = \frac{H^3}{\rho \nu v_0 x} \beta \tag{3-19}$$

and

$$\beta = \frac{\partial p}{\partial x} \quad . \tag{3-20}$$

It is also convenient to redefine the coefficients b, c, and d as follows:

$$b = \frac{24 - \beta_1}{R + 6} \tag{3-21}$$

$$c = \frac{12 R + 3 \beta_1}{R + 6} \tag{3-22}$$

$$d = \frac{-12 R - 24 - 2 \beta_1}{R + 6} \quad . \tag{3-23}$$

The solution at this point remains incomplete, however, since β is still unknown. In order to determine β, Equation (3-18) must be substituted into the integral momentum Equation (3-2) which can then be solved for the pressure distribution.

Substituting Equation (3-18) into Equation (3-2) gives

$$\frac{2 v_0^2 x}{H^2} \left(\frac{bb'}{3} + \frac{bc'}{4} + \frac{bd'}{5} + \frac{cb'}{4} + \frac{cc'}{5} + \frac{cd'}{6} + \frac{db'}{5} + \frac{dc'}{6} + \frac{dd'}{7} \right)$$

$$= - \frac{1}{\rho} \beta + \frac{\nu}{H^2} \frac{v_0 x}{H} (2c+3d) \quad , \tag{3-24}$$

where the primes denote differentiation with respect to x. The terms b, c, and d are used for convenience, but it must be remembered that they contain β also. Note that substitution of $u(x,\xi)$ into the second term on the right side of Equation (3-2) reduces that term to zero. Hence, the x-direction viscous forces are canceled out.

Substituting for b, c, and d from Equations (3-21) through (3-23) and carrying out the indicated operations results in a differential equation of the form

$$C_2\beta\beta' + C_3x\beta' + C_4\beta + C_5x = 0 \tag{3-25}$$

where

$$C_2 = \frac{H^7}{210\ \rho^2} \tag{3-26}$$

$$C_3 = \frac{2\nu v_0 H^4}{35\ \rho} + \frac{v_0^2 H^5}{35\ \rho} \tag{3-27}$$

$$C_4 = \frac{212}{35}\ \nu v_0 H^4 + \frac{37}{70}\ v_0^2 H^5 + 18\ \nu^2 H^3 \tag{3-28}$$

$$C_5 = \frac{48}{35}\ v_0^4 H^3 + \frac{738}{35}\ \nu v_0^3 H^2 + \frac{2520}{35}\ \nu^2 v_0^2 H + 216\ \nu^3 v_0 \quad . \tag{3-29}$$

In terms of the pressure p, Equation (3-25) becomes

$$C_2p'p'' + C_3xp'' + C_4p' + C_5x = 0 \quad . \tag{3-30}$$

Equation (3-30) is an ordinary differential equation with variable

coefficients, and as such a solution in the form of an infinite series provides the most practical method of solution. A power series solution of the following form is assumed to exist.

$$p = g_0 + g_1 x + g_2 x^2 + g_3 x^3 + \ldots \quad . \tag{3-31}$$

Substitution of Equation (3-31) into Equation (3-30) and grouping coefficients of like powers yields

$$(2\,C_2 g_1 g_2 + C_4 g_1) + (6\,C_2 g_1 g_3 + 4\,C_2 g_2 g_2 + 2\,C_3 g_2 + 2\,C_4 g_2 + C_5)x$$
$$+ (12\,C_2 g_1 g_4 + 12\,C_2 g_2 g_3 + 6\,C_2 g_2 g_3 + 6\,C_3 g_3 + 3\,C_4 g_3)x^2$$
$$+ \ldots = 0 \quad . \tag{3-32}$$

Since each coefficient of the x-powers must equal zero, it follows that

$$g_1 = 0 \tag{3-33}$$

and

$$g_2 = -\frac{(C_3+C_4)}{4\,C_2} \pm \frac{1}{2}\left\{\left(\frac{C_3 + C_4}{2\,C_2}\right)^2 - \frac{C_5}{C_2}\right\}^{\frac{1}{2}} \quad . \tag{3-34}$$

It is assumed here that three terms of the series of Equation (3-31) are sufficient to describe the pressure distribution. Substitution of Equations (3-33) and (3-34) into Equation (3-31) and noting that $g_0 = p_0$, the pressure at x = 0 gives for the pressure distribution in the x-direction

$$p = p_0 + \left[-\frac{(C_3+C_4)}{4\,C_2} \pm \frac{1}{2}\left\{\left(\frac{C_3 + C_4}{2\,C_2}\right)^2 - \frac{C_5}{C_2}\right\}^{\frac{1}{2}}\right] x^2 \quad . \tag{3-35}$$

Note that Equation (3-35) does not represent the complete pressure distribution but only amounts to a solution for the first term on the right side of Equation (2-16). In other words, it is only the x-direction component of the total pressure distribution. However, to complete the solution for the velocity profiles all that is necessary is β or $\frac{\partial p}{\partial x}$; and hence, Equation (3-35) is all that is necessary. Calculation of β gives

$$\beta = \frac{\partial p}{\partial x} = 2\left[-\left(\frac{C_3 + C_4}{4\,C_2}\right) \pm \frac{1}{2}\left\{\left(\frac{C_3 + C_4}{2\,C_2}\right)^2 - \frac{C_5}{C_2}\right\}^{\frac{1}{2}}\right] x \quad . \tag{3-36}$$

For Equation (3-18), the quantity β_1 defined by Equation (3-19) is required. Multiplication of Equation (3-36) by $\frac{H^3}{\rho\nu v_{0x}}$ and substitution of Equations (3-26) through (3-29) gives

$$\beta_1 = \frac{H^3}{\rho\nu v_{0x}}\frac{\partial p}{\partial x} = -\left(\frac{\frac{214}{35} + \frac{39}{70}R + \frac{18}{R}}{\frac{1}{105}}\right) + \left\{\left(\frac{\frac{214}{35} + \frac{39}{70}R + \frac{18}{R}}{\frac{1}{105}}\right)^2 - \left(\frac{\frac{48}{35}R^2 + \frac{738}{35}R + \frac{4056}{35} + \frac{216}{R}}{\frac{1}{210}}\right)\right\}^{\frac{1}{2}} , \tag{3-37}$$

where for the case of fluid injection at the wall, the plus (+) sign is retained in front of the square root quantity. For the case of suction at the wall, which is not considered here, the minus (-) sign should be used.

Equation (3-37) used in conjunction with Equation (3-18) completes the solution for the x-component of the velocity distribution. In the integral energy and diffusion equations, only the x-component is required.

Pressure Distribution

To complete the calculation of the pressure distribution, the y-direction component of velocity $v(\xi)$ must first be determined. Substitution of Equation (3-18) into Equation (2-9) and integrating with respect to v from v_0 to $v(\xi)$ and ξ from 0 to ξ gives

$$v(\xi) = v_0 - \frac{v_0 y}{H}\left\{\frac{b}{2}\xi + \frac{c}{3}\xi^2 + \frac{d}{4}\xi^3\right\} \quad . \tag{3-38}$$

The symbols b, c, and d defined by Equations (3-21) through (3-23) are used as a matter of convenience.

Substitution of Equation (3-38) into Equation (2-13) then gives

$$\frac{\partial p}{\partial y} = -\frac{\rho v_0^2}{RH}\left\{b + 2c\xi + 3d\xi^2\right\} - \frac{\rho v_0^2}{H}\left\{-b\xi - c\xi^2 - \left(d - \frac{b^2}{2}\right)\xi^3 + \left(\frac{5bc}{6}\right)\xi^4 + \left(\frac{3bd}{4} + \frac{c^2}{3}\right)\xi^5 + \frac{7cd}{12}\xi^6 + \frac{d^2}{4}\xi^7\right\} \quad . \tag{3-39}$$

Integration of $dp(x,\xi) = \frac{\partial p}{\partial x}dx + \frac{\partial p}{\partial \xi}d\xi$ using Equations (3-36) and (3-39) results in the complete pressure distribution.

$$p(x,\xi) = p(0,0) + \frac{\rho v_0^2}{2} \frac{\beta_1}{R} \left(\frac{x}{H}\right)^2 + \left[- \frac{\rho v_0^2}{R} f_1 - \frac{\rho v_0^2}{2} f_2 \right] , \qquad (3\text{-}40)$$

where

$$f_1 = b\xi + c\xi^2 + d\xi^3 \qquad (3\text{-}41)$$

and

$$f_2 = - b\xi^2 - \frac{2c}{3} \xi^3 - \left(d - \frac{b^2}{2}\right) \frac{1}{2} \xi^4 + \frac{bc}{3} \xi^5 + \left(\frac{3bd}{4} + \frac{c^2}{3}\right) \frac{1}{3} \xi^6 + \frac{cd}{6} \xi^7 + \frac{d^2}{16} \xi^8 \qquad (3\text{-}42)$$

The pressure change in the x-direction may then be found from Equation (3-40):

$$\Delta p_x = \frac{p(x,\xi) - p(0,\xi)}{\frac{1}{2} \rho v_0^2} = \frac{\beta_1}{R} \left(\frac{x}{H}\right)^2 . \qquad (3\text{-}43)$$

Similarly, the pressure change in the y-direction is

$$\Delta p_y = \frac{p(\xi,x) - p(0,x)}{\frac{1}{2} \rho v_0^2} = - \frac{2}{R} f_1 - f_2 . \qquad (3\text{-}44)$$

The velocity profile and pressure distribution derived in this chapter are compared with the results of previous investigators in Chapter VI. The results of this chapter are used in Chapter IV and Chapter V in obtaining solutions of the energy and diffusion equations.

CHAPTER IV

ENERGY SOLUTION

General

In this chapter a solution of the integral energy Equation (2-22) is presented for the temperature profile of a mixture of air and water-vapor flowing in a semi-porous channel with asymmetric wall temperatures. All of the mass flowing in the channel is assumed to originate at the porous wall. The boundary conditions are selected in order that the temperature profile may be obtained independently of the radiant heat exchange between the walls.

Once the temperature profile is known, the heat transfer to the wall by radiation and convection is equated to the heat required for sublimation. This energy balance is used to establish the functional relationship between the two wall temperatures.

The first term on the right side of Equation (2-22) represents heat transfer by conduction in the x-direction in the channel. In this work, it is assumed that the longitudinal conduction effect is small over most of the channel length. Hence, the x-direction conduction term is neglected. This assumption is commonly made in fully developed channel and tube flow and in boundary layer flow problems. It greatly simplifies the solutions without significantly affecting the accuracy of the final results.

Temperature Distribution

Again, it is convenient to define the dimensionless distance

$$\xi = \frac{y}{H} \quad . \tag{4-1}$$

Neglecting the x-conduction term, Equation (2-22) then becomes

$$\int_0^1 \frac{\partial uT}{\partial x}\, d\xi - \frac{v_0 T_0}{H} = \frac{\alpha}{H^2} \frac{\partial T}{\partial \xi}\bigg|_1 - \frac{\alpha}{H^2} \frac{\partial T}{\partial \xi}\bigg|_0 \quad . \tag{4-2}$$

The assumed polynomial temperature profile is

$$T(x,\xi) = a_1(x) + b_1(x)\, H\xi + c_1(x)\, H^2\xi^2 + d_1(x)\, H^3\xi^3 \quad . \tag{4-3}$$

The x in parenthesis again implies that the coefficients are functions of x.

The coefficients in Equation (4-3) must be calculated subject to conditions at the boundaries. With reference to Figure 4, these conditions are

at $\xi = 0$: $$T(x,0) = T_0 \tag{4-4}$$

$$\frac{v_0}{H} \frac{\partial T}{\partial \xi}\bigg|_0 = \frac{\alpha}{H^2} \frac{\partial^2 T}{\partial \xi^2}\bigg|_0 \quad , \tag{4-5}$$

and at $\xi = 1$: $$\frac{\partial^2 T}{\partial \xi^2}\bigg|_1 = 0 \quad . \tag{4-6}$$

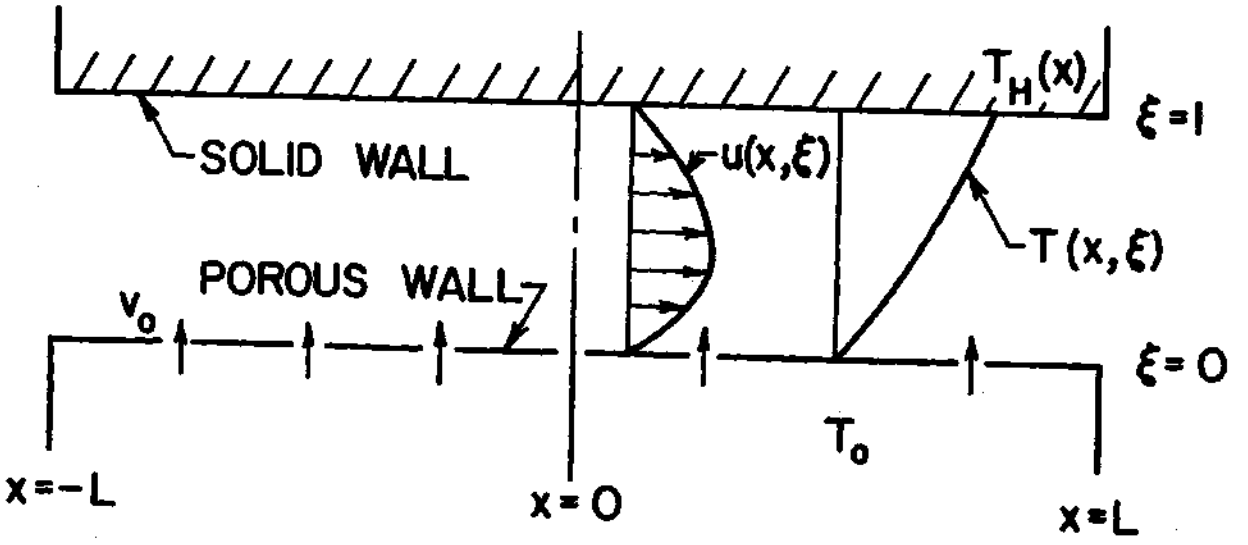

Figure 4. Typical Semi-Porous Channel Temperature Distribution for Different Wall Temperatures

Equation (4-4) is a result of specifying the surface temperature and assuming it to be constant with respect to position along the surface. An assumption of a constant heat flux at $\xi = 0$ instead of a constant temperature would be more compatible with the constant velocity assumption used in Chapter III. However, a constant heat flux boundary condition would necessitate including the radiation terms in the boundary condition making them non-linear. This problem is avoided by specifying the temperature instead.

Equations (4-5) and (4-6) are the results of evaluating the differential energy Equation (2-5) at the lower and upper boundaries.

Another condition is required in order to completely determine the four coefficients in Equation (4-3). The most obvious choice is to use Equation (4-2), the integral energy equation, to complete the determination of the coefficients.

The temperature distribution along the impermeable wall is given in Chapter II as a boundary condition. However, the actual distribution is unknown and must be determined as part of the solution. Hence, in place of using the surface temperature at $\xi = 1$ as a condition with which to determine the coefficients in Equation (4-3), it is more convenient to obtain the necessary conditions from the differential equation.

Application of the boundary conditions in Equations (4-4) through (4-6) to Equation (4-3) yields the following set of equations.

$$a_1 = T_0 \tag{4-7}$$

$$v_0 b_1 = 2 \alpha c_1 \tag{4-8}$$

$$2\,c_1 + 6\,d_1\,H = 0 \quad . \tag{4-9}$$

Now it is necessary to substitute the temperature profile and the x-component of the velocity profile $u(x,\xi)$ given by Equation (3-18) into Equation (4-2). This gives

$$(xb_1'+b_1)\,H\,C_6 + (xc_1'+c_1)\,H^2C_7 + (xd_1'+d_1)\,H^3C_8 - 2\,\frac{c_1\alpha H}{v_0} - 3\,\frac{d_1\alpha H^2}{v_0} = 0 \quad , \tag{4-10}$$

where

$$C_6 = \frac{b}{3} + \frac{c}{4} + \frac{d}{5} \tag{4-11}$$

$$C_7 = \frac{b}{4} + \frac{c}{5} + \frac{d}{6} \tag{4-12}$$

$$C_8 = \frac{b}{5} + \frac{c}{6} + \frac{d}{7} \tag{4-13}$$

Substituting Equations (4-8) and (4-9) into Equation (4-10) gives

$$c_1' + \frac{\gamma}{x}\,c_1 = 0 \quad , \tag{4-14}$$

where

$$\gamma = 1 - \frac{(18 + 3R)}{\left(\frac{96}{5} + \frac{18R}{5} + \frac{\beta_1}{10} + \frac{162RPr}{35} + \frac{RPr\beta_1}{28} + \frac{32R^2Pr}{35}\right)} \quad . \tag{4-15}$$

The combination RPr is the wall Reynolds number times the Prandtl number

and is defined by

$$RPr = \frac{v_0 H}{\alpha} \quad . \tag{4-16}$$

The first order differential Equation (4-14) may be solved by means of multiplication with an integrating factor.

$$I.F. = e^{\int \frac{\gamma}{x} dx} = e^{\gamma \ln x} = x^{\gamma} \quad . \tag{4-17}$$

The solution becomes

$$c_1 = C_9 x^{-\gamma} \quad , \tag{4-18}$$

where C_9 is a constant of integration to be determined. Using Equation (4-18), the coefficients b_1 and d_1 are easily determined from Equations (4-8) and (4-9), and upon substitution of all the coefficients into Equation (4-3) there results

$$T - T_0 = C_9 x^{-\gamma} H^2 \left(\frac{2}{RPr} \xi + \xi^2 - \frac{1}{3} \xi^3 \right) \quad . \tag{4-19}$$

The term γ defined by Equation (4-15) is always positive, and hence as x approaches zero the temperature approaches infinity. This behavior is a result of neglecting the x-direction conduction term in Equation (2-22). Near x = 0 conduction in the x-direction is the same order of magnitude as convection in the x-direction. Further, in the limit as x approaches zero, neglecting the x-conduction term causes a physically impossible situation. That is, the solution presented in Equation (4-19)

attempts to compensate for the absence of the conduction term by increasing the temperature to infinity at x = 0. This type of behavior is also observed in boundary layer analysis at the leading edge of a flat plate. At this location, the heat transfer coefficient approaches infinity, again as a result of neglecting terms which are important at the leading edge. However, when considering a long plate, the overall error introduced is considered negligible. Similarly, if the analysis here is confined to long narrow channels, the resulting error near x = 0 may be overlooked.

The constant C_9 in Equation (4-19) must now be evaluated. It is convenient to introduce the temperature of the heater surface into the solution. The final boundary condition will then be taken as the temperature of the heater surface at x = L.

$$\text{at } x = L,\ \xi = 1: \qquad T(L,1) = T_{LH} \quad . \tag{4-20}$$

Evaluation of Equation (4-19) subject to Equation (4-20) gives

$$C_9 = \frac{\left(T_{LH}-T_0\right)\left(3\ RPr\right)}{L^{-\gamma}H^2(6+2\ RPr)} \tag{4-21}$$

Hence, the complete solution for the temperature profile becomes

$$\frac{T(x,\xi) - T_0}{T_{LH} - T_0} = \left(\frac{x}{L}\right)^{-\gamma}\left(\frac{3}{3 + RPr}\,\xi + \frac{3\ RPr}{6 + 2\ RPr}\,\xi^2 - \frac{RPr}{6 + 2\ RPr}\,\xi^3\right) . \tag{4-22}$$

It is convenient to define a dimensionless temperature.

$$\theta(x,\xi) = \frac{T(x,\xi) - T_0}{T_{LH} - T_0} \quad . \tag{4-23}$$

In ordinary channel flow problems, the temperature is usually non-dimensionalized in terms of a fluid temperature entering a heated or cooled section. This entrance temperature serves as the usual boundary condition with respect to x. This is convenient because in general the increase or decrease of the fluid bulk temperature above or below the initial value is of interest.

However, no such convenient or useful reference temperature exists in this problem. The temperatures of most interest are those of the porous surface and the heater surface and these are not independently controlled in freeze-drying. It is not possible to specify a temperature at $x = 0$ since the solution is discontinuous at this location. This means that another location must be selected for a boundary condition and the logical one is at $x = L$. But, the average bulk temperature of the water-vapor is of little interest at this location. However, the heater surface temperature is of primary interest, and hence at $x = L$, $\xi = 1$, it is assumed that the temperature is known in order to put the solution in the form given by Equation (4-22). Once the temperature T_{LH} is known, then the temperature at any location along the heater surface may be determined or a mean heater surface temperature may be defined. Also, the rates of heat transfer from the heater to the porous surface may be determined for convection and radiation. However, the surface temperatures are not independently controlled, and in the next section an energy balance at $\xi = 0$ is used to relate those quantities.

From the temperature profile of Equation (4-22), it is now possible to calculate the heat transfer between the porous wall and the fluid layer next to the wall using the equation

$$q_c = - k \left.\frac{\partial T}{\partial y}\right|_0 \quad , \tag{4-24}$$

or in terms of θ and ξ,

$$q_c = - \frac{k\left(T_{LH}-T_0\right)}{H} \left.\frac{\partial \theta}{\partial \xi}\right|_0 \quad . \tag{4-25}$$

Heat Transfer

The heat balance at the surface $\xi = 0$ is given by Equation (2-27). The energy convected across the channel and conducted to the surface may be calculated using Equation (4-25) to give

$$q_c = \frac{- k\left(T_{LH}-T_0\right)}{H}\left(\frac{3}{3 + RPr}\right)\left(\frac{x}{L}\right)^{-\gamma} \quad . \tag{4-26}$$

The mean temperature of the heater may be calculated from

$$T_m = \frac{1}{2L} \int_{-L}^{L} T(x,1)\, dx \quad . \tag{4-27}$$

Substitution of Equation (4-22) into Equation (4-27) gives

$$T_m = T_0 + \frac{\left(T_{LH}-T_0\right)}{(1-\gamma)} \quad , \tag{4-28}$$

and Equation (4-26) may be written

$$q_c = \frac{-k\left(T_m - T_0\right)\left(1-\gamma\right)}{H}\left(\frac{3}{3 + RPr}\right)\left(\frac{x}{L}\right)^{-\gamma} \quad . \tag{4-29}$$

The mean temperature of the heater surface T_m is a more practical quantity to measure and to use in subsequent calculations.

The energy per unit area conducted away from the porous surface toward the frozen-region is given by

$$q_d = \rho_0 v_0 \, \Delta H + \rho_0 v_0 \, c_p\left(T_0 - T_d\right) \quad , \tag{4-30}$$

where ρ_0 is the density of water-vapor at $y = 0$, ΔH is the latent heat of sublimation of the frozen food juices, c_p is the specific heat of water-vapor, and T_d is the temperature of the frozen-region.

Equation (2-27) then becomes upon substitution of Equations (4-29) and (4-30)

$$q_r - \frac{k\left(T_m - T_0\right)\left(1-\gamma\right)}{H}\left(\frac{3}{3 + RPr}\right)\left(\frac{x}{L}\right)^{-\gamma} = \rho_0 v_0 \, \Delta H + \rho_0 v_0 c_p\left(T_0 - T_d\right) \, . \tag{4-31}$$

The net radiation flux to the porous surface is a complex function of geometry, further complicated by the variable temperature of the heater surface. The equations presented here utilize the methods and terminology of Sparrow and Cess (49). A derivation of the equations presented here is contained in Appendix A.

The net radiation heat flux from surface i of a system of surfaces is given by

$$q_i(x_i) = \frac{\epsilon_i}{1 - \epsilon_i} \left[\sigma T_i^4(x_i) - B_i(x_i) \right] , \qquad (4\text{-}32)$$

where ϵ_i is the emissivity of surface i, σ is the Stefen-Boltzmann constant, and $B_i(x_i)$ is the radiosity, the total emitted radiation energy per unit area, and is in general a function of position on surface i.

The radiosity of surface i may be written as

$$B_i(x_i) = \epsilon_i \sigma T_i^4(x_i) + (1-\epsilon_i) \sum_j \int_{A_j} B_j(x_j) \frac{dF_{i-j}}{dA_j} dA_j , \qquad (4\text{-}33)$$

where $B_j(x_j)$ is the radiosity function of a typical j surface of the system and dF_{i-j} is the incremental view factor from an elemental area dA_i on surface i to area dA_j on surface j. The summation is extended over all surfaces of the system including surface i if it can see part of itself. Each radiosity term must in general be integrated over the corresponding surface.

The $B_j(x_j)$'s are in general unknown and hence an equation similar to (4-33) must be written for each of the surfaces, and the set of equations solved simultaneously in order to obtain the radiosity of each surface. For a system of non-black, non-isothermal surfaces this is a formendable task, and only with computers can a complex system be analyzed.

The system pictured in Figure 5 has four surfaces. The two exits are treated as black isothermal windows for radiation calculations, and the heater surface at y = H is treated as a black non-isothermal surface. The porous surface is, of course, isothermal, but it must be treated as gray for calculations.

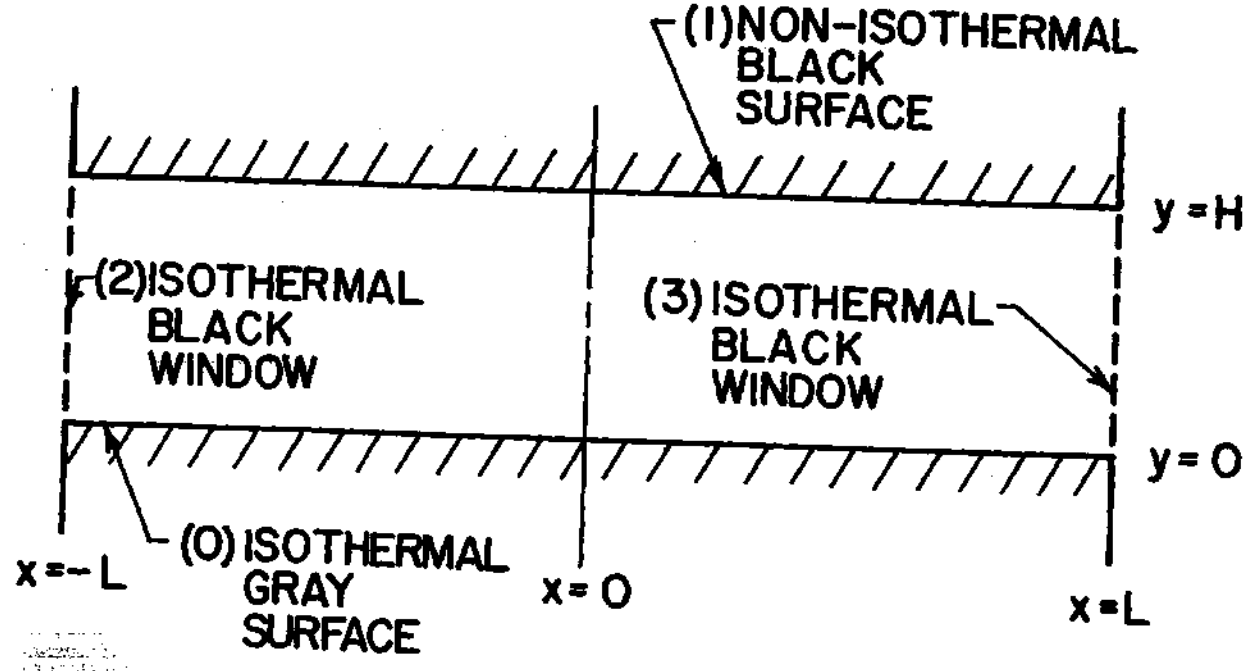

Figure 5. Enclosure Illustrating Types of Radiating Surfaces in Semi-Porous Channel

For freeze-dried beef, measurements by Sevcik and Sunderland (58) showed that the emissivity is 0.75. Hence, it cannot be treated as a black surface. Heater surfaces may be specially coated so that the emissivity is greater than 0.9, and thus for calculations may be considered black.

Using the subscripts 0, 1, 2, and 3 to indicate respectively the porous surface, the heater, the exit at x = -L, and the exit at x = L, the radiosities may be evaluated for each surface. Since $\epsilon_1 = \epsilon_2 = \epsilon_3 = 1$, the radiosities for surfaces 1, 2, and 3 may be successively evaluated from the general Equation (4-33) to be

$$B_1(x_1) = \sigma T_1^4(x_1) \tag{4-34}$$

$$B_2 = \sigma T_2^4 \tag{4-35}$$

$$B_3 = \sigma T_3^4 \quad . \tag{4-36}$$

The fact that the emissivities of surfaces 1, 2, and 3 are equal to one eliminates any contribution from the summation term in Equation (4-33) to the respective radiosities. Since the emissivity of surface 0 is not equal to one, the expression for $B_0(x_0)$ is not as simple. It must also include the radiosities of the other surfaces. Writing Equation (4-33) for $B_0(x_0)$ and substituting Equations (4-34) through (4-36), gives

$$B_0(x_0) = \epsilon_0 \sigma T_0^4 + (1-\epsilon_0) \int_{A_1} \sigma T_1^4(x_1) \frac{dF_{0-1}}{dA_1} dA_1 \tag{4-37}$$

$$+ (1-\epsilon_0) \int_{A_2} \sigma T_2^4 \frac{dF_{0-2}}{dA_2} dA_2 + (1-\epsilon_0) \int_{A_3} \sigma T_3^4 \frac{dF_{0-3}}{dA_3} dA_3 \quad .$$

Obviously the assumption of three black surfaces greatly simplifies the radiosity expressions. The terms B_1, B_2, and B_3 were reduced to simple functions of temperature only, and the interdependence among the radiosities eliminated. The expression, $B_0(x_0)$, is now a function of the four surface temperatures and the geometric view factors. The incremental view factors, derived in Appendix B, in terms of the surface coordinates of the four surfaces are

$$dF_{0-1} = \frac{H^2 \, dx_1 \, dz_1}{\pi \left[z_1^2 + H^2 + (x_1 - x_0)^2 \right]^2} \tag{4-38}$$

$$dF_{0-2} = \frac{y_2 (L+x_0) \, dy_2 \, dz_2}{\pi \left[z_2^2 + y_2^2 + (L+x_0)^2 \right]^2} \tag{4-39}$$

$$dF_{0-3} = \frac{y_3 (L-x_0) \, dy_3 \, dz_3}{\pi \left[z_3^2 + y_3^2 + (L-x_0)^2 \right]^2} \quad . \tag{4-40}$$

The coordinates z_1, z_2, and z_3 are in the direction into and out of the page. Integration with respect to the z-coordinate is made from $-\infty$ to $+\infty$. The coordinates y_2 and y_3 are the vertical coordinates at each end of the channel and these range from 0 to H. Note that

$$dA_1 = dx_1 \, dz_1 \tag{4-41}$$

$$dA_2 = dy_2 \, dz_2 \tag{4-42}$$

$$dA_3 = dy_3\, dz_3 \quad . \tag{4-43}$$

The incremental view factors, Equations (4-38) through (4-40) must be substituted in Equation (4-37) and the indicated integrals evaluated. The last two integrals in Equation (4-37) are relatively straightforward to integrate because the temperatures T_2 and T_3 may be assumed independent of the position coordinates. These integrals are evaluated in Appendix C. The first integral, however, is complicated by having the temperature a function x_1 and raised to the fourth power. The integration with respect to the z_1 coordinate may be performed independently, however, and it too is included in Appendix C.

The results of substituting the view factors, performing all the integrations mentioned except with respect to x_1, and then substituting $B_0(x_0)$ into Equation (4-32) for $q_0(x_0)$ gives

$$q_0(x_0) = \frac{\epsilon_0}{1-\epsilon_0}\left\{(1-\epsilon_0)\sigma T_0^4 - (1-\epsilon_0)\,\sigma \int_{x_1} \frac{T_1^4(x_1)\, H^2\, dx_1}{2\left[(x_1-x_0)^2 + H^2\right]^{3/2}}\right.$$

$$- \frac{(1-\epsilon_0)\,\sigma\, T_2^4}{2}\left[1 - \frac{(L+x_0)}{\left[(L+x_0)^2 + H^2\right]^{1/2}}\right] \tag{4-44}$$

$$\left. - \frac{(1-\epsilon_0)\,\sigma\, T_3^4}{2}\left[1 - \frac{(L-x_0)}{\left[(L-x_0)^2 + H^2\right]^{1/2}}\right]\right\}$$

Substituting $q_0(x_0)$ from Equation (4-44) for q_r in Equation (4-31) completes the energy balance at $y = 0$. The result is still a function of

x_0, however, making it a local heat balance. To obtain an overall energy balance, integration must be performed with respect to x_0 from -L to L. Thus, substituting Equation (4-44) into Equation (4-31) and integrating term by term with respect to x_0 from -L to +L gives

$$\frac{\epsilon_0}{1-\epsilon_0}\left\{(1-\epsilon_0)\,\sigma\,T_0^4\left(\frac{2L}{H}\right) - \frac{(1-\epsilon_0)\,\sigma\,H}{2}\int_{-L}^{L}\int_{-L}^{L}\frac{T_1^4(x_1)\,dx_1\,dx_0}{\left[(x_1-x_0)^2+H^2\right]^{3/2}}\right.$$

$$\left. - \frac{(1-\epsilon_0)\,\sigma\,T_2^4}{2}\left[\frac{2L}{H}+1-\sqrt{4\left(\frac{L}{H}\right)^2+1}\right] - \frac{(1-\epsilon_0)\,\sigma\,T_3^4}{2}\left[\frac{2L}{H}+1-\sqrt{4\left(\frac{L}{H}\right)^2+1}\right]\right\} \qquad (4\text{-}45)$$

$$- \frac{k(T_m-T_0)}{H}\left(\frac{6}{3+RPr}\right)\left(\frac{L}{H}\right) = 2\,\rho_0 v_0\,\Delta H\left(\frac{L}{H}\right) + 2\,\rho_0 v_0 c_p (T_0-T_a)\left(\frac{L}{H}\right) \quad .$$

Integrations with respect to x_0 may be found in Appendix C. Equation (4-45) has been divided by H in order to produce the non-dimensional quantity L/H a length to width ratio. Note that if $T_2 = T_3$, the contributions from the exits are identical as would be expected.

There now remains the task of substituting T(x,1) from Equation (4-22) for $T_1(x_1)$ and performing the indicated integrations. The result of this substitution yields sixteen integrals which must be integrated numerically. The details are rather tedious, and an outline of the steps is presented in Appendix D. Performing the substitution, the double integral in Equation (4-45) may be written as

$$I = \frac{(1-\epsilon_0)\,\sigma}{2}\left[2\,T_0^4\sqrt{4\left(\frac{L}{H}\right)^2+1} - 2\,T_0^4 + 4\,T_0^3\left(T_{LH}-T_0\right)I_1\right.$$

$$\left. + 6\,T_0^2\left(T_{LH}-T_0\right)^2 I_2 + 4\,T_0\left(T_{LH}-T_0\right)^3 I_3 + \left(T_{LH}-T_0\right)^4 I_4\right] \qquad (4\text{-}46)$$

where I represents the double integral in Equation (4-45) and I_1, I_2, I_3, and I_4 are defined in Appendix D and are functions of γ and L/H and must be numerically evaluated.

Procedure

In Equation (4-45) either the product surface temperature or the mean heater surface temperature must be considered as an unknown. All other temperatures and properties are considered to be known quantities. The injection Reynolds number R is a known parameter which is free to vary over any desired range of values. If one then chooses either T_0 or T_m as known, then the other may be calculated from Equation (4-45). In some instances, the heater temperature is fixed at a certain level throughout the drying cycle. For this case, it is desirable to know how the product surface temperature will vary as drying progresses. On the other hand, it may be convenient to raise the product surface temperature to a certain level and maintain it fixed throughout the cycle. In this case, it is desirable to know how the heater temperature must vary during drying. Equation (4-45) will predict either one of these temperatures when the other is given.

During drying, the flow rate decreases steadily with time as the thickness of the dried porous region increases. For a particular value of R, Equation (4-45) is applicable for a short period of time during the

freeze-drying process. Since R is actually slowly changing, then it must be considered as an average injection Reynolds number during the time period. In this work, T_0 or T_m and R are treated as known parameters in the problem. In order to relate a set of flow conditions in the channel to a particular stage of the drying cycle, it is necessary to know the depth of the dried layer or the interface position, X_d. The interface position is defined as the boundary between the dried and frozen regions of the sample. The interface position and in certain cases the time τ required to dry to a specified thickness may be related to R from the internal drying rate solutions of Dyer, et al. (5). It will be seen in Chapter VI that the channel flow conditions and surface temperatures for a complete drying process may be related to X_d or time by simply allowing R to vary over a sufficient range of values. When X_d is zero or near zero, then R has a relatively high value. As X_d increases, R slowly decreases and eventually approaches zero. This simply means that the flow rate is high at the start of drying when the dried layer is thin. As the dried layer becomes thicker, the resistance to heat transfer and fluid flow becomes greater, and the flow rate necessarily decreases.

For a large number of calculations, Equation (4-45) is most conveniently solved on a digital computer. Equation (4-45) is transcendental for either T_m or T_0 and must be solved by trial and error. The additional complication of the integrals which require numerical evaluation makes a computer solution almost a necessity.

The momentum and energy equations have been solved for the case of constant properties, and hence all properties in Equation (4-45) are to be taken at the average of the mean heater surface temperature and the porous surface temperature. In particular, R is evaluated at the average

fluid properties. However, certain of the quantities in Equation (4-45) are evaluated at the heater surface and others at the product surface. For example, the quantity γ is introduced when the temperature is evaluated at the heater surface and again when the amount of heat by conduction is calculated at $\xi = 0$. Hence, γ should be evaluated at the respective surface temperature to improve the accuracy of the results.

The procedure for solving Equation (4-45) for T_0, as an example, is as follows:

1. The quantities L/H, H, T_2, and T_3 are selected. The chamber pressure, p_c, is selected and this establishes the interface temperature T_d.

2. A range of values for R is selected and the initial value substituted into Equation (4-45). The desired mean heater surface temperature, T_m, is also substituted.

3. The quantity γ is calculated at the temperature, T_m.

4. The integrals included in Equation (4-46) are numerically evaluated using the well known trapezoidal rule.

5. Trial values for T_0 are then systematically tried and rejected until the two sides of Equation (4-45) are balanced.

6. Using T_m and the value calculated for T_0, the average Reynolds number is corrected to the temperatures of the two walls. This is achieved by correcting the density and viscosity values in the Reynolds number.

7. The quantity γ is then re-evaluated for the corrected Rs. In Equation (4-46) γ is evaluated at the mean heater surface temperature. In calculating the heat conducted to the porous wall, γ is evaluated at the porous wall temperature.

8. Equation (4-45) is solved again by trial and error for T_0.

9. Steps 4 through 8 are repeated until T_0 does not change.

10. The average injection Reynolds number is then changed by a selected amount and the process is repeated.

In this way, T_0 is calculated for steadily changing flow conditions. In the case where T_0 is known and the heater surface temperature distribution is desired, the process is exactly the same.

For each R, the following quantities are also calculated:

1. The overall convection heat transfer coefficient $\bar{h}_c$ at $\xi = 0$.

2. The radiation heat transfer coefficient $\bar{h}_r$ and the sum of the radiation and convection coefficients $\bar{h}_{cr}$.

3. The depth of the dried layer X_d.

4. The overall heat transfer coefficient $\bar{U}$ between the heater and the frozen region.

5. The pressure at $x = 0$ and $\xi = 0$, $p(0,0)$.

6. The time τ to dry to the depth calculated in Step 3.

The equations used to calculate the above quantities are presented in Appendix E and Appendix F. The drying time equation is based on the model defined by Dyer, et al. (5) where all heat transfer to the frozen region occurs through the dried layer, and no back face heating is present. Only for this case is the frozen region temperature constant with respect to time.

Results based on the equations derived in this chapter are presented in Chapter VI. Comparison is made with experimental data of Lusk, et al.(54).

CHAPTER V

CONCENTRATION SOLUTION

General

In this chapter an approximate solution for the mass concentration profile of water-vapor in the semi-porous channel is presented. In the energy solution, it was convenient and necessary to neglect the x-direction conduction term in the differential equation. Hence, it might seem necessary to do the same in the diffusion Equation (2-23), and neglect the x-direction diffusion term. However, as will be seen in the solution, by carefully choosing the boundary conditions it was possible to retain this term and obtain a more general solution to the diffusion equation.

Concentration Distribution

Again, it is convenient to non-dimensionalize the y-coordinate as was done in Equations (3-1) and (4-1). The integral diffusion Equation (2-23) then becomes

$$\int_0^1 \frac{\partial u\omega}{\partial x}\, d\xi - \frac{v_0\omega_0}{H} = D\int_0^1 \frac{\partial^2\omega}{\partial x^2}\, d\xi + \frac{D}{H^2}\frac{\partial\omega}{\partial\xi}\bigg|_1 - \frac{D}{H^2}\frac{\partial\omega}{\partial\xi}\bigg|_0 \quad . \tag{5-1}$$

For the concentration solution, a fourth order polynomial profile was chosen to represent the mass concentration of water-vapor in the channel. Thus,

$$\omega(x,\xi) = a_2(x) + b_2(x)H\xi + c_2(x)H^2\xi^2 + d_2(x)H^3\xi^3 + e_2(x)H^4\xi^4 \qquad (5\text{-}2)$$

where again the coefficients are functions of x. The coordinate system is the same used in the momentum and energy solutions, and reference may be made to either Figure 3 or Figure 4.

Five conditions are required to evaluate the coefficients in Equation (5-2). Two are found by evaluating the differential Equation (2-6) at $\xi = 0$ and $\xi = 1$. These are

$$v_0 \left.\frac{\partial \omega}{\partial \xi}\right|_0 = \frac{D}{H} \left.\frac{\partial^2 \omega}{\partial \xi^2}\right|_0 \qquad (5\text{-}3)$$

$$\left.\frac{\partial^2 \omega}{\partial \xi^2}\right|_1 = 0 \quad . \qquad (5\text{-}4)$$

Note in Equations (5-3) and (5-4) the x-direction diffusion term has been eliminated. In evaluating the differential equation at each wall, it is necessary to let

$$D \left.\frac{\partial^2 \omega}{\partial x^2}\right|_{0,1} \approx 0 \qquad (5\text{-}5)$$

because the diffusion coefficient D at the wall in the x-direction must necessarily be much smaller than it is in the channel. This appears logical since there is no movement of fluid on the walls under continuum flow conditions. It is important to note that Equation (5-5) is valid because D is approximately zero on the walls, and not because the second derivative

is zero. This observation makes obtaining a solution to the diffusion equation including x-direction diffusion possible. Note on the right side of Equation (5-3) that D is not zero because water-vapor does diffuse in the y-direction through the pores into the channel.

In Chapter II the water-vapor mass concentration at each wall is given as a boundary condition. However, in practice this quantity is not actually known. The concentration and the normal derivatives at the wall may be related to the injection velocity at the wall by using Ficks law which is for the water-vapor species

$$N_w = -\rho D \frac{\partial \omega}{\partial y} + \omega(N_w+N_a) \quad . \tag{5-6}$$

The net mass flux of air N_a, at the interface between the dried region and the frozen region is zero, and hence must remain zero through the dried layer and in the channel. Therefore, Equation (5-6) may be rearranged to give

$$N_w = - \frac{\rho D}{(1-\omega)} \frac{\partial \omega}{\partial y} \quad . \tag{5-7}$$

Noting that $N_w = \rho_w v_w$ and that the definition of the average mass velocity given by

$$v = \frac{\rho_w v_w + \rho_a v_a}{\rho} \tag{5-8}$$

reduces to $\rho v = \rho_w v_w$ when $v_a = 0$, Equation (5-7) may be written

$$\frac{\partial \omega}{\partial y} = \frac{v(\omega-1)}{D} \quad . \tag{5-9}$$

Hence, two more conditions at the walls are found by evaluating Equation (5-9) at each wall. These are in terms of ξ.

$$\left.\frac{\partial \omega}{\partial \xi}\right|_0 = \frac{v_0 H}{D}(\omega_0 - 1) \tag{5-10}$$

$$\left.\frac{\partial \omega}{\partial \xi}\right|_1 = 0 \quad . \tag{5-11}$$

The fifth equation to be used is, of course, the integral diffusion Equation (5-1).

Substituting Equation (5-2) into each of Equations (5-3), (5-4), (5-10), and (5-11) results in the following set of equations:

$$v_0 b_2 = 2 D c_2 \tag{5-12}$$

$$2 c_2 + 6 d_2 H + 12 e_2 H^2 = 0 \tag{5-13}$$

$$b_2 = \frac{v_0}{D}(a_2 - 1) \tag{5-14}$$

$$b_2 + 2 c_2 H + 3 d_2 H^2 + 4 e_2 H^3 = 0 \quad . \tag{5-15}$$

From Equations (5-12) through (5-15), it is possible to express four of the five coefficients in terms of the remaining one. Thus, expressing a_2, b_2, c_2, and d_2 in terms of e_2 results in

$$a_2 = 1 + \frac{H^4}{RSc}\left(\frac{4}{2 + RSc}\right) e_2 \tag{5-16}$$

$$b_2 = H^3 \left(\frac{4}{2 + RSc} \right) e_2 \tag{5-17}$$

$$c_2 = H^2 \left(\frac{2\ RSc}{2 + RSc} \right) e_2 \tag{5-18}$$

$$d_2 = -H \left(\frac{12 + 8\ RSc}{6 + 3\ RSc} \right) e_2 \quad . \tag{5-19}$$

The coefficients are written in terms of the wall Reynolds number R times the Schmidt number Sc. This product is defined by

$$RSc = \frac{v_o H}{D} \quad . \tag{5-20}$$

Substitution of the velocity profile, Equation (3-18), the concentration profile, Equation (5-2), and the coefficients, Equations (5-16) through (5-19), into the integral diffusion Equation (5-1) yields, after considerable rearrangement, the following differential equation for e_2:

$$e_2'' - \frac{\eta x}{H^2} e_2' - \frac{\eta}{H^2} e_2 = 0 \quad . \tag{5-21}$$

The quantity η is defined by

$$\eta = \frac{60\ RSc + (RSc)^2\ (60\ C_6 - 60\ C_8 + 30\ C_{10}) + (RSc)^3\ (30\ C_7 - 40\ C_8 + 15\ C_{10})}{60 + 21\ RSc + 3\ (RSc)^2} \tag{5-22}$$

The quantities C_6, C_7, and C_8 are defined by Equations (4-11) through (4-13) and

$$C_{10} = \frac{b}{6} + \frac{c}{7} + \frac{d}{8} \quad . \tag{5-23}$$

Equation (5-21) may be rewritten by noting that

$$\frac{d(xe_2)}{dx} = e_2 + x\frac{de_2}{dx} \quad . \tag{5-24}$$

Therefore, giving for Equation (5-21)

$$\frac{d^2e_2}{dx^2} - \frac{\eta}{H^2}\left(\frac{d(xe_2)}{dx} - e_2\right) - \frac{\eta}{H^2}e_2 = 0 \quad , \tag{5-25}$$

or

$$\frac{d^2e_2}{dx^2} - \frac{\eta}{H^2}\frac{d(xe_2)}{dx} = 0 \quad . \tag{5-26}$$

Equation (5-26) may be integrated once to give

$$\frac{de_2}{dx} - \frac{\eta}{H^2}xe_2 = C_{11} \quad , \tag{5-27}$$

where C_{11} is a constant of integration.

Defining an integrating factor

$$I.F. = e^{-\int \frac{\eta x}{H^2}dx} = \exp\left(-\frac{\eta}{H^2}\frac{x^2}{2}\right) \tag{5-28}$$

multiplying it through Equation (5-27) and rearranging gives

$$\frac{d\left[e_2\exp(-Z)\right]}{dx} = C_{11}\exp(-Z) \tag{5-29}$$

where

$$Z = \frac{\eta}{2}\left(\frac{x}{H}\right)^2 \quad . \tag{5-30}$$

The solution of Equation (5-29) may be written in the form

$$e_2 = C_{11}\exp(Z)\frac{\sqrt{\pi}}{2}\frac{H}{\sqrt{\frac{\eta}{2}}}\left[\frac{2}{\sqrt{\pi}}\int_0^{\sqrt{Z}}\exp(-Z)\,dZ\right] + C_{12}\exp(Z) \tag{5-31}$$

and C_{12} is the second constant of integration. The term in brackets in Equation (5-31) is the familiar error function.

Before evaluating the constants C_{11} and C_{12}, it is convenient to express the mass concentration profile in terms of e_2. Substituting Equations (5-16) through (5-19) into Equation (5-2) will give

$$\omega(x,\xi) = 1 + e_2 f_3(\xi) \tag{5-32}$$

where $f_3(\xi)$ is a polynomial function of ξ. Its exact form is not necessary to the development here and hence is omitted.

Two conditions on x are necessary to evaluate C_{11} and C_{12}. Due to symmetry at x = 0, one condition is

$$\left.\frac{\partial\omega}{\partial x}\right|_{x=0} = 0 \quad . \tag{5-33}$$

From Equation (5-32) then

$$\left.\frac{\partial e_2}{\partial x}\right|_{x=0} = 0 \quad . \tag{5-34}$$

Performing this operation on Equation (5-31) results in

$$C_{11} = 0 \tag{5-35}$$

and thus

$$e_2 = C_{12} \exp(Z) \quad . \tag{5-36}$$

Another condition results from the assumption that at x = L the average concentration $\bar{\omega}_L$ is equal to the chamber concentration ω_c. Thus,

$$\bar{\omega}_L = \omega_c = \frac{\int_0^1 \omega_L \, d\xi}{\int_0^1 d\xi} \quad . \tag{5-37}$$

Therefore, evaluation of Equation (5-32) at x = L and substitution into Equation (5-37) will give the constant C_{12} in terms of the known chamber concentration, ω_c. Hence, the final result for the mass concentration profile of water-vapor in the channel is

$$\frac{\omega(x,\xi) - 1}{\omega_c - 1} = \left\{ \exp\left[\frac{\eta}{2}\left(\frac{L}{H}\right)^2 \left\{ \left(\frac{x}{L}\right)^2 - 1 \right\} \right] \right\} \left\{ \frac{20}{C_{13}} + \frac{20\,RSc}{C_{13}}\xi + \frac{10(RSc)^2}{C_{13}}\xi^2 - \frac{20 + \frac{40}{3}(RSc)^2}{C_{13}}\xi^3 + \frac{5\,RSc(2+RSc)}{C_{13}}\xi^4 \right\} \tag{5-38}$$

where

$$C_{13} = 20 + 7\,RSc + (RSc)^2 \quad . \tag{5-39}$$

The concentration profiles are seen to be influenced by the injection Reynolds number R and the Schmidt number Sc. More important, as will be seen in Chapter VI, is the influence of the parameter L/H. Typical mass concentration profiles are presented in Chapter VI under various flow conditions and for short and long channels.

CHAPTER VI

DISCUSSION OF THEORETICAL RESULTS

General

In this chapter the results of the solutions found in Chapters III, IV, and V are presented. First, typical velocity, temperature, and water-vapor mass concentration profiles are shown, and the influence on these of R and other basic variables are discussed. The results of the simple polynomial velocity profile are compared with the more exact perturbation solutions given by Donoughe (16). Based on this comparison, it is possible to establish the relative accuracy of the momentum solution presented here. This also serves to establish limits on the accuracy of the energy and concentration solutions.

The momentum, energy, and concentration solutions are applied to some typical freeze-drying situations. Two broad cases are considered here. First, the surface at $\xi = 1$ corresponding to a heater surface is allowed to assume a mean temperature, T_m, which is invarient with respect to time. For this case, the variation of the product temperature, T_0, at $\xi = 0$ is shown for typical drying conditions. In particular, the theoretically predicted surface temperatures are compared with experimental results given by Lusk, et al. (54). The second case considered is where the surface at $\xi = 0$, which is the product surface, assumes a constant temperature T_0, invarient with respect to time. For this case, the variation of the mean heater surface temperature, T_m, with respect to time is

shown under typical drying conditions.

Also discussed in this chapter are the relative effects of radiation and convection heat transfer between the heater and product in freeze-drying. In connection with this, some typical heat transfer coefficients are presented.

Momentum Solution

In this section, the results of the momentum solution presented in Chapter III are discussed and comparison is made with similar solutions by Donoughe (16). Equation (3-18) may be written in the form

$$u(x,\xi) = \frac{v_o x}{H} f(\xi) \quad , \tag{6-1}$$

where

$$f(\xi) = \left(\frac{24-\beta_1}{R+6}\right)\xi + \left(\frac{12R+3\beta_1}{R+6}\right)\xi^2 + \left(\frac{-12R-24-2\beta_1}{R+6}\right)\xi^3 \quad . \tag{6-2}$$

When considering the velocity $u(x,\xi)$ in porous channels with continuous mass addition along one wall, fully developed flow cannot be achieved because the velocity component in the flow direction is a function of x. However, Equation (6-1) may be rewritten in the following form:

$$\frac{u(x,\xi)}{\bar{u}(x)} = f(\xi) \quad , \tag{6-3}$$

where $\bar{u}(x)$ is defined by

$$\bar{u}(x) = \frac{v_o x}{H} \quad . \tag{6-4}$$

The velocity ratio given in Equation (6-3) is a function of R and position ξ only, but not position x. As Donoughe (16) suggests, if fully developed flow is defined as a constant value of $f(\xi)$ for increasing flow direction x, then analytically fully developed flow is obtained for fixed R.

The solution given by Donoughe (16) and other investigators has the form

$$u(x,\xi) = \left[\bar{U}(0) + \frac{v_o x}{H}\right] f(\xi) \quad , \tag{6-5}$$

where $\bar{U}(0)$ is the average flow velocity at x = 0. For the special case considered here, $\bar{U}(0)$ is zero and hence Equation (6-5) reduces to the form in Equation (6-1).

The velocity ratio given by Equation (6-3) may be plotted using R as a parameter to give a qualitative feel for what happens to the velocity distribution as R changes. This is shown in Figure 6 for values of R equal to 0.1, 1.0, and 4.0. As the amount of injection increases at the porous wall, the shape of the profile is seen to shift toward the solid wall. As R approaches zero, the profile approaches the typical parabolic profile for laminar flow between impermeable walls. Of course, in this case when R is equal to zero there is no flow in the channel since all the mass originates at the wall.

Figure 6 also shows a comparison between the velocity profiles for R = 4.0 given by Equation (6-2) and the results of Donoughe (16). The curve by Donoughe is shown to be shifted slightly closer to the solid wall. For values of R less than four, the difference is too small to illustrate graphically. The numerical values of $f(\xi)$ given by Equation (6-2) and the

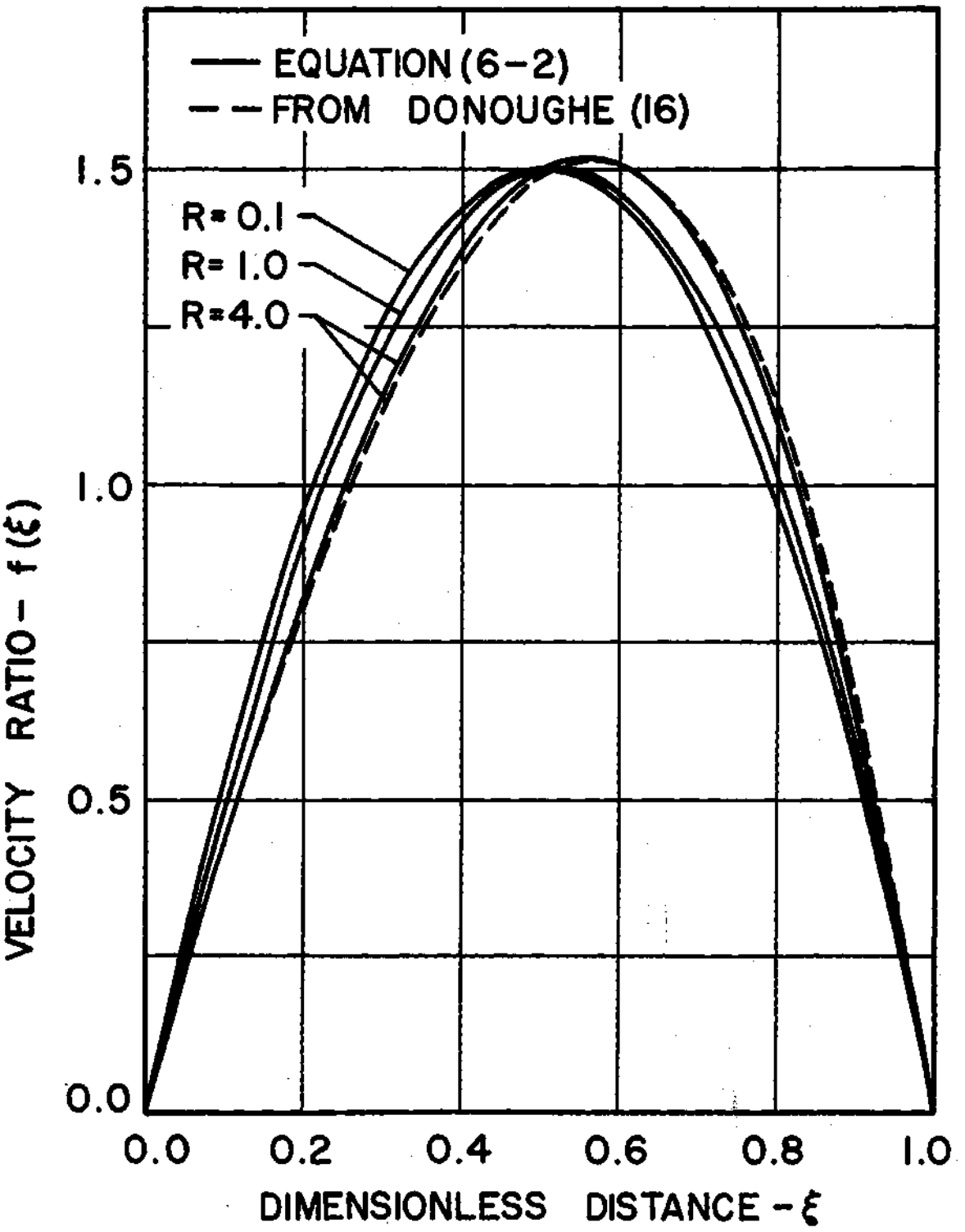

Figure 6. Semi-Porous Channel Velocity Distributions, Polynomial Solution and Perturbation Solution

more exact results given by Donoughe (16) are given in Appendix G for several values of R.

The pressure change in the flow direction is given by Equation (3-43). It shows that the pressure drop in a semi-porous channel is proportional to the second power of x and describes a parabolic curve. The term β_1 in Equation (3-43) defined by Equation (3-37) is tabulated in Table 1 with the corresponding results given by Donoughe (16) for comparison.

Table 1. Pressure Parameter β_1 from Integral Momentum Solution and Perturbation Solution

R	β_1, Equation (3-37)	β_1, Donoughe (16)
0	Approaches -12.000	-12.000
0.1	-12.240	-12.232
0.5	-13.200	-13.170
1.0	-14.402	-14.366
2.0	-16.815	-16.824
3.0	-19.240	-19.359
4.0	-21.678	-21.953

Donoughe (16) shows that for $R \leq 4.0$ his perturbation solution is accurate to within 0.1 per cent of an exact numerical solution. Similar accuracy for the polynomial solution presented here occurs for $R \leq 3$. This figure is well above the usual maximum injection Reynolds numbers which occur in freeze-drying. Hence, the simplified polynomial solution is entirely adequate for the purposes of this work.

Energy Solution

In this section some typical temperature profiles from the energy solution given in Equation (4-22) are considered. The effect of the singularity which arises at $x = 0$ will be seen. Also, local and average heat transfer rates must be considered with regard to the effect the injection Reynolds number has on them. The temperature profiles are of course non-similar in every respect. In order to obtain a qualitative feel for the behavior of the temperature distribution within the channel, it is necessary to first consider a fixed position in the flow direction and allow the coordinate ξ to vary. Then it is necessary to choose a position for ξ and allow the coordinate x (or x/L) to vary. All of the graphical data presented is for a Prandtl number of unity which is the value for pure water-vapor.

The first situation to be considered is the effect of R on $\theta(x,\xi)$ at a fixed position of x. In Figure 7, the dimensionless temperature is plotted against ξ at $x/L = 0.5$ for values of R equal to 0.1, 0.5, and 2.0. For small R, the temperature profile appears to be nearly linear, and at the solid wall is nearly equal to one, the value at the exit of the channel. This indicates that the disturbance at the porous wall caused by the fluid injection into the main flow has a very small effect on the energy transport mechanisms. Hence, at low R the heat transfer across the channel approaches the situation of heat transfer through a stagnant gas layer. Both walls become isothermal in this case. As R increases, the injection at the porous wall exerts a cooling effect on the gases near this wall. At the same time, θ at the solid wall increases for increasing R, and the temperature profile along the solid wall must

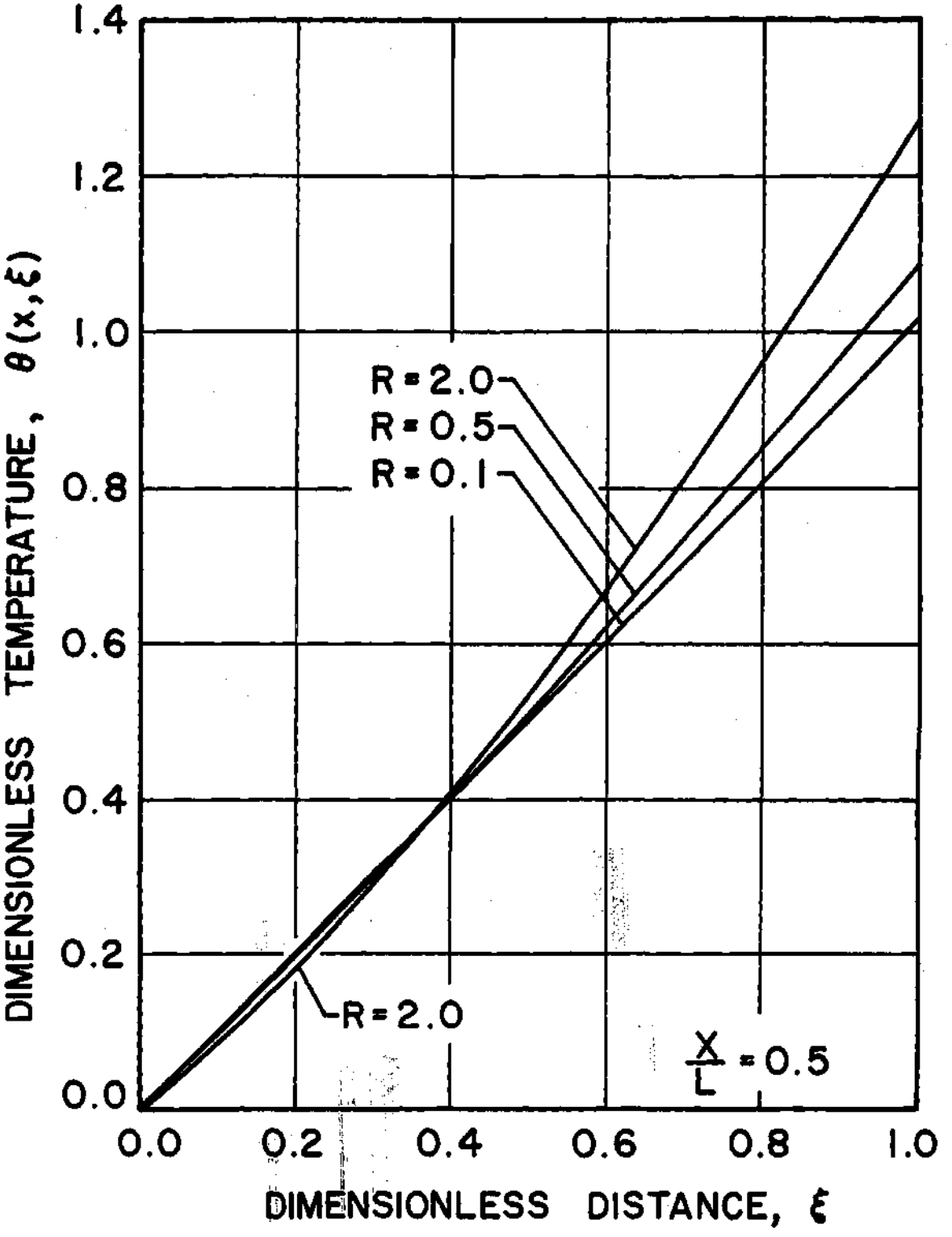

Figure 7. Influence of Injection Reynolds Number R on Semi-Porous Channel Temperature Distribution, R = 0.1, 0.5, 2.0

become increasingly non-isothermal.

In Figure 8, the temperature profile is plotted with respect to ξ for several values of x/L at R = 0.5 to illustrate the changing nature of the profile in the flow direction. This is further illustrated in Figure 9 where the non-dimensional temperature is plotted versus x/L for several values of R at ξ = 1, the solid wall. Figure 9 shows the singularity at x = 0 where the temperature approaches infinity. Here it is clearly seen that as R approaches zero the temperature of the solid surface becomes isothermal. As R increases, the solid wall temperature profile must necessarily become increasingly non-isothermal in order to maintain the porous surface isothermal. This requirement can be met with individually controlled heat cells placed in the solid wall. Later in this chapter it will be seen that the range of R for freeze-drying is ordinarily less than 0.5. Hence, the deviation from an isothermal heating surface will be small.

The average convection heat transfer coefficient $\bar{h}_c$ at the porous surface is derived along with the corresponding Nusselt number $\overline{Nu}$ in Appendix E. This coefficient is based on the arithmetic mean temperature difference between the two walls. The Nusselt number based on the channel width is

$$\overline{Nu} = \frac{\bar{h}_c H}{k} = \frac{3}{3 + R} \quad . \tag{6-6}$$

The average Nusselt number is plotted versus R in Figure 10. As can be seen, when R increases or the injection rate at the wall increases then $\overline{Nu}$ decreases. This observation has also been made by Terrill (30)

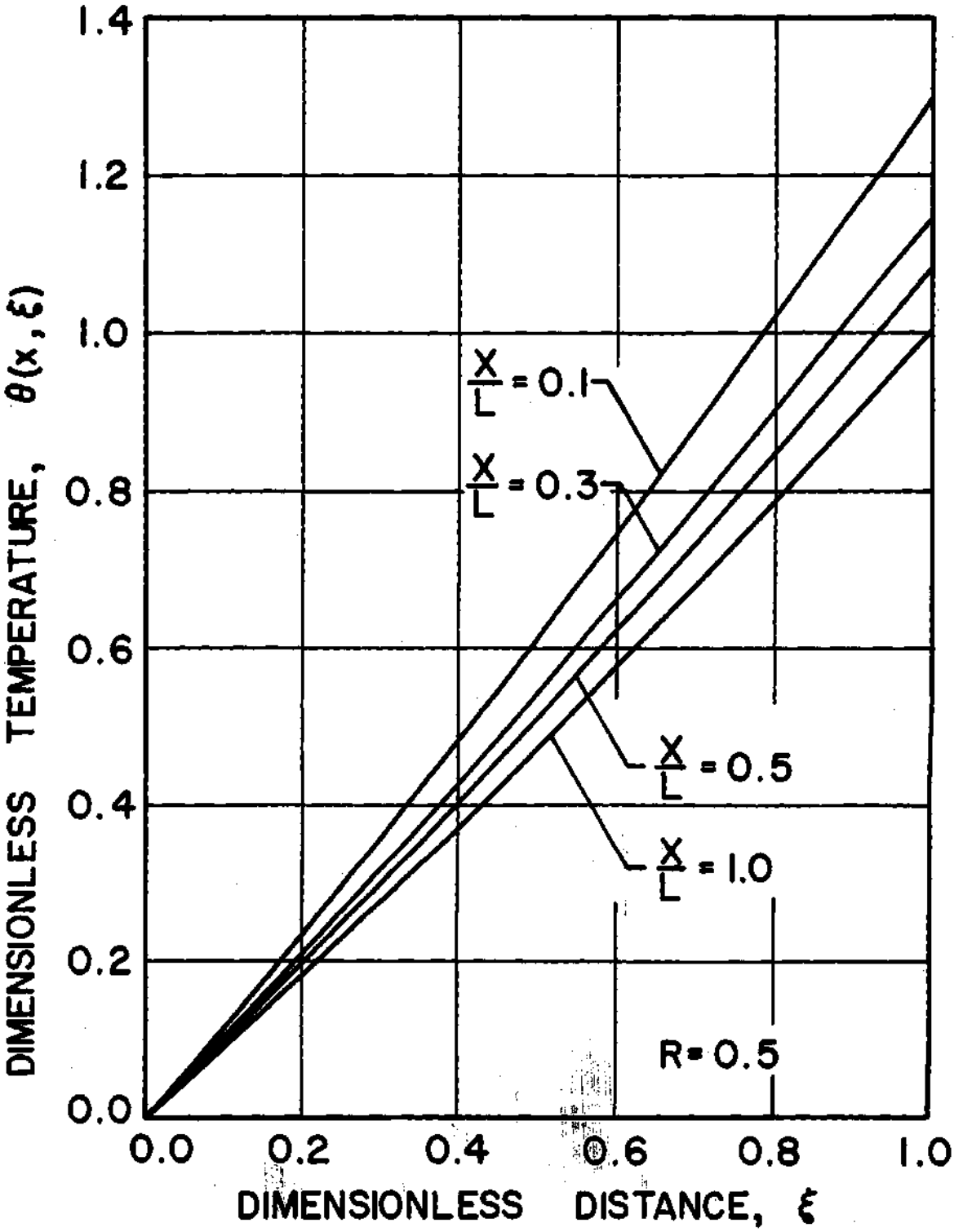

Figure 8. Influence of x-Direction Position on Semi-Porous Channel Temperature Distributions

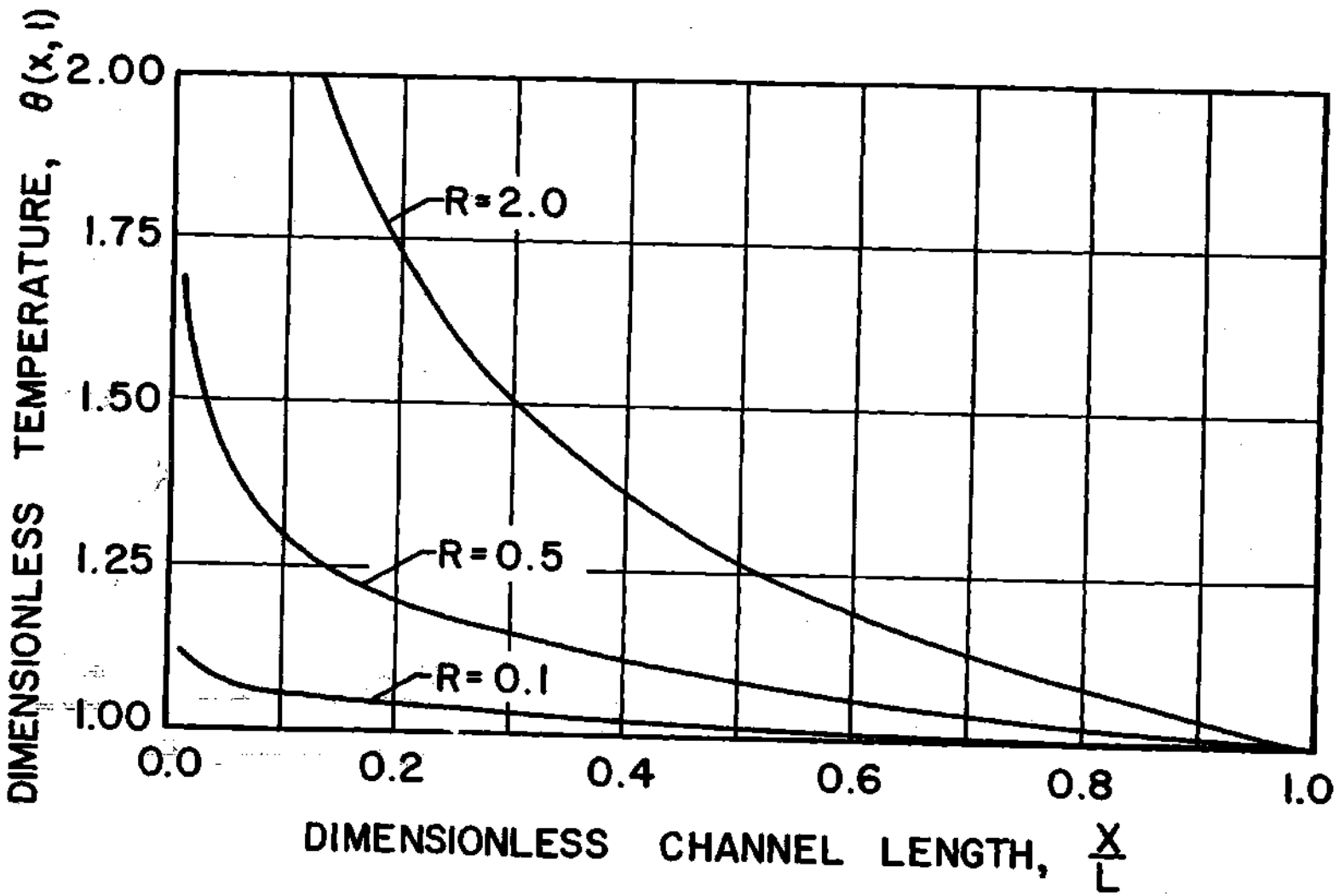

Figure 9. Solid Wall Temperature Distributions Illustrating Effect of Singularity at x = 0

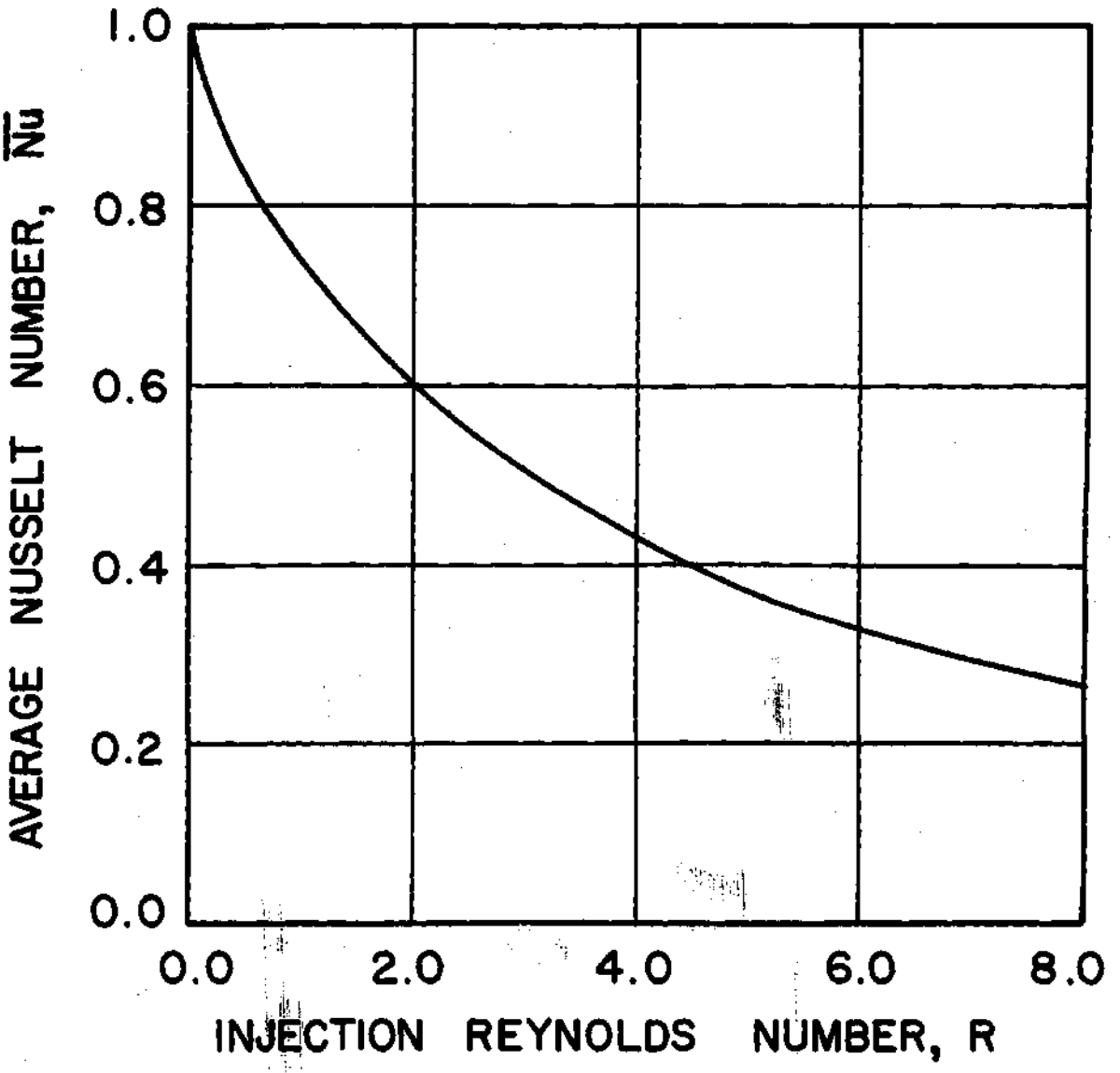

Figure 10. The Effect of Injection Reynolds Number R on Average Nusselt Number at Porous Wall

for heat transfer in a fully porous channel with symmetric wall temperatures. Note in Equation (6-6) that as R approaches zero, $\overline{Nu}$ approaches unity and

$$\overline{h}_c = \frac{k}{H} \quad , \tag{6-7}$$

which simply means that the mode of heat transfer is pure conduction through a stagnant gas layer between the walls.

The local Nusselt number along the porous surface, also derived in Appendix E, is given by

$$Nu = (1-\gamma)\left(\frac{3}{3+R}\right)\left(\frac{x}{L}\right)^{-\gamma} \quad . \tag{6-8}$$

Figure 11 shows the variation of the local Nusselt number along the channel length for values of R equal to 0.1, 0.5, and 2.0, and the average value given by Equation (6-6). Again, the singularity at $x = 0$ is illustrated when local conditions are considered, but, as shown, when the average values are considered the singularity disappears.

It is important to note that as R approaches zero the local Nusselt number approaches the average Nusselt number at all locations along the channel. This means that the heat flux as well as the temperature becomes nearly constant in the flow direction at $\xi = 0$. In obtaining the momentum and energy solutions of Chapter III and Chapter IV, it was convenient and necessary to assume both v_0 and T_0 constant with respect to x. This is tantamount to assuming that both the heat flux and the temperature at $\xi = 0$ are constant. This, however, cannot be true unless, as has been shown here, the injection rate is very low which is true for freeze-drying, as

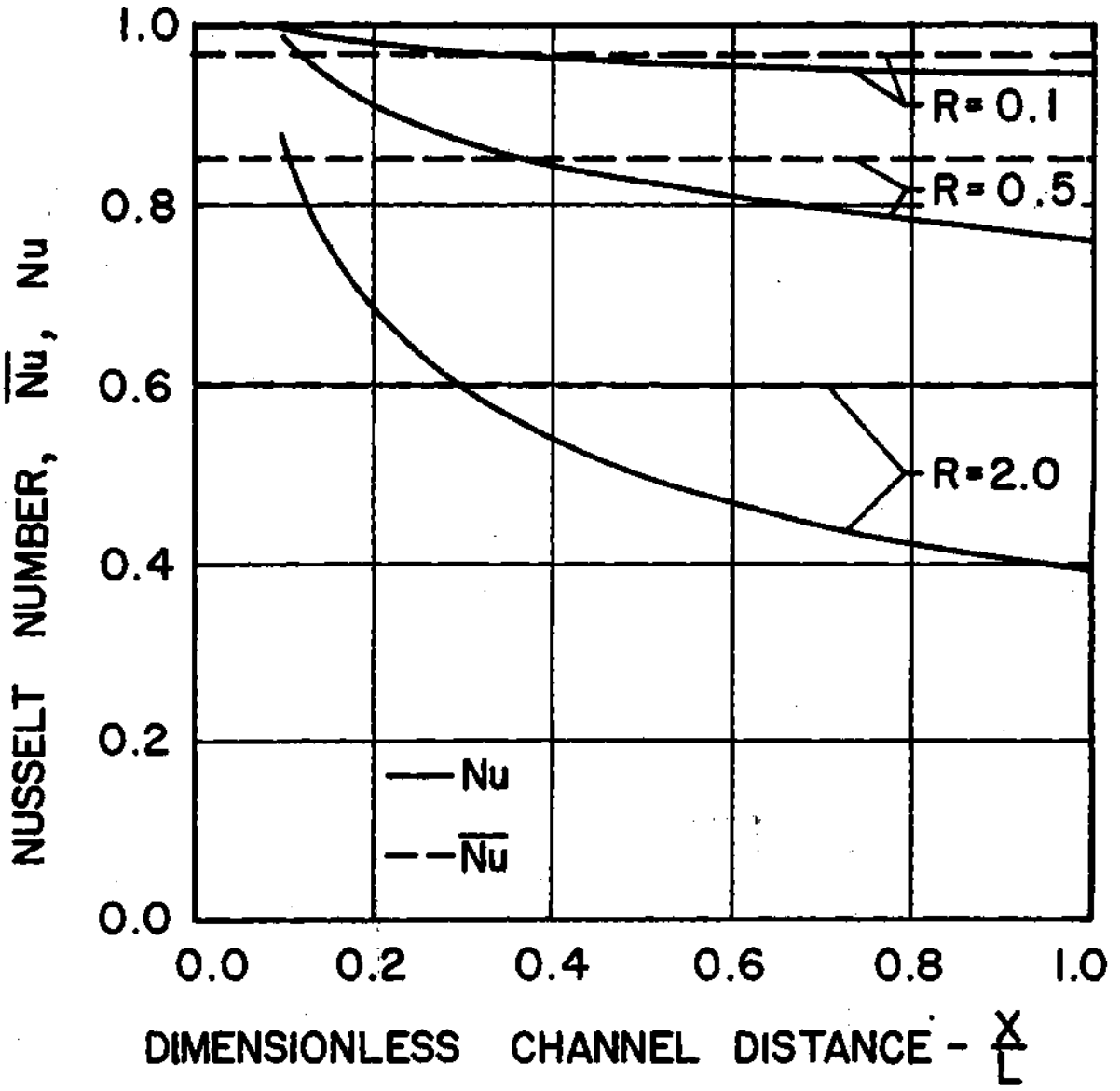

Figure 11. Local and Average Porous Surface Nusselt Numbers as a Function of x-Direction

will be seen in a later section of this chapter.

It was mentioned earlier that the momentum solution is considered quite accurate for $R \leq 3$. Since the approximate momentum solution is used to obtain the approximate energy solution, the range of accuracy for the energy solution must be somewhat less than that for the momentum solution. The exact limits of accuracy are not estimated here. In a later section in this chapter the results of the energy solution are used to correlate some experimental data of Lusk, et al. (54) wherein the accuracy is then established.

Concentration Solution

In this section the results of the concentration solution derived in Chapter V are presented. The water-vapor mass concentration, $\omega(x,\xi)$, with respect to the ξ direction is practically unchanging. Some typical profiles with respect to ξ at various x-direction locations are tabulated in Appendix H. The results of greatest interest in freeze-drying are the profiles in the flow direction at the porous surface, that is $\omega(x,0)$ or ω_0.

The solution given by Equation (5-38) is seen to be a function of R and Sc, the Schmidt number, as well as location. The Schmidt number for typical conditions encountered in freeze-drying ranges from 0.4 to 0.6. Another important quantity in Equation (5-38) is the length to width ratio L/H of the channel. Note that L is actually half the total length of the channel, as illustrated in Figure 1. A typical industrial vacuum chamber may have trays and heaters with a channel half length L equal to 18 inches and a width H equal to 0.5 inch. Hence, L/H would equal 36. This ratio could, of course, be higher or, for pilot plants used in experimental work,

L/H may be as low as 10, or even lower.

For the results presented here, the chamber concentration ω_c is taken to be 0.6 lbm H_2O/lbm mixture. Figures 12 and 13 show the surface concentration $\omega(x,0)$ plotted as a function of x/L using R as a parameter. Figure 12 is for L/H equal to 10 and Figure 13 has curves for L/H equal to 24 and 36. It should be obvious that as L/H increases the water-vapor concentration in the channel approaches unity at all locations in the flow direction except of course in the immediate vicinity of the exits, and for all but the lowest values of R. Even for low values of L/H and R, as in Figure 12, the concentration is greater than 0.9 lbm H_2O/lbm mixture for over half the channel length. In Figure 13 for L/H = 36, the curve for R = 0.02 is included to illustrate how small a value for R must be chosen to get any profile other than a straight horizontal line. This extremely low value of R would rarely be encountered in freeze-drying as can be seen in Figures 18 and 32. Calculations were also made for ω_c = 0.2 lbm H_2O/lbm mixture. For long narrow channels and the range of R normally encountered in freeze-drying, they show that the concentration in the channel is still almost pure water-vapor over the entire length.

Physically the results shown here simply mean that the convective contribution to mass transfer is much greater than the diffusion contribution in the flow direction for large values of L/H. In Equation (2-6), this means that the first term on the left side is much greater than the first term on the right side. This conclusion may be more clearly seen by writing the diffusion Equation (2-6) in dimensionless form. The dimensionless coordinates to be used are

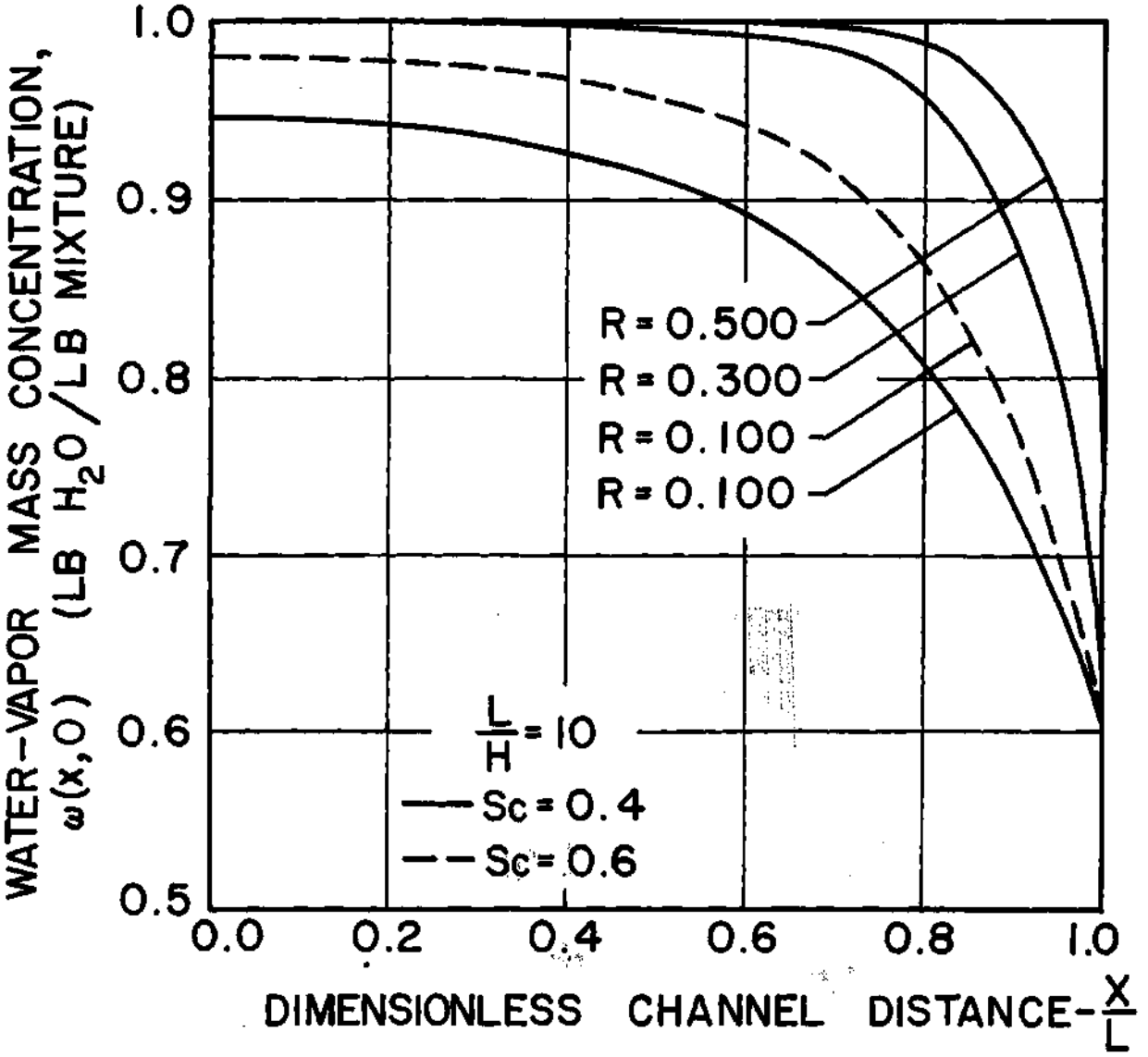

Figure 12. Influence of R and Sc on x-Direction Semi-Porous Channel Mass Concentration Distributions, L/H = 10

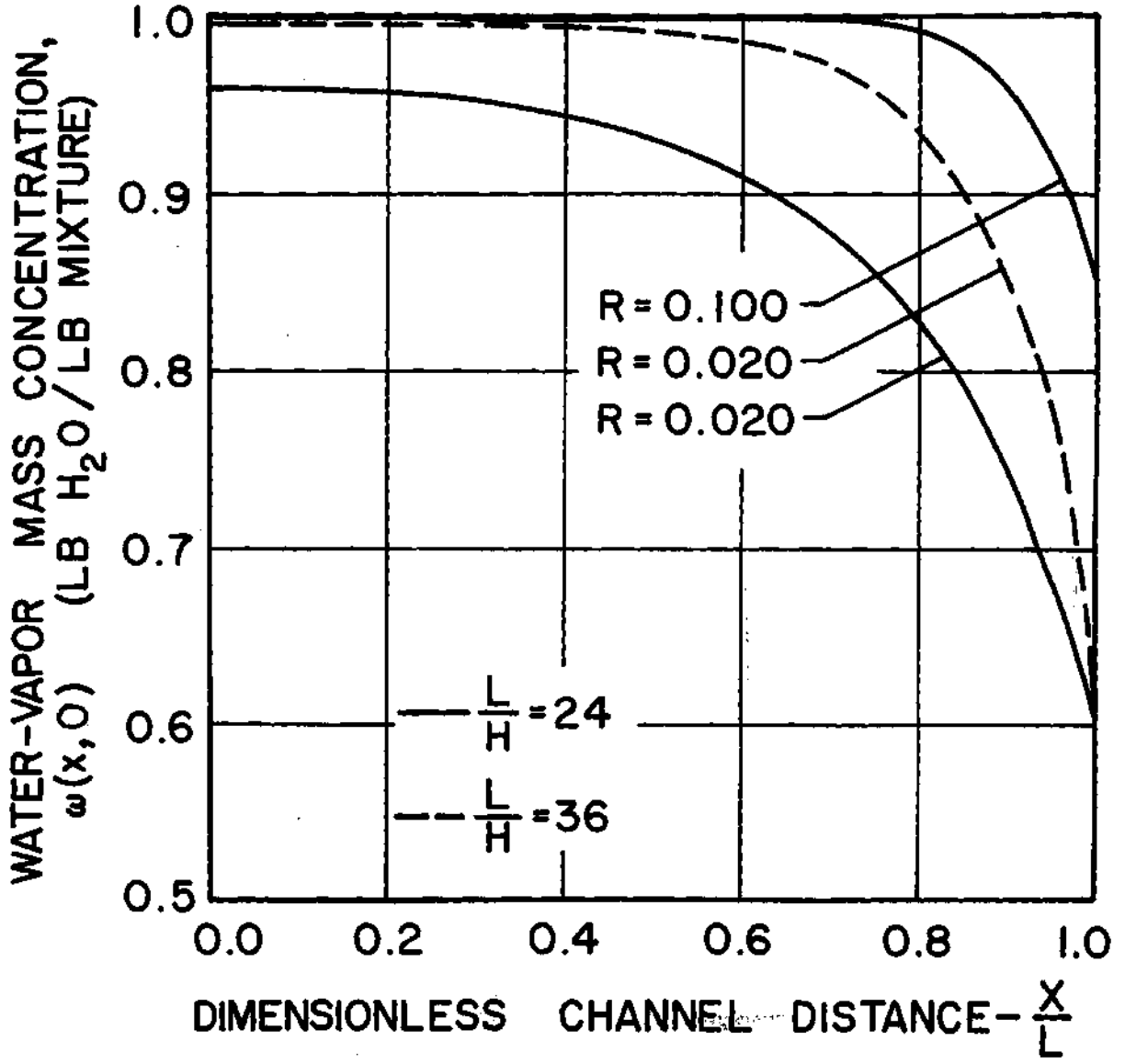

Figure 13. Influence of R on x-Direction Semi-Porous Channel Mass Concentration Distributions, L/H = 24, 36

$$X = x/L \tag{6-9}$$

and

$$\xi = \frac{y}{H} \quad . \tag{6-10}$$

Equation (6-1) is substituted for $u(x,\xi)$ and Equation (3-38) rewritten

$$v(\xi) = v_0 g(\xi) \tag{6-11}$$

is substituted for $v(\xi)$ in Equation (2-6). The dimensionless diffusion equation becomes

$$f(\xi)\, X \frac{\partial \omega}{\partial X} + g(\xi) \frac{\partial \omega}{\partial \xi} = \frac{1}{RSc} \left(\frac{H}{L}\right)^2 \frac{\partial^2 \omega}{\partial X^2} + \frac{1}{RSc} \frac{\partial^2 \omega}{\partial \xi^2} \quad . \tag{6-12}$$

A simple order of magnitude analysis shows all the quantities in Equation (6-12) to be of the same order of magnitude. However, when L/H is large and hence its reciprocal small, the first term on the right side of Equation (6-12) is made small compared with the other terms. This term corresponds to the x-direction diffusion and as a result could well be neglected for long narrow channels.

These results have far-reaching implications when one considers the type of flow which must be present in the channel and in the dried portion of the product. The results imply that all or nearly all the air in and above the product is swept away leaving an atmosphere of nearly pure water-vapor. Sample calculations of the average velocity near the channel exit show that average velocities as high as 90 fps can occur in the early stages of drying. As such, the flow mechanism must be purely hydrodynamic

viscous flow in the pores of the product and in the channel. For this type of flow only, a total pressure gradient is necessary to maintain the flow. In the absence of a partial pressure gradient, diffusional flow as a result of a binary mixture of two gases does not occur.

Previous investigators in their theoretical work have assumed that a fixed concentration of water-vapor could be maintained at the product surface, and hence both diffusional and hydrodynamic flow would be present. This situation could possibly exist where the space above the product surface were open and unconfined and the water-vapor able to migrate directly to a condenser. However, the typical industrial model resembles the semi-porous channel arrangement analyzed in this thesis, and for this model the solution shows that for long narrow channels, the fluid consists almost completely of water-vapor with no air present. In the region between the channel exits and the condenser surface, the flow will of course revert to a diffusional type flow providing the condenser is efficiently removing the water-vapor and converting it to ice again.

In passing, it should be noted that neglecting the effect of surface water-vapor concentration on v_0 in Chapter II proved to be a valid assumption since the variation of ω along the surface has been shown to be small or non-existent.

Application to Freeze-Drying

The results of the energy solution discussed previously are not complete for application to the freeze-drying process. As was outlined in Chapter IV, it is necessary to consider an energy balance at the porous product surface to establish the relationship between the two wall tempera-

tures under a prescribed set of flow conditions. In the energy balance which was derived in Chapter IV, the radiant heat exchange among the surfaces was included. As has been discussed by Burke and Decareau (6), there is much controversy over the exact role played by the modes of heat transfer from the heater surface to the product surface. The relative effects of radiation and convection are illustrated in this section.

Equation (4-45) of Chapter IV may be used to determine either the product surface temperature or the heater surface temperature depending on which is assumed to be known. The heater surface is non-isothermal, and hence in dealing with this surface the mean temperature with respect to length defined by Equation (4-28) will be used. In addition to one of the surface temperatures being specified, the injection Reynolds number R is also treated as known. Specification of R also establishes the injection velocity v_o and the flow rate N_w. From the known value of R, Equation (F-3) of Appendix F is then used to determine the interface position X_d of the product which establishes the first link between the external and the internal process. This is important because it is then possible to relate a set of external flow conditions and surface temperatures to a particular stage in the drying cycle. As discussed in Chapter IV, it is possible to predict the complete range of external conditions associated with a drying cycle. Finally, in the case where the product surface temperature, T_o, is known and fixed with respect to time, Equation (F-5) may be used to calculate the time required to dry the product to a particular depth.

The equation used to calculate dried layer thickness and drying time are taken from solutions presented by Dyer, et. al. (5). The solutions

establish the relationship of the surface temperature, T_o, and the rate of heat transfer across the dry layer to the interface position X_d, and the corresponding drying rate and drying time. The model analyzed by Dyer, et al. is for a uniformly retreating ice interface through the product and hence is a one-dimensional treatment. Also, the only heat transfer to the interface is across the dried layer as opposed to the situation where heat transfer could also occur through the frozen region. His boundary conditions at the surface assume a uniform and constant surface temperature and a uniform drying rate with respect to the cross-section of the product. The external solution in the channel, however, is a two-dimensional treatment. Hence, the necessity of choosing the porous surface boundary conditions v_o and T_o constant with respect to flow direction becomes more apparent. Only by doing so is it possible to match the existing internal drying rate and time solutions with the external solutions. The analysis of the problem under more rigorous boundary conditions of a constant heat flux at $\xi = 0$ instead of a constant temperature would have been very difficult and would have rendered the internal solutions useless. The approach used in this work yields excellent qualitative results and enables one to grasp a clear picture of the important characteristics of the transport phenomena.

The first of the next two subsections considers the case where the heater surface temperature distribution is assumed known and the product surface temperature unknown. Solutions are presented showing the surface temperatures and other quantities as a function of interface position. The next subsection considers the case where the product surface temperature is known and the mean heater temperature is unknown. Solutions are pre-

sented which show the mean heater surface temperature, T_m, and other quantities as a function of time. The formulas used to evaluate the various heat transfer coefficients are found in Appendix E.

Constant Heater Temperature

In this section the mean heater surface temperature, T_m, is treated as known and fixed with respect to time. Equation (4-45) is solved for the product surface temperature T_0, according to the procedure outlined in Chapter IV. A range for R is selected which covers the flow rates encountered in the typical drying cycle. There are no drying time equations for the case where T_0 varies with respect to time. Hence, in this section T_0 and other quantities can only be related to the interface position.

Lusk, et al. (54) experimentally measured the thermal conductivities of Haddock fish during freeze-drying. Included in their work are plots relating moisture content of the sample, the product surface temperature, and the interface temperature to time for a constant T_m. In this case, the plots show that the surface temperature of the Haddock begins the process at a very low temperature equal to the equilibrium temperature of the frozen product at the chamber pressure involved. This is, of course, because the surface is covered with ice at the start of the process. As drying continues and the interface retreats into the product, the surface temperature rises sharply at first and then levels off. Then T_0 slowly increases until at the end of the process it approaches the heater temperature. In order to provide accurate thermal conductivity data, these experiments were necessarily carefully controlled and monitored, hence providing an excellent means for correlating the analytical work presented

here with experimental data.

Data for two test runs are presented by Lusk, et al. (54). One sample was 0.75 inch thick and the other was 1 inch thick. Both samples were 8 by 10 inch slabs. For the theoretical calculations, the dimension L was taken to be 5 inches. The samples were dried between heaters that were 2 inches apart, and hence H was respectively 0.625 inch and 0.5 inch. The samples were dried at a chamber pressure of 0.08 torr at which the temperature of the frozen region T_d was $440^{\circ}R$. Since the samples were symmetrically dried from both sides, the frozen region temperature remained nearly constant throughout the cycle. Also, due to the symmetry only one side of the sample need be considered for calculations. The heater temperature, T_m, was held at $635^{\circ}R$ throughout the drying cycle, except for a very short start-up time. The physical property data necessary for use in Equation (4-45) is given in Appendix I. Based on the results of the concentration solution, the properties of the fluid in the channel were taken to be those of pure water-vapor.

Lusk, et al. (54) in calculating the thermal conductivity of the freeze-dried Haddock used a heat of sublimation ΔH equal to that of pure ice. The work of Dyer, et al. (59) and Hill, et al. (60) on heats of sublimation of various meat and poultry products casts some doubt on the validity of this assumption. They show that the heat of sublimation of meat and poultry is consistently higher than that of pure ice. However, since no measurements exist at this writing for the heat of sublimation of Haddock or any other fish, it is necessary to use that of pure ice in the calculations presented here. The heat of sublimation is quite critical to the accuracy of the heat transfer calculations presented here. As can

be seen on the right side of Equation (4-45), the heat of sublimation ΔH directly influences the magnitude of that side. This in turn will affect the values of the temperature on the left side of Equation (4-45) necessary to maintain the equality.

The low chamber pressure used forces the flow regime in the channel to border between continuum and slip flow. However, it is assumed that the continuum flow results presented here may be satisfactorily applied in this situation.

From the data given by Lusk, et al. (54), it is possible to compare the experimentally measured product surface temperature at various stages of drying with those analytically predicted by Equation (4-45). However, as mentioned above, it is not possible to analytically predict the variation of the temperature with time as is presented by Lusk, et al. However, Lusk, et al. also give the variation of moisture content of the test sample with respect to time. Given this information it is possible to calculate the interface position on one side of the sample at successive times during the drying cycle and thus relate the changing surface temperature to the corresponding X_d.

The interface position on one side of the product is equal to the difference between the total product thickness X_t, and the frozen region thickness, X_f, divided by two. That is,

$$X_d = \frac{X_t - X_f}{2} \quad . \tag{6-13}$$

The thickness of the frozen region is simply the total product thickness multiplied by the per cent moisture m remaining in the product which is

given by Lusk, et al. in the experimental data. Thus,

$$X_d = \frac{X_t - mX_t}{2} \quad , \tag{6-14}$$

or

$$X_d = \frac{X_t}{2}(1-m) \quad . \tag{6-15}$$

Hence, it is possible to replot the data of Lusk, et al. for the surface temperature and interface temperature as a function of the interface position. Equation (4-45) is then solved for T_o as a function of R and the corresponding X_d calculated using Equation (F-3).

The experimental temperature, T_o, as a function of X_d and the corresponding theoretically predicted temperature are shown in Figure 14 for both samples of Haddock. The correlation between the theoretically predicted surface temperature and the experimentally measured surface temperature is excellent especially for the 1-inch thick sample. The theoretical curve for T_o is shown to approach the mean heater surface temperature T_m asymtotically for an infinitely thick sample where, of course, the actual sample is of finite thickness and its final surface temperature is shown to be that of the heater temperature.

Note that in Equation (F-3) it is necessary to use the thermal conductivity of the dried layer to calculate its thickness. Lusk, et al.(54) list three values for the thermal conductivity of freeze-dried Haddock according to the sample thickness. These are 0.011, 0.013, and 0.015 Btu/hr ft $^{\circ}$F for respectively 0.5, 0.75, and 1.0 inch thick samples. The variation in conductivity values is attributed to side drying effects on

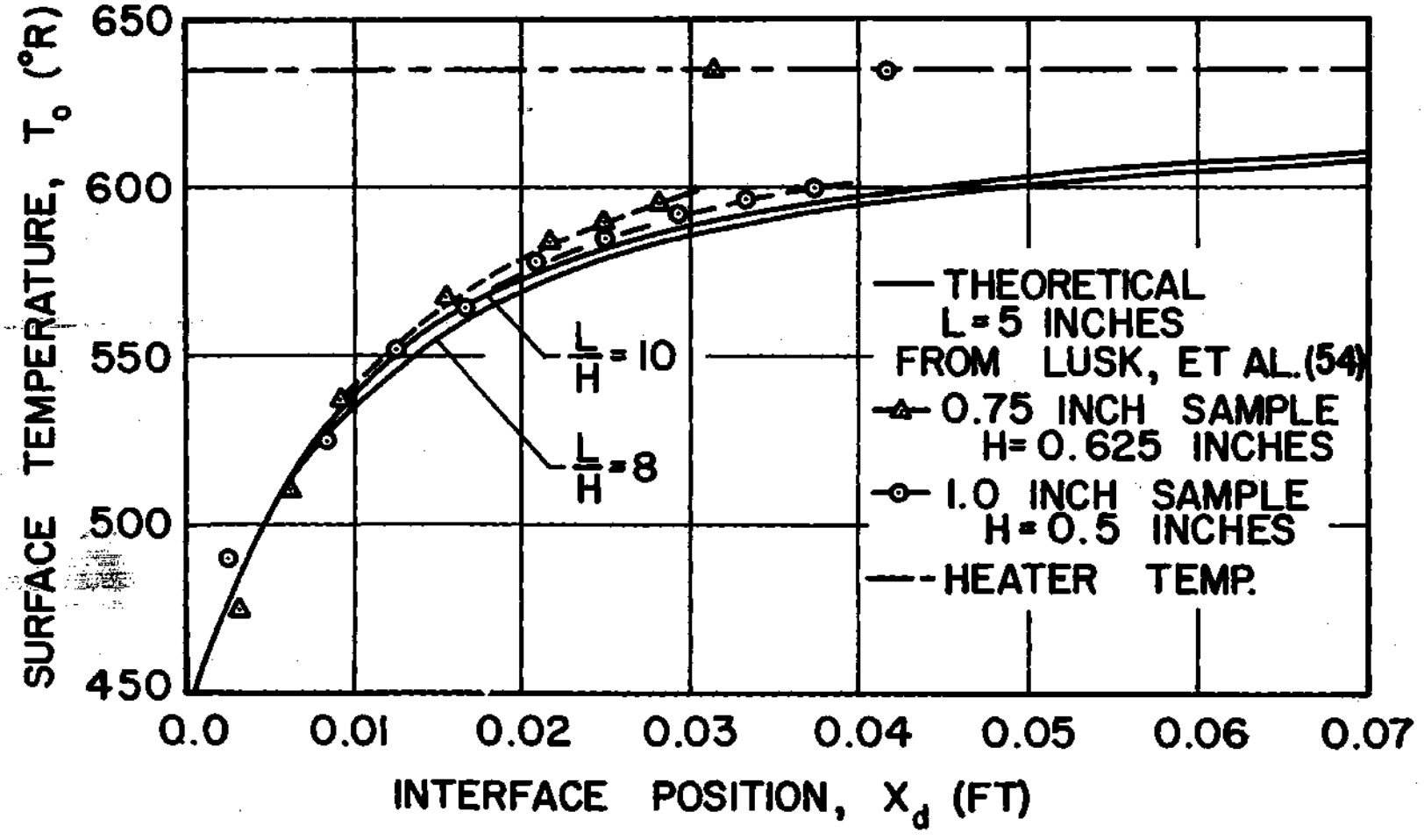

Figure 14. Comparison of Theoretically Predicted and Experimentally Measured Surface Temperatures of Haddock During Freeze-Drying for 0.75 and One-Inch Thick Samples

the samples. However, other experimental errors may have been present contributing to this variation. Hence, for Figure 14, the conductivity used to calculate X_d from Equation (F-3) was 0.013 Btu/hr ft ^{o}F. Figure 15 illustrates the effect of the variation of the dried layer thermal conductivity by plotting T_0 versus X_d for all three conductivities. The variation in the predicted surface temperature still compares well with the experimental data regardless of which value is used.

It is interesting to observe the effects that certain variables have on the prediction of T_0. For Figure 14, the ratio L/H was taken to be 8 and 10. In Figure 16, a comparison is made for the case where L/H is increased to 36. The dashed line for L/H = 36 and the solid line for L/H = 10 are both for H = 0.5 inch, and hence serve as a comparison for a change in L. This corresponds to an increase in channel length to a size typically used in commercial plants. As can be seen, the effect on T_0 is small and further increases in L have relatively the same effect. The small increase in efficiency noted is due to the smaller overall effect the exits of the channel have on radiation losses.

Of more interest is the effect produced when H is varied. This is also illustrated in Figure 16 where for the solid line H ranges from 0.25 to 2.0 inch while L remains constant at 5 inches. As can be seen for correspondingly equal interface positions, T_0 is considerably higher for small H than for large H. Since T_0 is higher, this implies that heat transfer across the dry layer is greater and hence the drying rate is greater for the same heater temperature.

The energy balance derived in Chapter IV considers the effect of radiation losses at the channel exits. For Figures 14 through 16, the

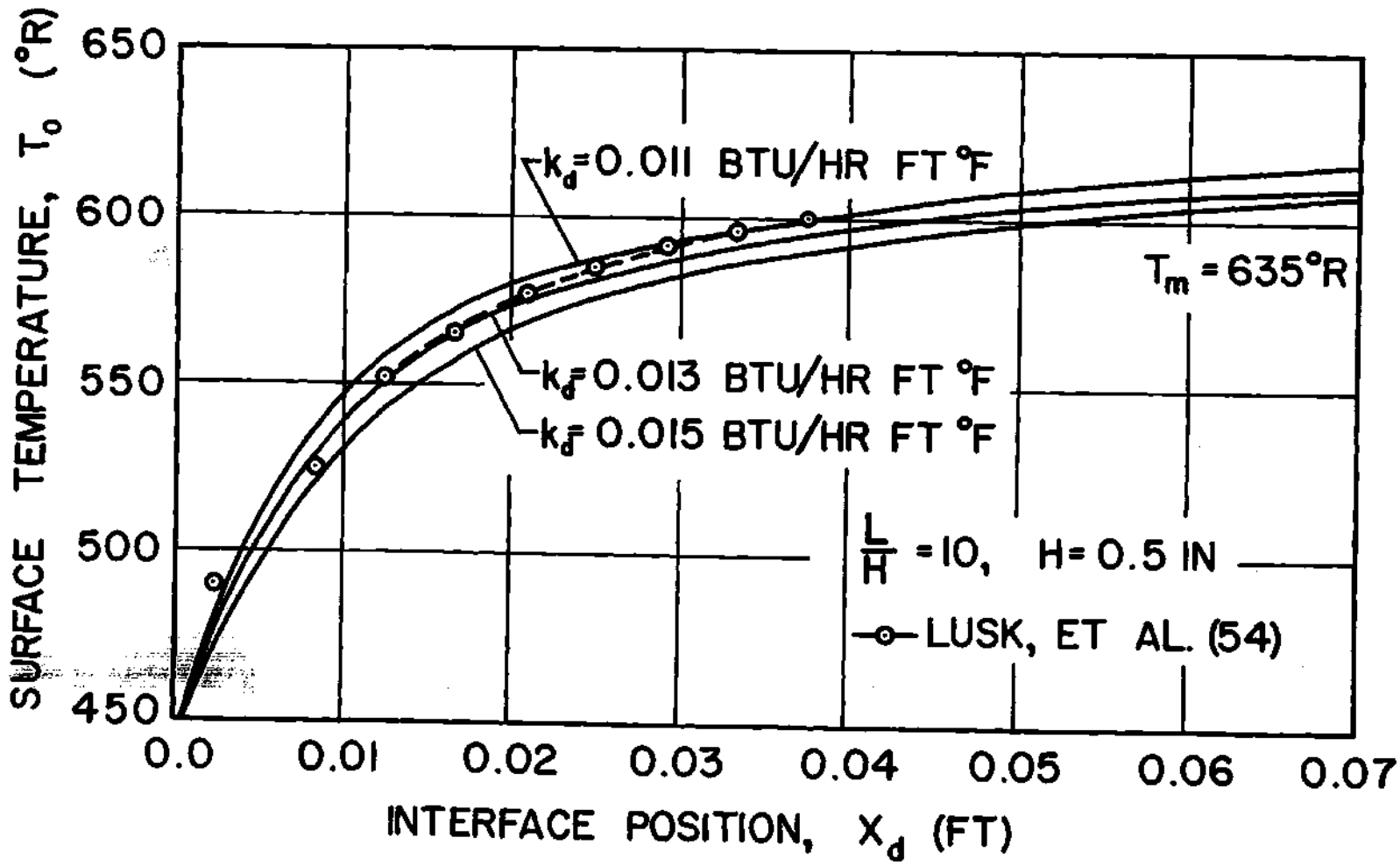

Figure 15. Influence of the Variation of the Thermal Conductivity of Dried Haddock on Prediction of Surface Temperature

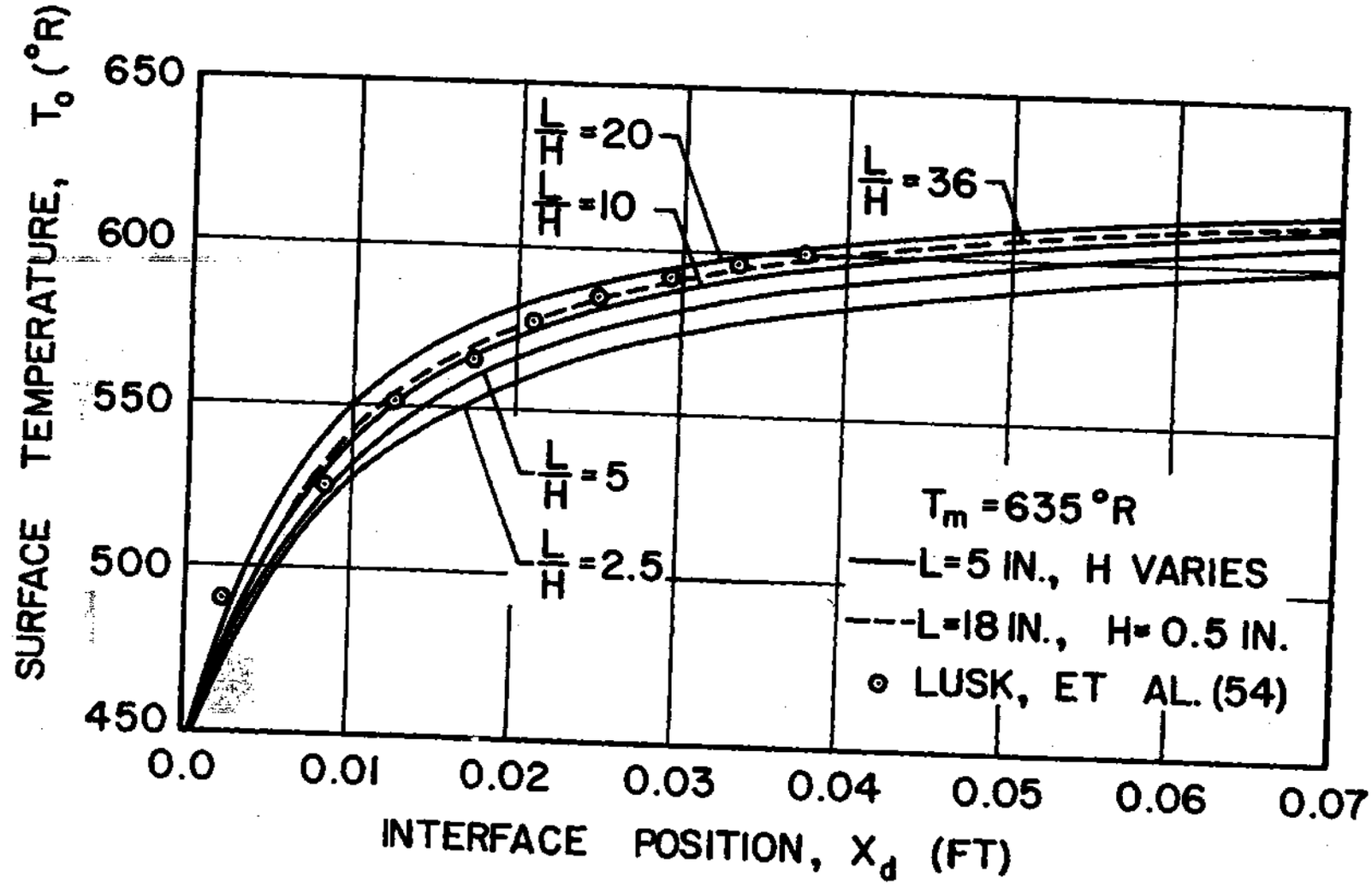

Figure 16. Influence of Variation of Channel Length and Width on Product Surface Temperature

exit temperature T_e (T_2 and T_3 in Figure 5) was arbitrarily allowed to be 530°R. The radiation losses from the channel with the exits at this temperature level for various L/H ratios was shown in Figure 16. Figure 17 shows the effect on T_0 of varying T_e from zero to 635°R for L/H equal to 10. As can be seen, the effect is small and the variation is at most approximately 1.5 per cent. For higher values of L/H, the effect of varying T_e is of course smaller.

The only known value for the emissivity of a freeze-dried product, as was mentioned earlier, is 0.75 for freeze-dried beef. Hence, this value was used for the calculation with Haddock. Figure 17 shows what happens when the emissivity is raised to 0.95 in Equation (4-45). The dashed line is for $\epsilon = 0.95$ and $T_e = 530°R$. Comparison is to be made with the solid line at $T_e = 530°R$ for which $\epsilon = 0.75$. Either curve is within acceptable limits for good comparison with the experimental data. Hence, if the emissivity used for Haddock is in error it does not significantly detract from the qualitative results shown here.

All of the data presented thus far has been for a mean heater or platen temperature T_m of 635°R, in accordance with that used by Lusk, et al. (54). Figure 17 also illustrates the effect on T_0 of lowering the heater temperature to 580°R.

The excellent agreement illustrated in Figures 14 through 17 between the theoretical solutions presented in this thesis and the independent experimental observations of Lusk, et al.(54) provides excellent confirmation of the validity of the momentum and energy solutions presented in Chapters III and IV for the range of R under consideration. The range of R is typically illustrated in Figure 18 and is seen to be well less than

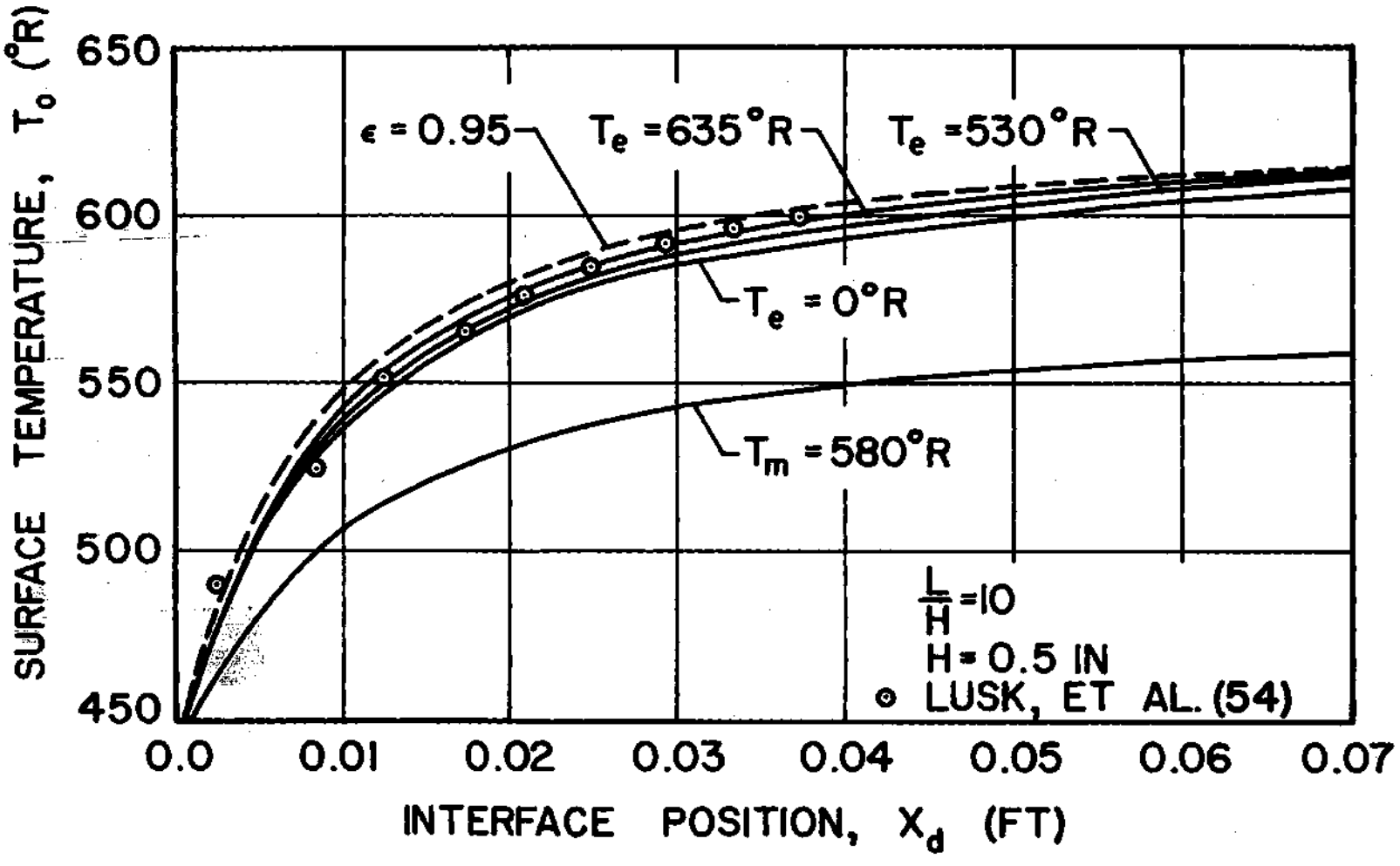

Figure 17. Influence of Channel Exit Temperature, Mean Heater Temperature, and Product Surface Emissivity on Product Surface Temperature

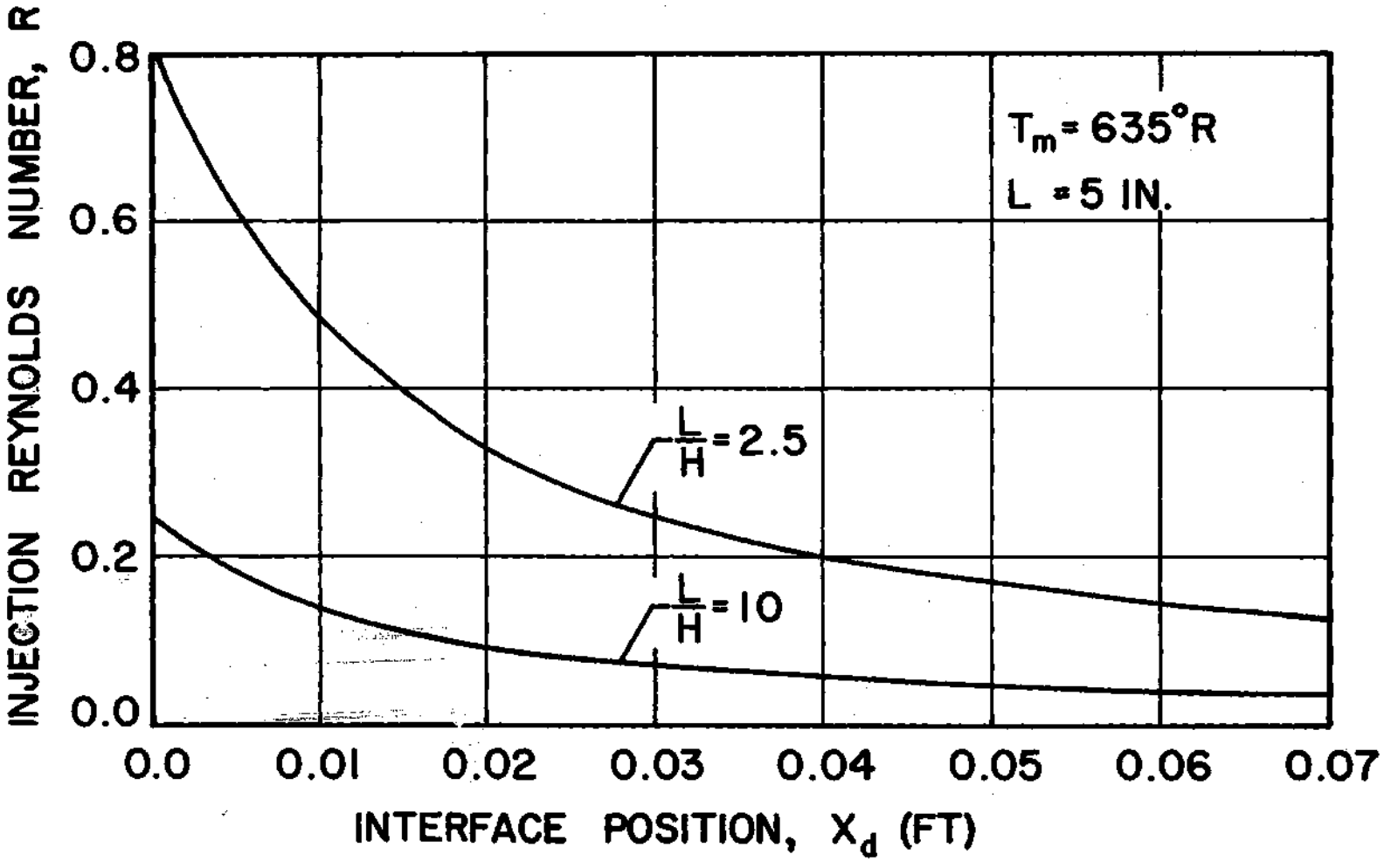

Figure 18. Variation of the Injection Reynolds Number During Freeze-Drying for the Case of Constant Mean Heater Temperature

unity for the majority of the drying cycle. It was mentioned earlier in this chapter that the expected range of accuracy for the momentum and energy solution would be rather limited, but the flow injection rates encountered in freeze-drying fall well within the most conservative limits of accuracy. The lower curve in Figure 18 is for the channel width H of 0.5 inch used by Lusk, et al. (54),whereas the upper curve is for a width of 2 inches which would seldom be used in practice because of the wasted space. Figure 19 shows that the amount of heat transfer to the product surface by radiation may range from 60 to almost 95 per cent of the total heat transfer. With this much heat transfer by radiation, small errors in the temperature profile solution of Equation (4-22) become less important in consideration of the total energy transfer process.

In connection with the amount of heat transfer by radiation from the heater to product, Figure 19 illustrates the variation of the per cent radiation with X_d for several values of H. This percentage is calculated by dividing the total contribution of the left side of Equation (4-45) into the contribution from the radiation terms after the correct temperature levels have been established. As can be seen, the greater the channel width the higher the percentage radiant heat transfer becomes. A look at the terms in Equation (4-45) will help explain these results. The convection term is inversely proportional to the channel width H and hence the greater H becomes the less the heat transfer by convection becomes. The radiation terms are a function of L/H but there is no direct influence of the channel width on the amount of radiation exchange between the two surfaces. Since the total amount of heat transfer must be the same regardless of what H is, then the percentage of radiant heat transfer must

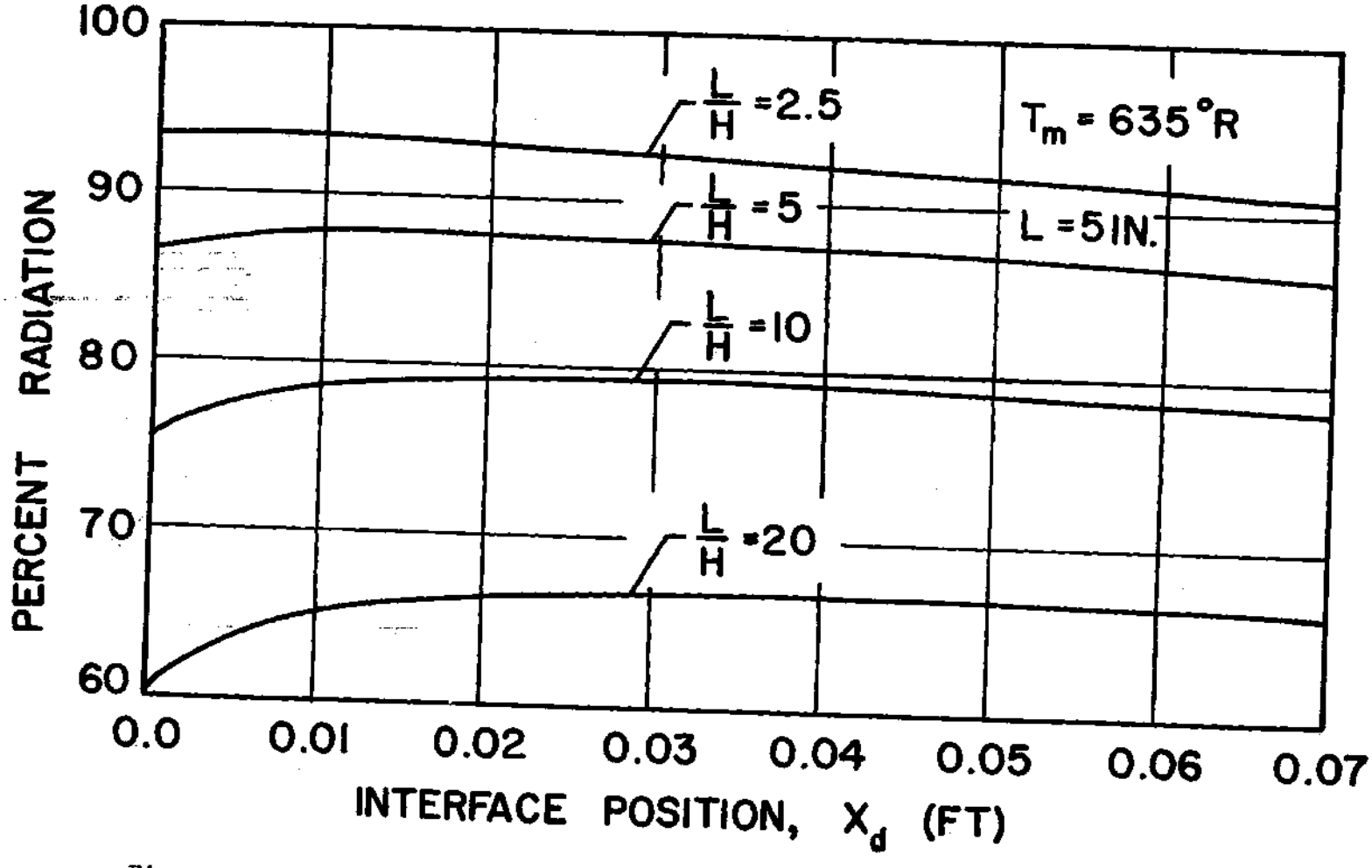

Figure 19. Influence of Channel Width on the Per Cent of Heat Transfer by Radiation to the Product Surface for the Case of Constant Mean Heater Temperature

increase as H increases. These results are very important and should help to clarify much of the existing confusion over the precise modes of heat transfer that occur between the heater and product. Radiation heat transfer is obviously the dominating mode in the process. The effects of channel length and exit temperature on the per cent radiation are insignificantly small when compared to the effect H has on the per cent radiation. These effects, however, are illustrated in the next subsection.

For the conditions described above for the 1-inch Haddock sample, some heat transfer coefficients are shown in Figure 20. These are as follows: the convection heat transfer coefficient $\bar{h}_c$, the radiation heat transfer coefficient $\bar{h}_r$, the combined convection and radiation coefficient $\bar{h}_{cr}$, and the overall heat transfer coefficient $\bar{U}$ between the heater surface and the frozen region of the product. The surface heat transfer coefficients are for the porous surface and are average coefficients for the entire length of the surface defined in Appendix E. The trends shown need little interpretation except that it is interesting to note the sharp decrease of $\bar{U}$ as X_d increases. The calculation of $\bar{U}$ of course includes the resistance of the dried layer and serves to illustrate the dominating effect that the dried layer has on the heat transfer.

The external surface coefficients experience relatively small change as drying proceeds when compared to $\bar{U}$. It is interesting to note that for the case of constant heater temperature, $\bar{h}_c$, $\bar{h}_r$, and $\bar{h}_{cr}$ experience a maximum at some point during drying and then slowly decrease as the cycle proceeds. This appears to suggest that drying beyond a certain thickness must be accomplished in an increasingly inefficient manner with respect to external as well as internal heat transfer.

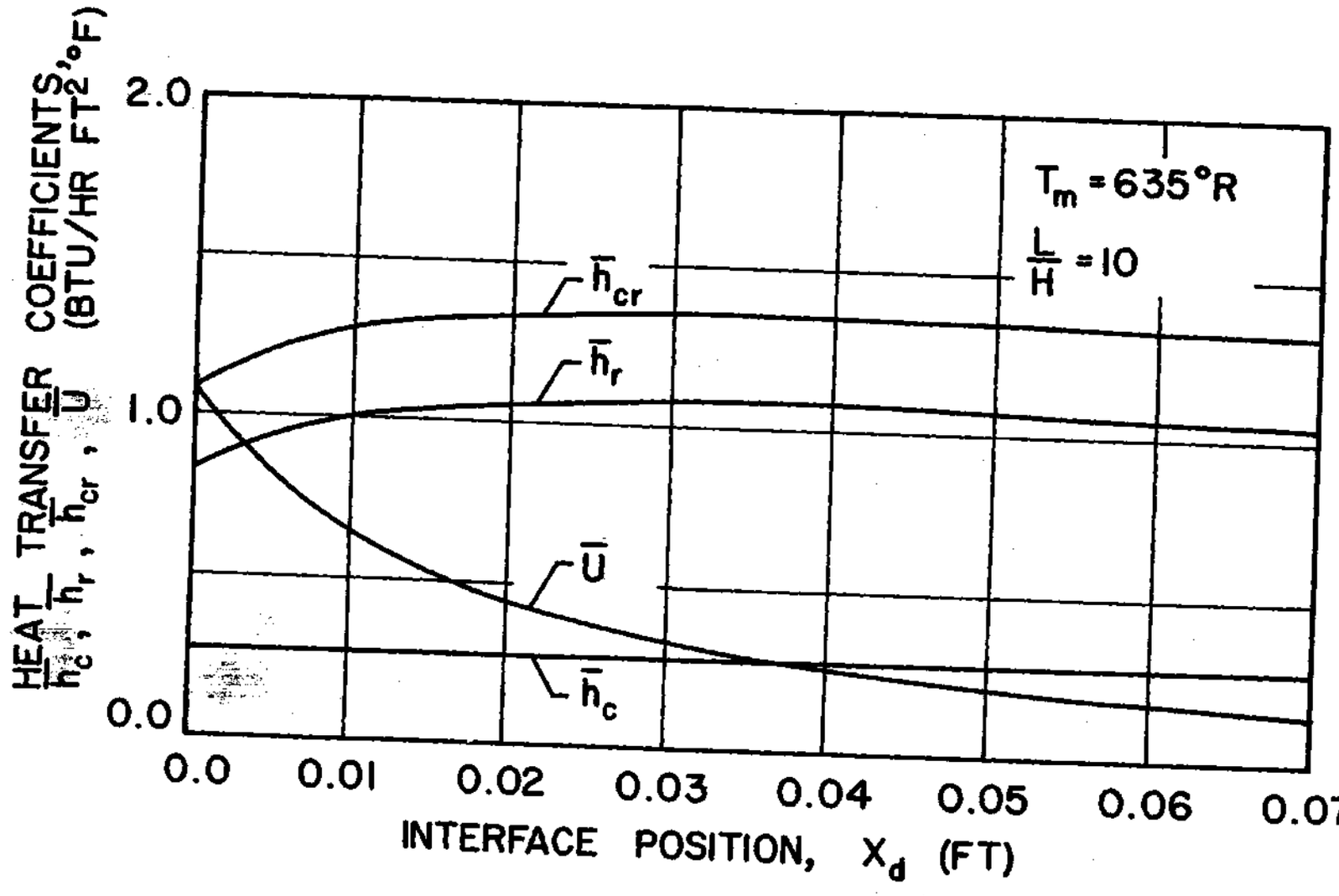

Figure 20. Heat Transfer Coefficients During Freeze-Drying for the Case of Constant Mean Heater Temperature

The most important coefficient in regard to the drying process is the overall heat transfer coefficient $\bar{U}$. A measurable increase in this coefficient by either external or internal means will directly influence the drying rates and times involved. The most influential variable noted in this work on the value of $\bar{U}$ is the channel width H. Figure 21 illustrates the effect that changing H has on the overall coefficient where all other conditions are the same as those employed by Lusk, et al. (54). It can be seen that up to an interface position of approximately 0.02 feet a decrease in H results in a significant increase in $\bar{U}$. Beyond this point the overwhelming resistance of the dried layer to heat transfer dampens any other influence on $\bar{U}$. Figure 22 shows the effect that changing H has on the flow rate at the porous surface.

Constant Product Surface Temperature

In this subsection the product surface temperature is considered as known and constant with respect to time and position. By selecting values of R, Equation (4-45) is used to calculate the mean heater temperature T_m required to maintain the product surface at the prescribed temperature and flow rate. Again, Equation (F-3) may be used to relate external flow conditions to the corresponding interface position. However, it is possible to go a step further in this section and use Equation (F-5) to calculate the length of time to dry to a particular interface position. Equation (F-5), derived by Dyer, et al. (5), is for the case where all heat transfer to the sublimating interface at X_d occurs across the dry layer, and the temperature of the frozen-region remains constant during the drying cycle. Hence, for this situation, it is possible to estimate the required heater temperature T_m at any particular time during the drying

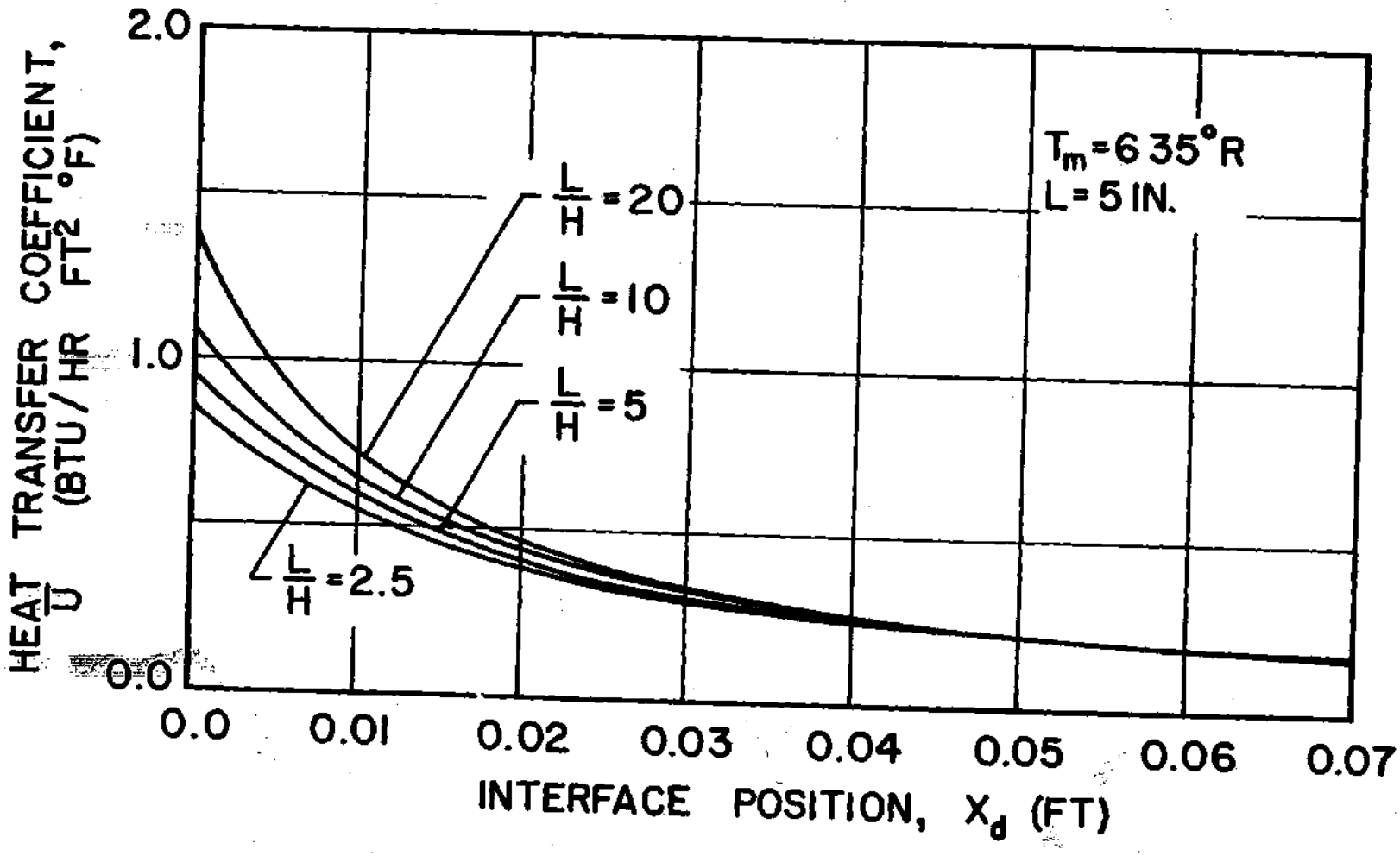

Figure 21. Influence of Channel Width on the Overall Heat Transfer Coefficient During Freeze-Drying for the Case of Constant Mean Heater Temperature

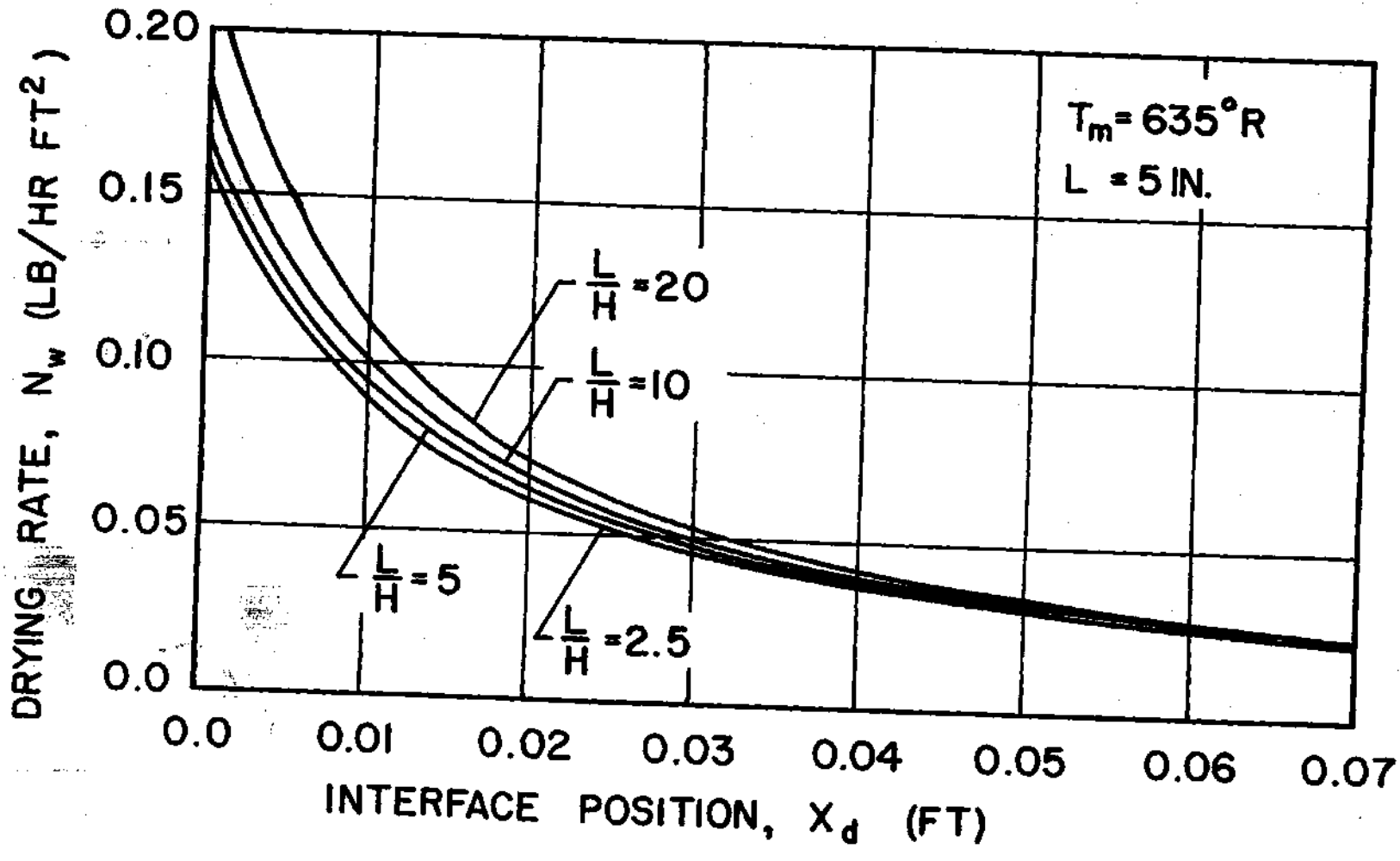

Figure 22. Influence of Channel Width on Freeze-Drying Rates for the Case of Constant Mean Heater Temperature

cycle and to graphically illustrate the variation on a plot of T_m versus time.

No experimental data is available for comparison with the analytical results for this case. However, the accuracy and reliability of the solution have been confirmed for the case considered in the last section.

Essentially the same quantities are considered in this section as in the last. First, the mean heater temperature is plotted versus time for a number of changing conditions. Also considered are several of the important heat transfer coefficients as they change with time. The physical property data used in this section is for freeze-dried beef. These properties are listed in Appendix I. Based on the results of the mass concentration solution outlined earlier which shows that nearly pure water-vapor exists in the channel, the properties of the mixture are taken to be those of pure water-vapor. The product surface temperature, T_O, unless otherwise specified is $560^\circ R$ and the absolute chamber pressure p_c is one torr. The interface temperature, T_d, which corresponds to a chamber pressure of one torr is $466^\circ R$. The channel exit temperature, T_e, unless otherwise specified is $530^\circ R$. The channel length to width ratio L/H is indicated on each figure.

Figures 23 through 25 are plots of the mean heater temperature versus time. Figure 23 illustrates the effect on T_m of varying the channel width H for a relatively long channel. Figure 24 shows the same thing for a short channel. The general effect is the same in both cases although slightly more pronounced for the shorter channel. The lower heater temperature required for the small widths is due in part to the increased convective heat flux across the channel and the reduced radiant

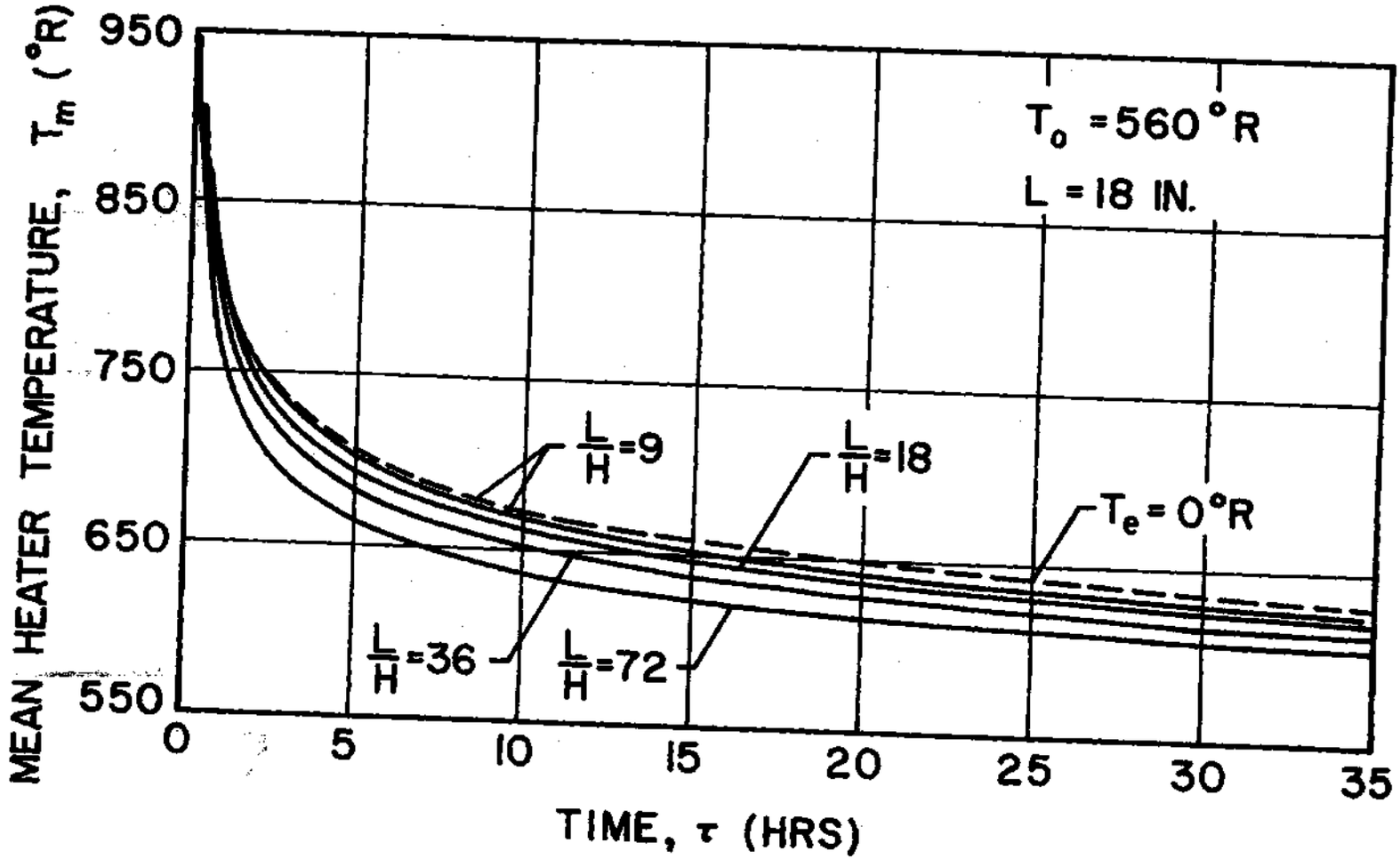

Figure 23. Influence of Channel Width and Exit Temperature on Mean Heater Surface Temperature for a Long Channel

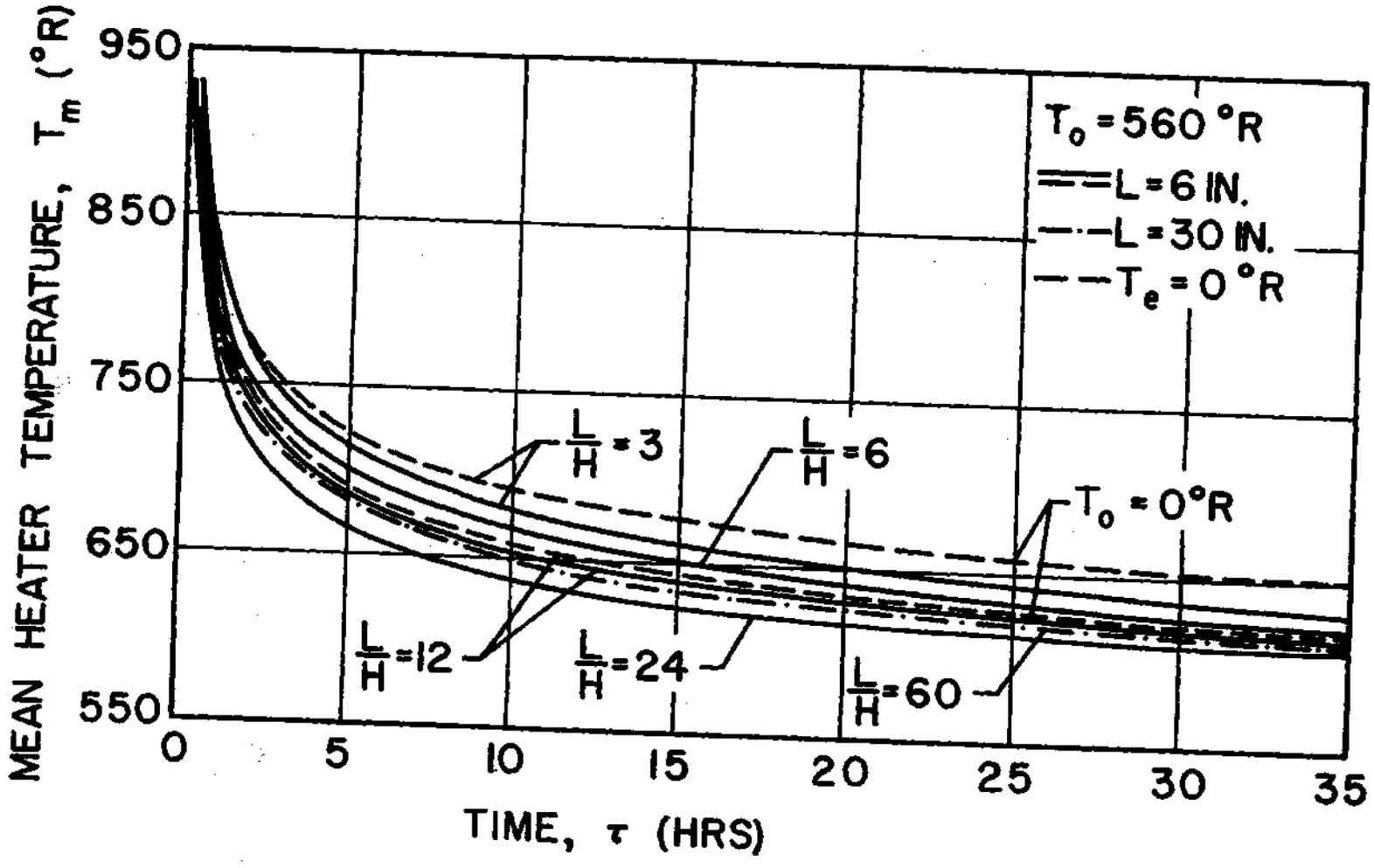

Figure 24. Influence of Channel Width, Length, and Exit Temperature on Mean Heater Surface Temperature

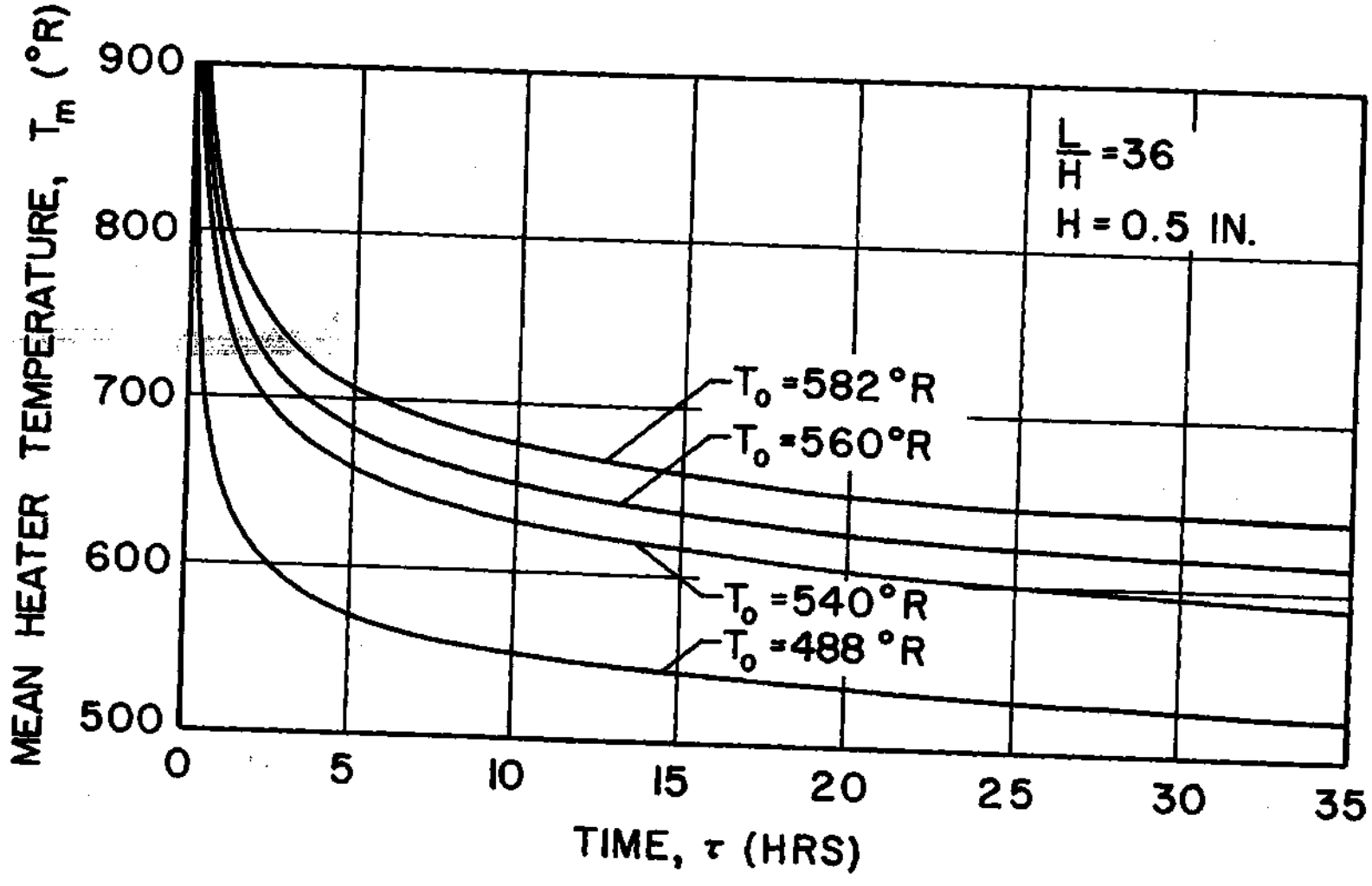

Figure 25. Influence of Product Surface Temperature on Mean Heater Surface Temperature

heat losses from the channel exits.

Figure 24 also shows the effect of changing length L when the channel width H is held constant. The curve for L/H = 60 has the same channel width as the one where L/H = 12. As can be seen, the effect is small when compared with the effect a change in H has on T_m. For the practical limits of the length to width ratio encountered in practice, there is little effect as a result of varying L. This simply illustrates that radiant heat losses from the channel exits are of negligible importance even for relatively short channels.

Figures 23 and 24 also illustrate the influence that a change in the exit temperature has on T_m for different channel gometries. The temperature was lowered to absolute zero since this would theoretically be the minimum temperature of the surroundings. On Figure 23, the effect of a lowered T_e is shown with the dashed line for the channel where L/H = 9. For the long narrow channels, there is no discernable effect on T_m. For the shorter channels of Figure 24, the effect of a lowered T_e is shown for two length to width ratios again with the dashed lines. As the geometry changes to a short wide channel, the effect becomes quite pronounced.

The effect that different values of T_0 has on the required value for T_m is shown in Figure 25. The only other external variable which could exert an influence on T_m would be the chamber pressure p_c. However, over the range of chamber pressures where freeze-drying normally occurs, in which the flow in the channel could be considered continuum (0.01 to 4 torr), there was no observed effect on T_m in the analytical work of this thesis. Of course, if the pressure is allowed to go consi-

derably lower, then other flow regimes are encountered and significant changes in the convective heat transfer would be expected to occur. This would then serve to alter the relative contributions of the radiant and convective modes of heat transfer.

Figure 26 shows the per cent of heat transfer by radiation to the product surface with respect to time under varying conditions. The effects of changing both L and H are illustrated. The solid lines are for a long channel and the dashed lines are for a short channel. As can be seen, the effect of a change in channel length for the same value of H is small. But when the channel length is held constant and H varies, it can be seen that the percentage of heat transfer by radiation undergoes large changes. The results shown in Figure 26 are very important and may help explain some seemingly contradictory observations made in freeze-drying. It is obvious that the further the heater surface is from the product the greater is the per cent radiant heat transfer. This may explain why one observer whose experimental equipment is arranged so that a large gap exists between heater and product reports that virtually all heat transfer is by radiation. However, another observer may arrange his equipment so that only a narrow space exists between heater and product, and as a result he reports that there is a significant contribution from the convective or conductive heat transfer mode. The analytical results presented here should help clear up some of the confusion that apparently exists in the literature.

Figure 26 also shows the change in per cent radiation which occurs for different values of the product surface temperature. All of the results demonstrate the dominant role played by radiation heat transfer between the heat source and the surface of the product in freeze-drying.

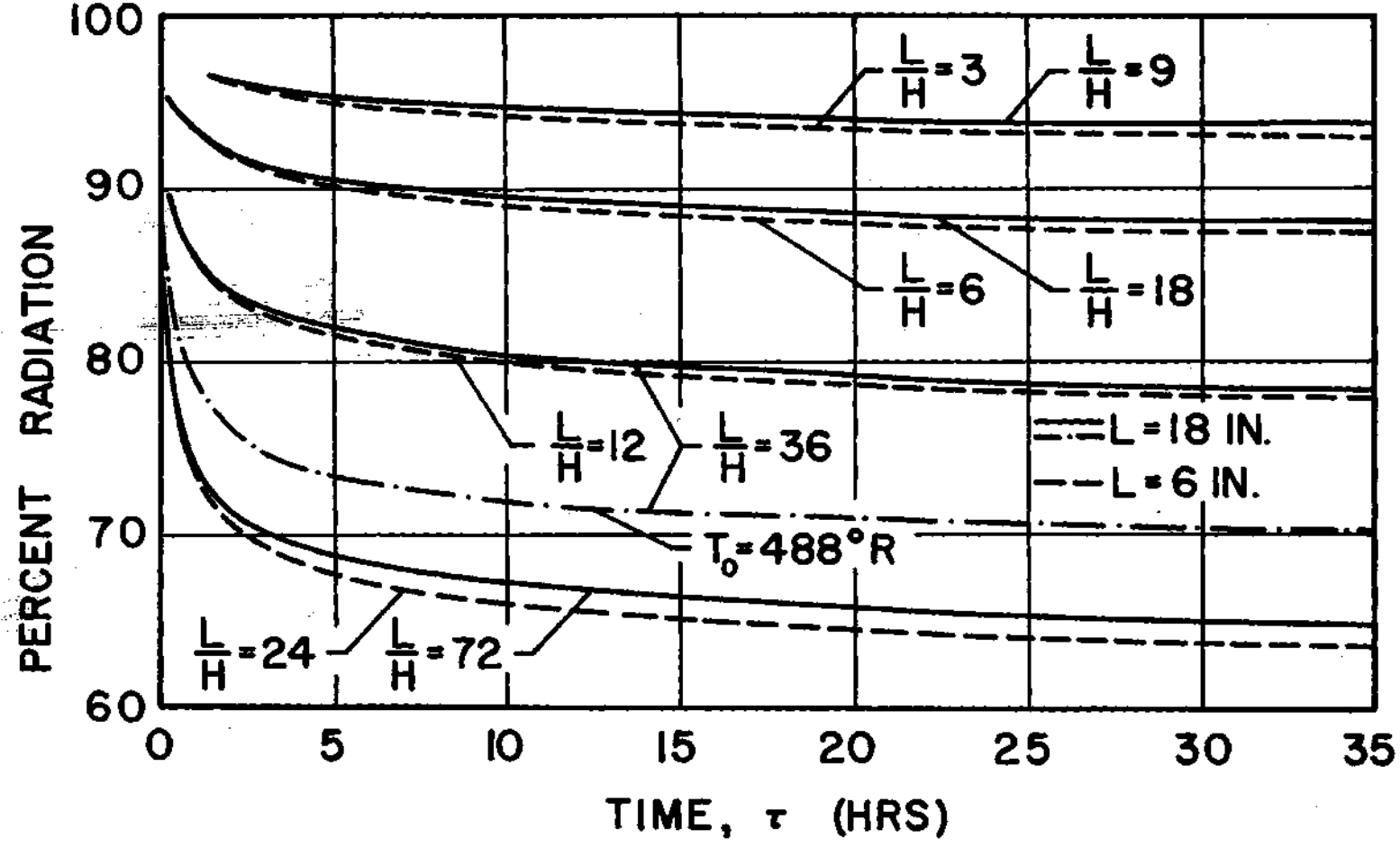

Figure 26. Influence of Channel Length, Width, and Product Surface Temperature on the Per Cent of Heat Transfer by Radiation to Product Surface for the Case of Constant Product Surface Temperature

Figure 27 is a plot of the convection heat transfer coefficient versus time. This figure illustrates the large effect that changing H has on $\bar{h}_c$. As was mentioned earlier, the convection heat transfer across the channel is directly influenced by H, and this applies to the convection heat transfer coefficient as well. Of course, the convection heat transfer is not affected by the channel length and neither is the coefficient. Figure 27 shows that at the beginning of the drying cycle the convection coefficient is somewhat lower than it is for the majority of the time. After the initial phase, $\bar{h}_c$ levels off and is relatively unchanging for the remainder of the cycle. This initial low value of $\bar{h}_c$ observed in each case is due to the higher injection Reynolds number which exists at the beginning of drying. As shown in Equation (6-6), as R increases, $\bar{h}_c$ decreases. No results are shown to illustrate the effect of the exit temperature T_e on $\bar{h}_c$ because the effect is negligible.

Figure 28 shows the radiation heat transfer coefficient $\bar{h}_r$ plotted with respect to time. The radiation heat transfer coefficient is a direct function of the temperature levels between the interacting surfaces. In Figure 28 this is shown by the sharp decrease in $\bar{h}_r$ which exists in the early stages of drying when T_m is also rapidly changing. The influence of the temperature levels is also illustrated by the effect a change in T_O has on $\bar{h}_r$. The same changes in the temperature levels of the walls results in very little effect on $\bar{h}_c$ since the convection heat transfer coefficient is not explicitly a function of temperature.

The effect of a change in L on $\bar{h}_r$ is also shown in Figure 28, and as can be seen, the effect is small. The effect of channel exit losses on $\bar{h}_r$ and on the per cent radiation is of the same order of magnitude

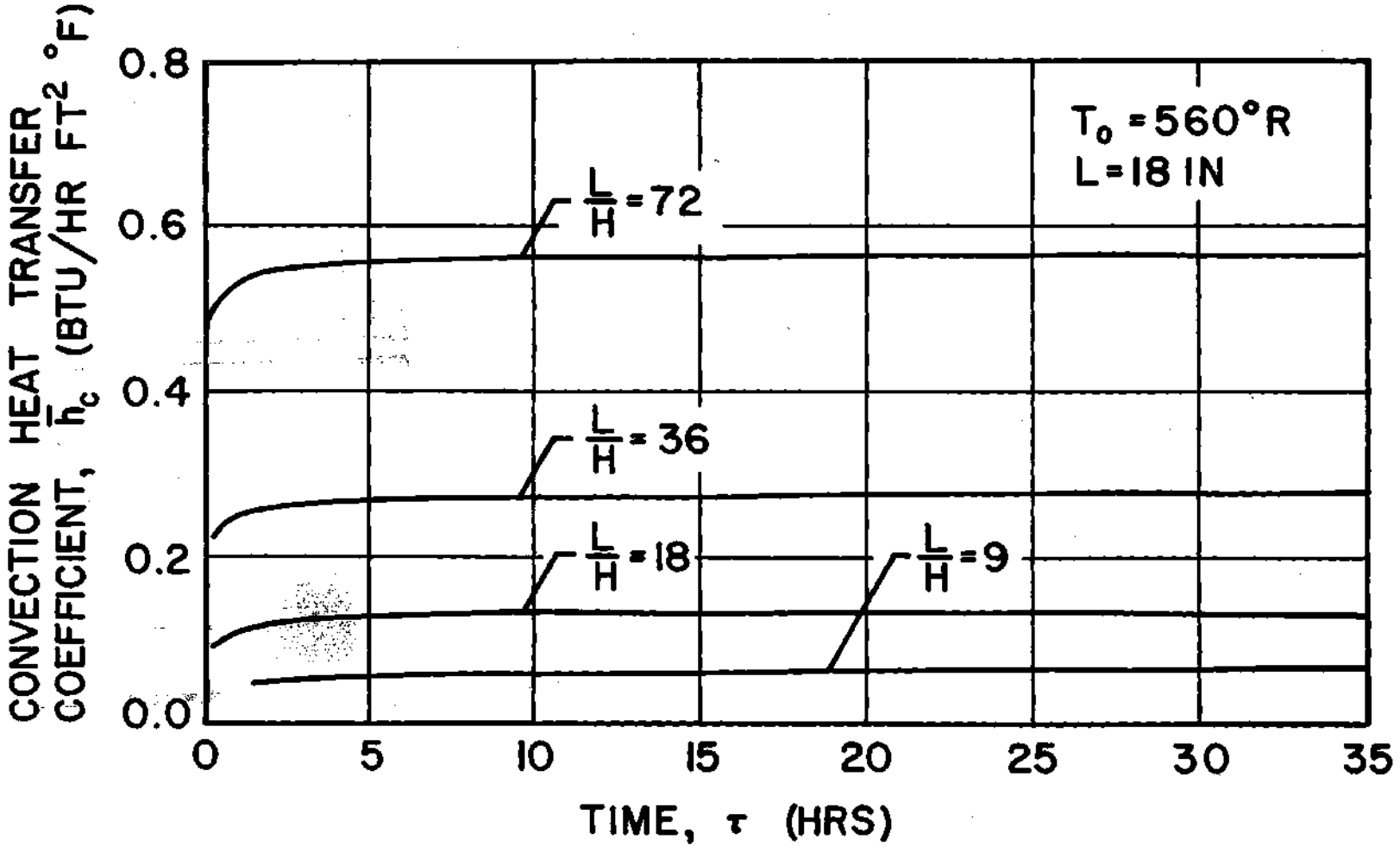

Figure 27. Influence of Channel Width on the Convection Heat Transfer Coefficient for the Case of Constant Product Surface Temperature

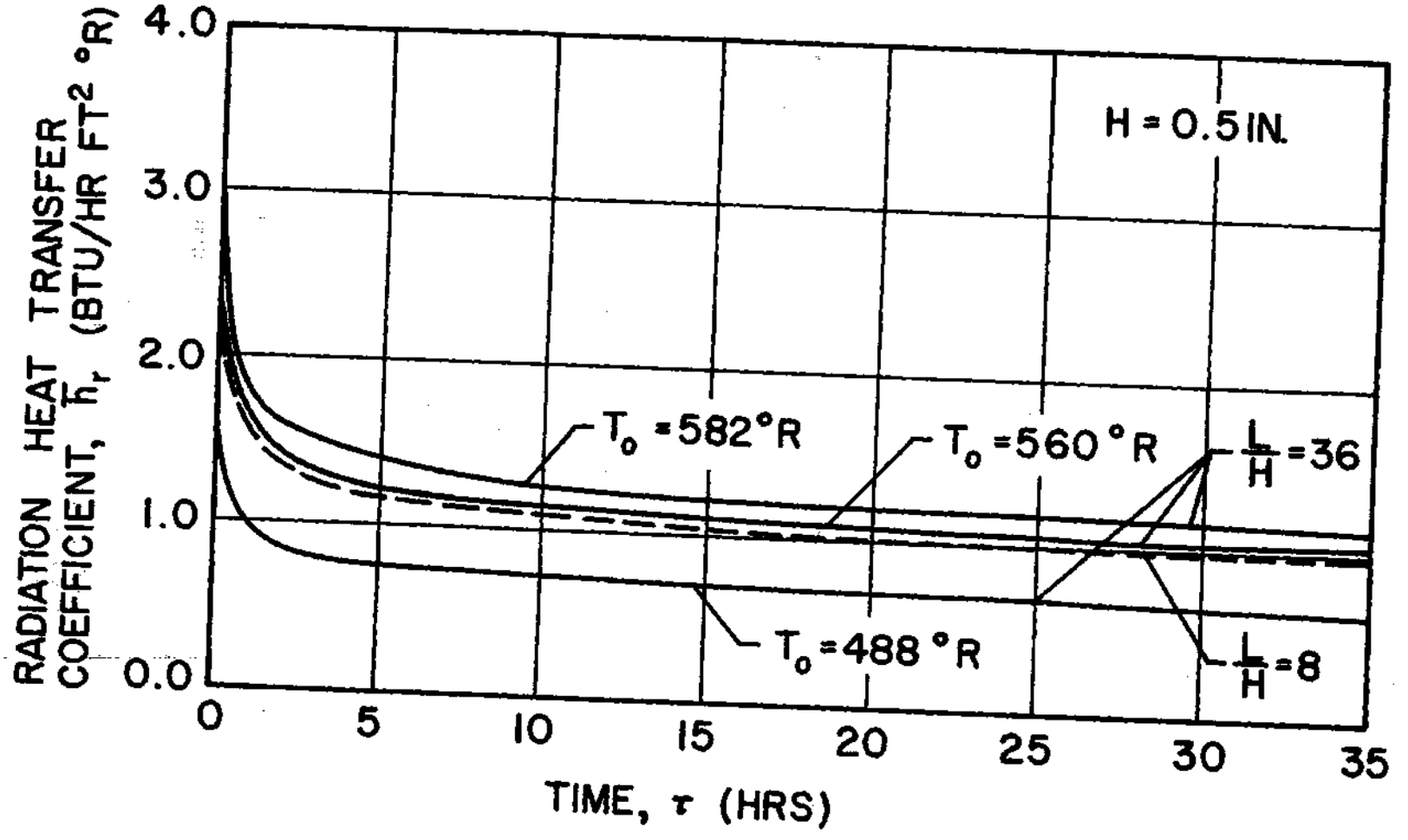

Figure 28. Influence of Channel Length and Product Surface Temperature on Radiation Heat Transfer Coefficient for the Case of Constant Product Surface Temperature

when L changes. For a change in H, the effect on $\bar{h}_r$ is even smaller and as a result is not shown in Figure 28. This is to be expected since the radiant heat flux is not explicitly a function of the channel width.

Figure 29 is a plot of the overall heat transfer coefficient $\bar{U}$ between the heater and the frozen region of the product. The effects of changing the channel width are shown and some benefit is gained at small values of H. As was mentioned earlier, an improvement in $\bar{U}$ represents a genuine increase in heat transfer to the frozen region and hence an improved drying rate. It should be observed though that in practice very narrow channels are often impractical due to the uneven nature of the product surface. Where the product surface is relatively flat, such as a granulated bed, the small advantage gained in improved overall heat transfer using the smallest possible channel width could, on a large commercial scale, result in significant savings. The effect of changing L on $\bar{U}$ is insignificantly small.

Calculations were also made of $\bar{U}$ where T_e is a parameter over a wide range of temperatures for the same channel geometries used in Figure 29. The overall coefficient is relatively unaffected by a temperature T_e as low as absolute zero. This result is of significant interest. In some commercial installations, the condensers which trap the removed water-vapor on a very cold surface are placed near the heating shelves. Worry over excessive heat losses from the heater to the condensers would appear to be largely unfounded. Of course, for a short wide channel configuration there is a measurable effect on $\bar{U}$ for the case where T_e is lowered to absolute zero. But for exit temperatures ordinarily found in practice, the effect on $\bar{U}$ is again negligible.

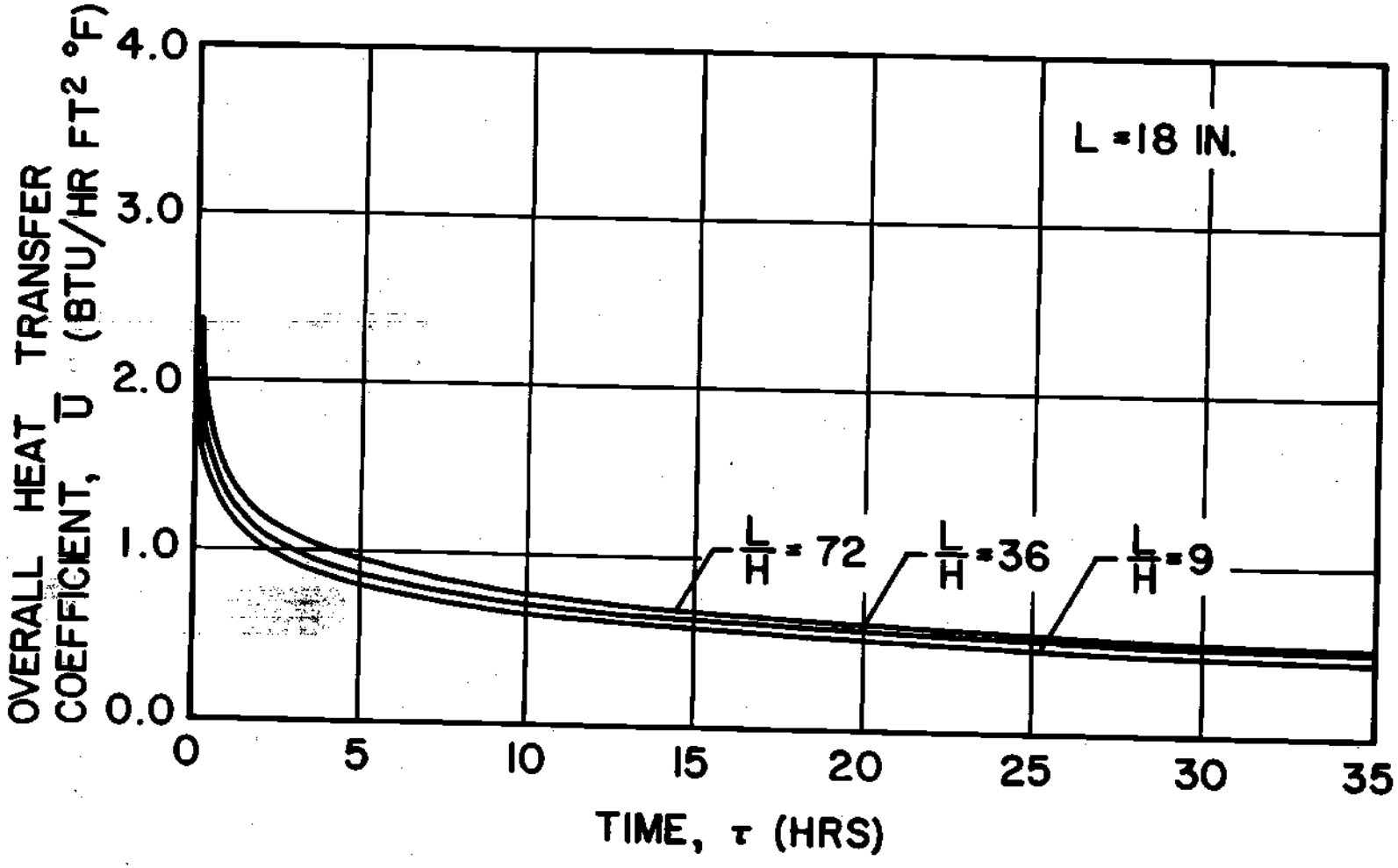

Figure 29. Influence of Channel Length on the Overall Coefficient of Heat Transfer for the Case of Constant Product Surface Temperature

The effects on $\bar{U}$ of varying the product surface temperature is shown in Figure 30. This figure shows some rather unexpected behavior for $\bar{U}$ when T_0 is the parameter. The different curves actually cross each other after an indicated amount of drying time elapses. For $T_0 = 488^{\circ}R$, the overall coefficient begins the process at a lower value than those for higher T_0, but eventually the coefficient becomes greater than those for higher T_0. This behavior is partially explained by a closer look at Figure 28 for $\bar{h}_r$. It is seen that for the lowest values of T_0, the curve exhibits a flatter aspect at an earlier time. Hence, when $\bar{U}$ is calculated using $\bar{h}_r$ in Equation (E-17), the effect in Figure 30 arises. This behavior is largely of academic interest only since the greatest overall advantage is still obtained when T_0 is kept as high as possible.

The pressure drop in the flow direction from the center of the channel to either exit is of considerable interest. If the pressure drop is too large, the pressure at the product surface near the middle of the channel may be high enough to allow some local thawing. The solution to the momentum equation presented in Chapter III includes the pressure distribution in the channel. Equation (3-40) gives the total pressure at any point in the channel while Equation (3-43) and Equation (3-44) give, respectively the pressure drop in the flow direction and across the channel. Since the chamber pressure is a known quantity, it is possible to calculate the total pressure at the center of the channel on the product surface using Equation (3-40). That is at $x = 0$ and $\xi = 0$ calculate $p(0,0)$. This is the point of maximum pressure in the channel and hence is sufficient to determine if the pressure is too high. The pressure at $x = L$ and $\xi = 0.5$ or $p(1,0.5)$ is taken to be the chamber pressure, p_c. Care must

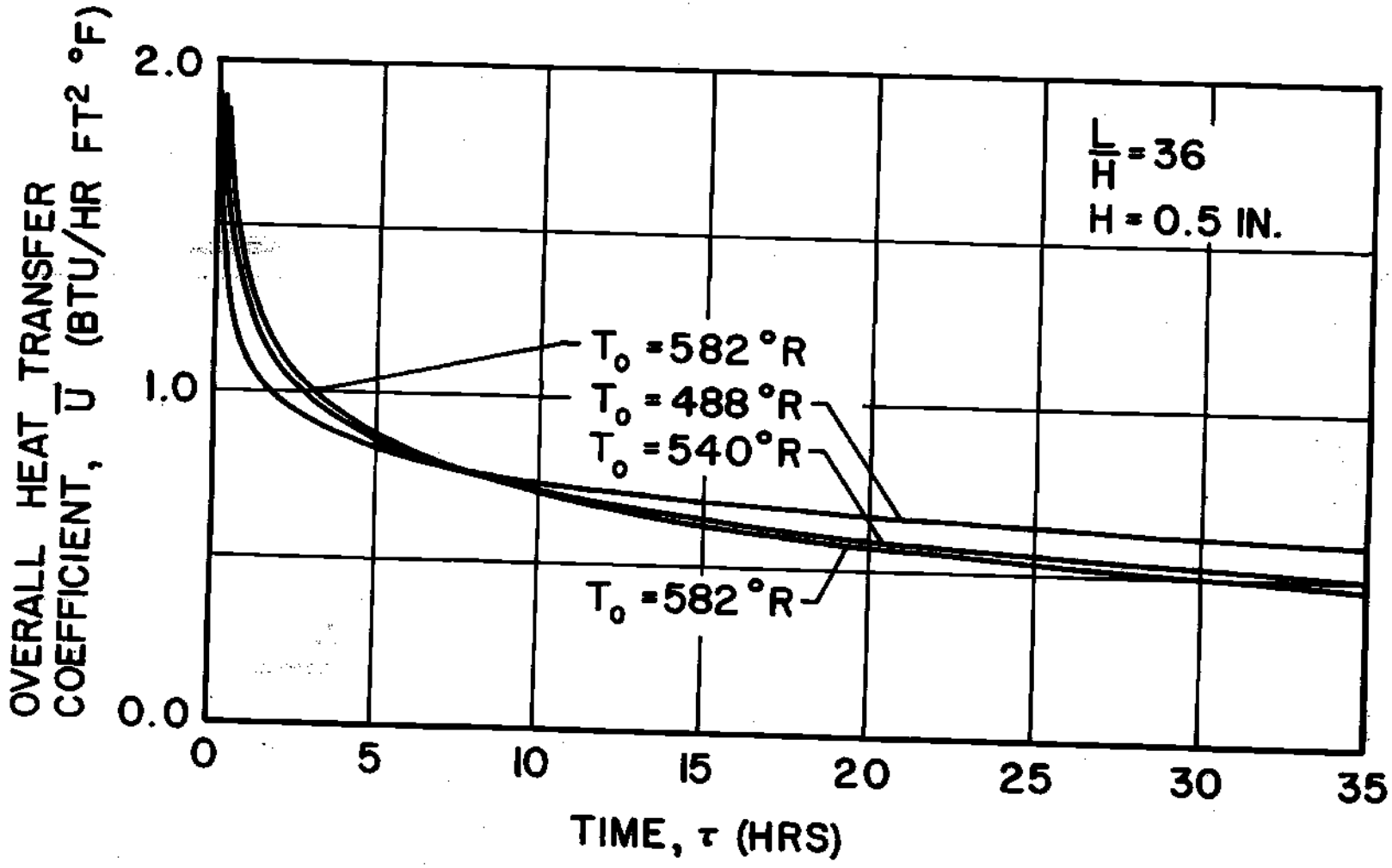

Figure 30. Influence of Product Surface Temperature on the Overall Coefficient of Heat Transfer for the Case of Constant Product Surface Temperature

be taken to use average properties in calculating the pressure change across the channel due to the temperature dependent properties. Since the product surface is isothermal with respect to the flow direction, no difficulty is encountered in evaluating properties for the pressure change along the porous surface.

Figure 31 shows the change of p(0,0) with respect to time for various channel geometries at a chamber pressure of one torr. As can be seen, during the early stages of drying when the flow rate is highest, the pressure near the center of the product can get relatively high, especially for the narrow channels. An increase in L at H = 0.25 inch, of course, results in even higher pressures. At wider channel widths, the increase in pressure near the center is insignificant for all practical channel lengths encountered in practice. In Figure 31 the chamber pressure, p_c, is seen to approach one as drying proceeds. Hence, the pressure drop along the porous surface from x = 0 to x = L, may be determined at any time by calculating the difference between p(0,0) and one. As can be seen, the pressure changes in the flow direction are quite small in freeze-drying. This result can be attributed to the very low densities encountered in normal freeze-drying situations. Reference to Equation (3-43) shows that the magnitude of the density directly influences the pressure changes.

Figure 32 shows the typical range of the injection Reynolds number for the case considered in this section. The variation is shown for two values of H to illustrate the widest range of R which might be encountered. Of course, the smaller channel width is most commonly found in industry for which values of R become quite small. Figure 33 and Figure 34 are,

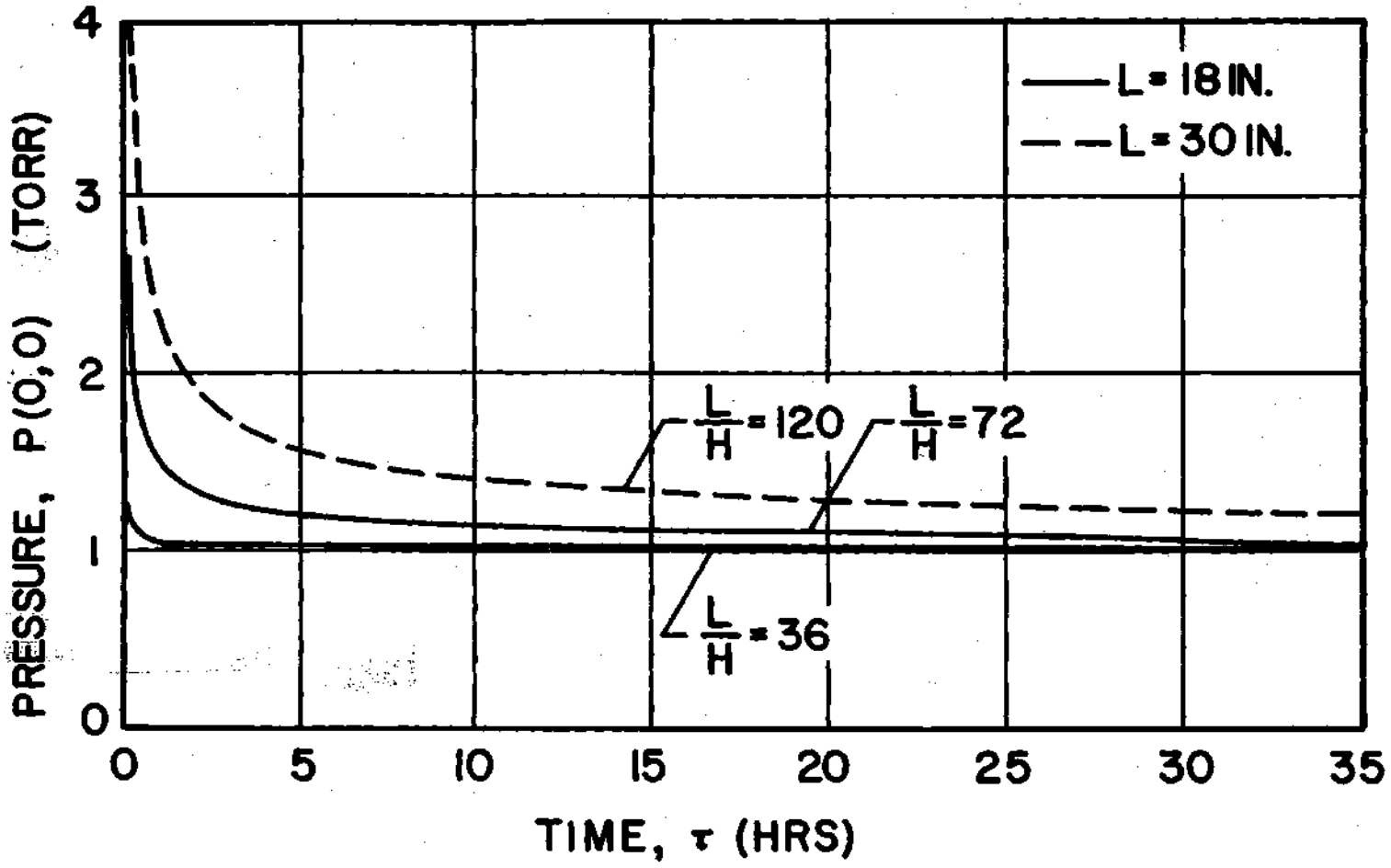

Figure 31. Variation of Porous Surface Pressure p(0,0) During Freeze-Drying for the Case of Constant Product Surface Temperature

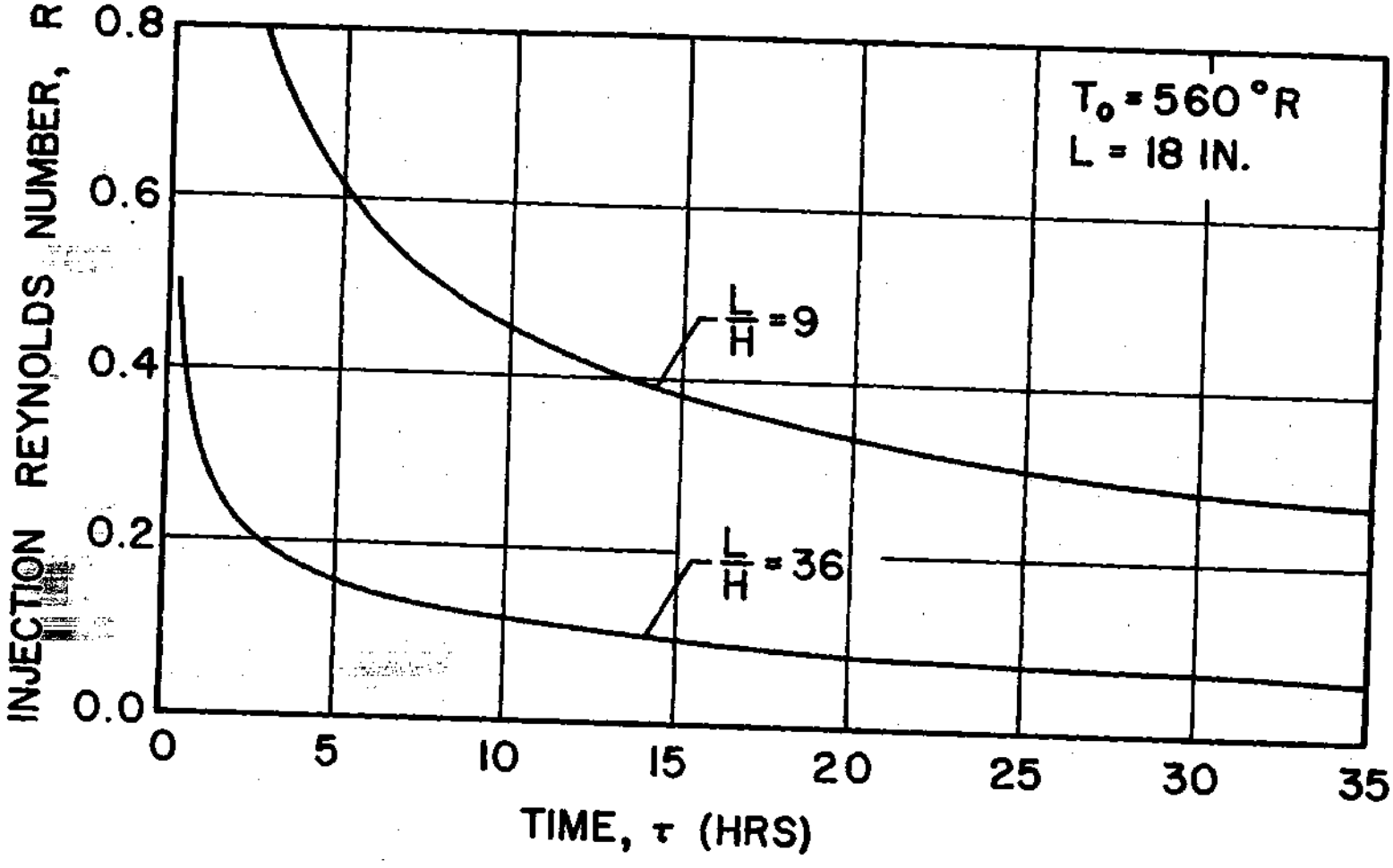

Figure 32. Variation of the Injection Reynolds Number During Freeze-Drying for the Case of Constant Product Surface Temperature

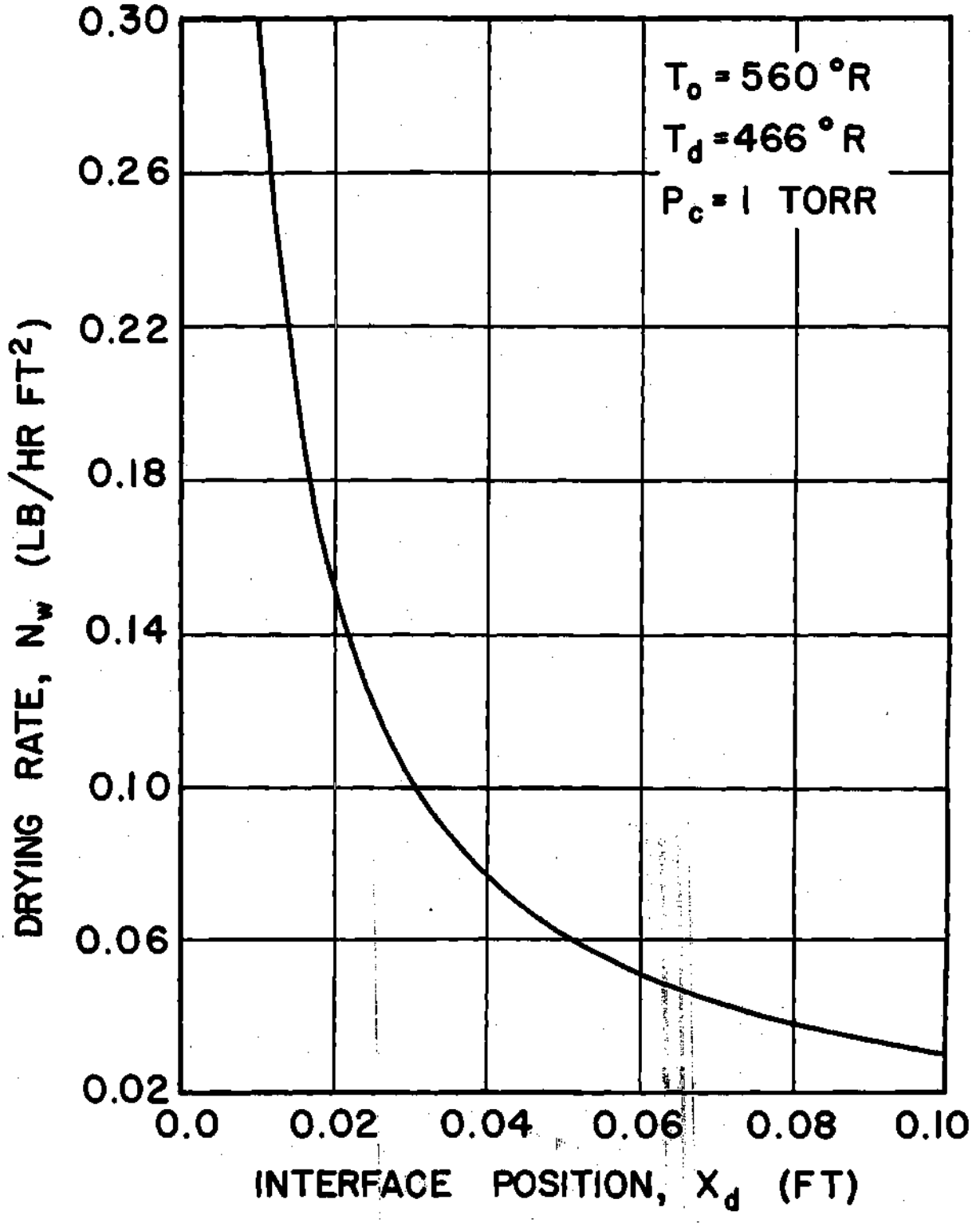

Figure 33. Drying Rate Versus Interface Position for Freeze-Drying of Beef at One Torr

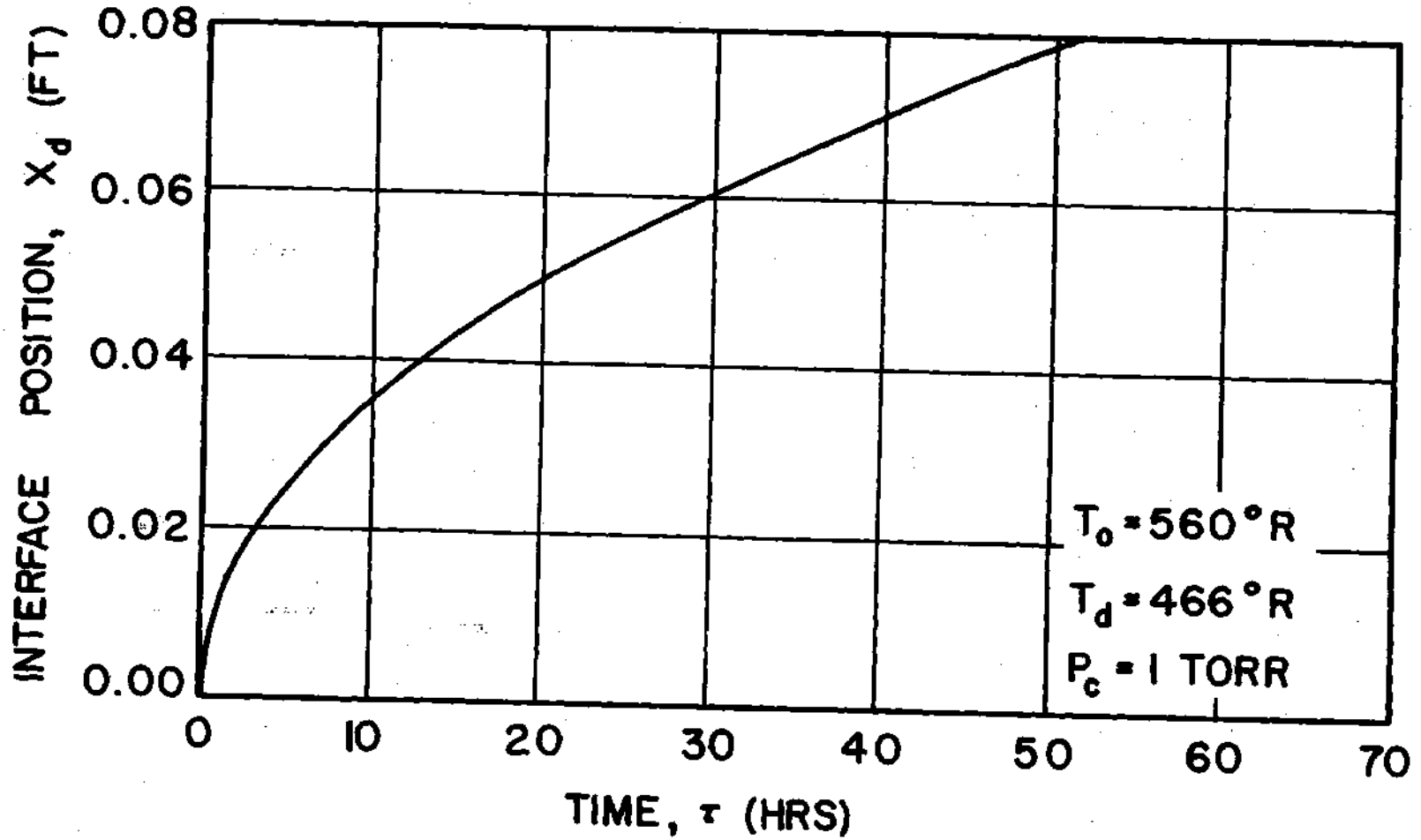

Figure 34. Interface Position Versus Time for Freeze-Drying of Beef at One Torr

respectively plots of flow rate versus interface position and interface position versus time for a surface temperature of 560°R and a chamber pressure of one torr. These curves are taken from the results of Dyer, et al. (5) and are presented here to provide a more complete picture of the combined external and internal mechanisms.

The material discussed in this chapter in connection with freeze-drying represents a very practical application of the theoretical analysis of a semi-porous channel. Previous work in the literature has consisted of very elegant mathematical analysis of porous channels of all types. However, few practical applications are considered, and the results usually appear too cumbersome to employ. The boundary conditions and solutions presented in this thesis were purposely simplified as much as possible in order to arrive at some practical results. Even so, the actual application to freeze-drying required considerable computer work in order to obtain a sufficient quantity of results.

CHAPTER VII

CONCLUSIONS AND RECOMMENDATIONS

The principal conclusions drawn from this investigation are discussed in the following paragraphs.

Based on the comparison with existing solutions, the polynomial solution for the velocity distribution in a semi-porous channel is shown to be quite accurate for $R \leq 3$. The accuracy of the polynomial solution for the temperature profile is established by comparison with published experimental results for a limited range of $RPr < 1$. The application of the semi-porous channel model to the heat transfer and fluid flow in the region between the heater platen and the food product in freeze-drying correlates well with the actual physical process since R is usually not greater than one.

In connection with freeze-drying, it is shown that radiation heat transfer is the dominant mode of heat transfer to the product surface where an open region separates the heater and the product. Depending on the channel width, the relative amount of radiation heat transfer may range from 60 to 95 per cent of the total heat transfer to the product surface. It is also shown that decreasing the channel width increases the convection heat transfer to the product surface and the overall heat transfer coefficient between the heater and the frozen region. The increase in the overall heat transfer coefficient results in slightly increased drying rates in the early stages of drying.

Other observations indicate that radiant heat losses from the channel exits are relatively unimportant for long narrow channels. Also, the hydrodynamic pressure drop in the flow direction of the channel in freeze-drying is ordinarily insignificant.

Finally, it is observed that for the long narrow channel usually found in commercial use, the fluid in the channel is almost pure water-vapor, and hence only hydrodynamic flow exists. Any residual air is swept away from the surface of the product at the start of drying, and diffusional flow in the channel is negligible.

The following items are presented as a logical extension of the work which has been presented in this thesis:

1. The complete set of differential equations describing the heat transfer and fluid flow characteristics in the semi-porous channel should be solved numerically using the most compatible set of boundary conditions. The solutions could also be extended to include the internal aspects of the flow processes.

2. Although the solutions presented in this thesis are apparently substantiated by experimental evidence, considerably more experimental work should be done in regard to the external transport mechanisms to confirm optimum drying conditions. Work especially needs to be done to verify the results of the mass concentration solution.

3. The diffusion equation should be solved under conditions where an inert gas is forcibly injected into the channel at some point to theoretically determine the feasibility of the use of such gases.

4. As data becomes available on the spectral and directional emissivities of food products, the external solutions should be refined

to include these effects.

APPENDICES

APPENDIX A

RADIATION EQUATIONS

The approach used here to derive the radiant exchange equations is based on the material in Chapter III of Sparrow and Cess (49). The nomenclature is also basically the same.

The rate at which radiant energy streams away from an incremental surface area, dA_i, is termed the radiosity and is given by

$$B_i(x_i) = \epsilon_i \sigma T^4(x_i) + \rho_i H_i(x_i) \quad , \tag{A-1}$$

where the symbol B denotes the radiosity. The first term on the right of Equation (A-1) represents the radiation emitted by the surface, and the second term represents the reflected radiation. The radiosity has units of energy per unit time and unit area. In general, the radiosity is a function of position, and hence the position coordinate, x_i, is used to show this dependence explicitly.

The radiant flux, H_i incident on the surface i comes from the other surfaces in the enclosure denoted by the symbol j. From an incremental area on j, an amount of energy $B_j(x_j)dA_j$ streams away in all directions. The amount of energy which arrives at i is $B_j(x_j)dA_j dF_{j-i}$, where dF_{j-i} is the incremental geometric factor between elements dA_j and dA_i. By employing one form of the recipiocity rule given by $dA_j dF_{j-i} = dA_i dF_{i-j}$, it follows that the rate at which energy arrives per unit area at dA_i from surface j is $B_j(x_j)dF_{i-j}$. The contribution from the entire j surface is

$$\int_{A_j} B_j(x_j) dF_{i-j} \quad . \tag{A-2}$$

Such a contribution arrives at dA_i from all surfaces in the enclosure and hence H_i is expressible as a sum

$$H_i(x_i) = \sum_j \int_{A_j} B_j(x_j) dF_{i-j} \quad . \tag{A-3}$$

Equation (A-3) may be used to eliminate H_i from Equation (A-1) to give

$$B_i(x_i) = \epsilon_i \sigma T_i^4(x_i) + (1-\epsilon_i) \sum_j \int_{A_j} B_j(x_j) \frac{dF_{i-j}}{dA_j} dA_j \quad , \tag{A-4}$$

where use of the fact that $\rho_i = 1 - \epsilon_i$ has been made.

The net rate of heat transfer leaving surface i per unit area is given by

$$q_i(x_i) = B_i(x_i) - H_i(x_i) \quad . \tag{A-5}$$

Solving Equation (A-1) for $H_i(x_i)$ and substituting the result into Equation (A-5) results in

$$q_i(x_i) = \frac{\epsilon_i}{1 - \epsilon_i} \left[\sigma T_i^4(x_i) - B_i(x_i) \right] \quad . \tag{A-6}$$

If the temperature distributions on each surface of the enclosure

are known, then Equation (A-4) applied at each surface yields a set of linear integral equations for the unknown radiosity functions of each surface. Solution methods can become quite complex and numerical computer solutions are commonly used. Once the radiosities are known, the heat flux at each surface may be calculated using Equation (A-6).

APPENDIX B

GEOMETRIC VIEW FACTORS

The general equation used to calculate radiation exchange geometric view factors may be found in any standard text on radiation heat transfer. For two elemental areas, dA_1 and dA_j, the equation is

$$dF_{i-j} = \frac{\cos \phi_i \cos \phi_j \, dA_j}{\pi r^2} \quad . \tag{B-1}$$

The angles ϕ_i and ϕ_j are formed by the respective normals to the area elements and the connecting line r between the elements.

The incremental view factor between two area elements located on opposing parallel plates may now be easily derived. Reference is made to Figure 35 where two infinitely long parallel strips are shown. Different locations of dA_0 and dA_1 with respect to z must be taken into account.

The connecting line between the elements is

$$r^2 = z_1^2 + H^2 + (x_1 - x_0)^2 \quad , \tag{B-2}$$

and $dA_1 = dx_1 dz_1$.

Evaluation of the cosines of the angles ϕ_0 and ϕ_1 gives

$$\cos \phi_0 = \frac{H}{\left[z_1^2 + H^2 + (x_1 - x_0)^2\right]^{1/2}} \tag{B-3}$$

and

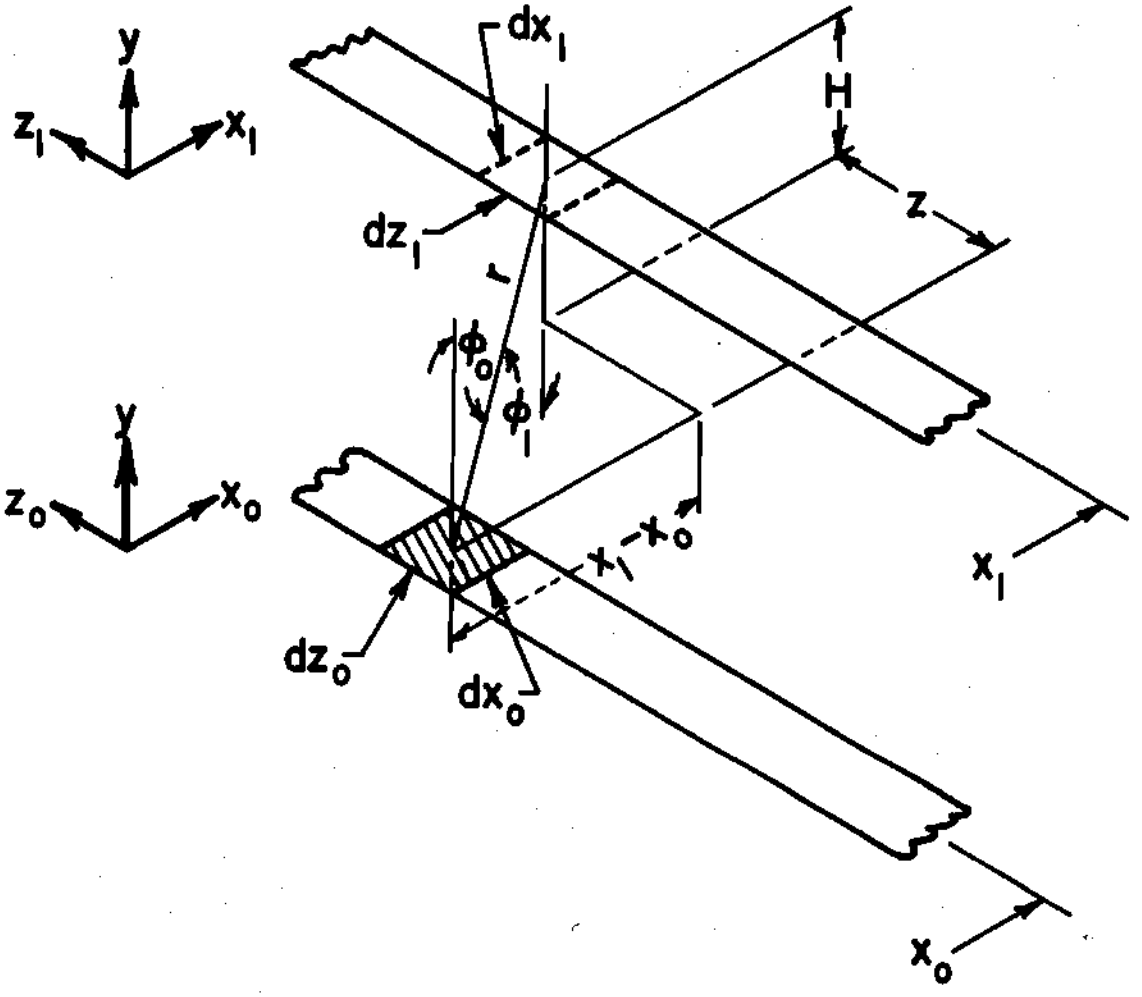

Figure 35. Relationship of Incremental Areas on Parallel Planes Illustrating Coordinate System for Calculation of Geometric View Factors

$$\cos \phi_1 = \frac{H}{\left[z_1^2 + H^2 + (x_1 - x_0)^2\right]^{1/2}} \quad . \tag{B-4}$$

The view factor then becomes

$$dF_{0-1} = \frac{H^2 \, dx_1 \, dz_1}{\pi \left[z_1^2 + H^2 + (x_1 - x_0)^2 \right]^2} \quad . \tag{B-5}$$

Integration with respect to z_1 from $-\infty$ to $+\infty$ will yield the view factor between a pair of infinite strips on the two surfaces. This integration is performed in Appendix C.

The geometric view factor between an area element on a horizontal surface and an element on a perpendicular surface may also be evaluated. Figure 36 illustrates the relative positions of the elements and the appropriate nomenclature. Again, the z-direction must be considered.

The connecting line between the element is

$$r^2 = z_3^2 + y_3^2 + (L - x_0)^2 \tag{B-6}$$

and $dA_3 = dy_3 dz_3$.

Evaluation of the cosines of the angles ϕ_0 and ϕ_3 yields

$$\cos \phi_0 = \frac{y_3}{\left[z_3^2 + y_3^2 + (L - x_0)^2\right]^{1/2}} \tag{B-7}$$

and

$$\cos \phi_3 = \frac{L - x_0}{\left[z_3^2 + y_3^2 + (L - x_0)^2\right]^{1/2}} \quad . \tag{B-8}$$

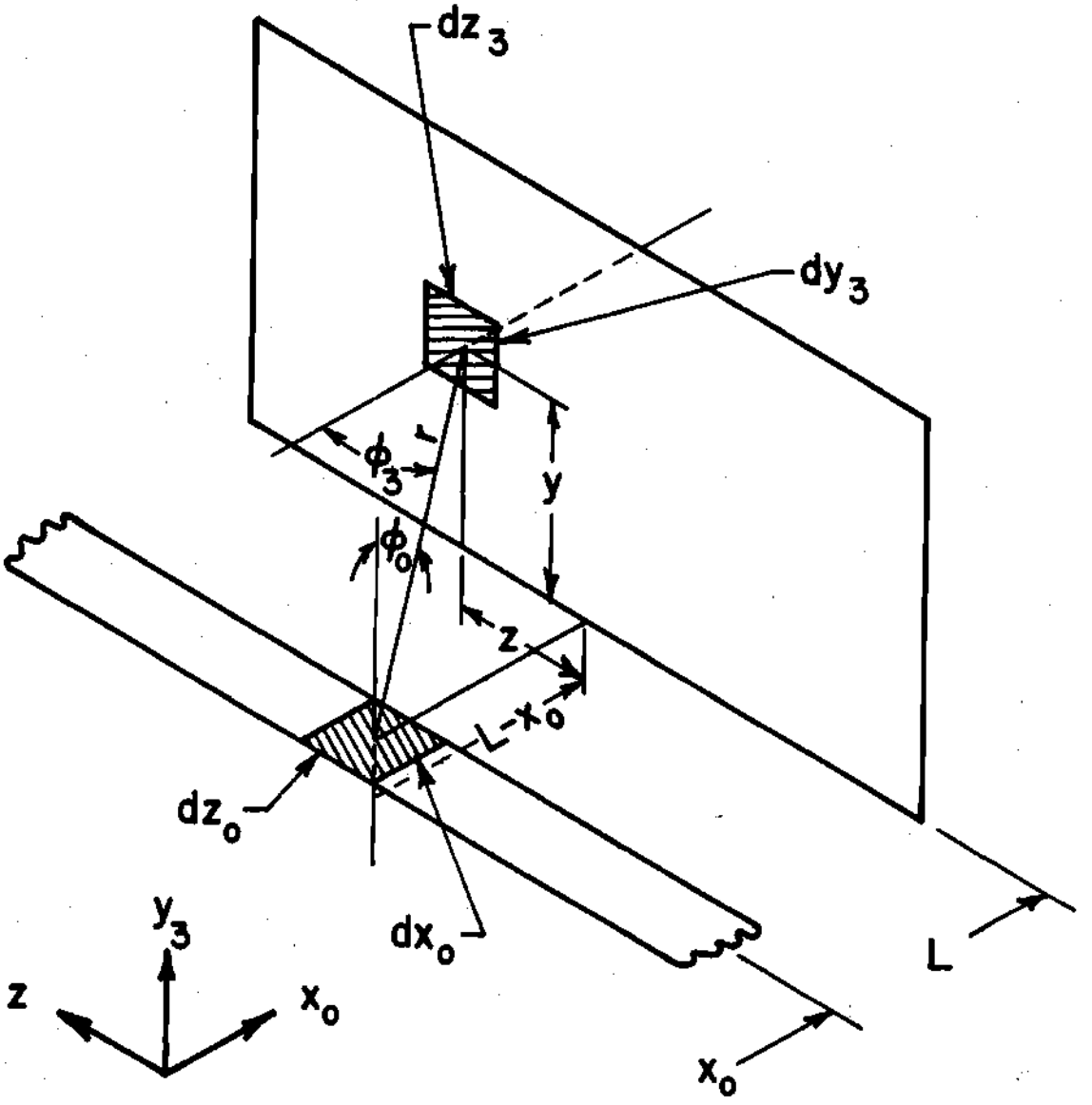

Figure 36. Relationship of Incremental Areas on Two Adjacent Perpendicular Planes Illustrating Coordinate System for Calculation of Geometric View Factors

Substitution into Equation (B-1) yields for the view factor

$$dF_{0-3} = \frac{y_3(L-x_0)\, dy_3\, dz_3}{\pi\left[z_3^2 + y_3^2 + (L-x_0)^2\right]^2} \quad . \tag{B-9}$$

Again, integration with respect to z_3 from $-\infty$ to $+\infty$ will yield the view factor between two infinite strips on the surfaces. This integration is performed in Appendix C.

The view factor between surface 0 and 2 of Figure 5 is derived in the very same manner and is

$$dF_{0-2} = \frac{y_2(L+x_0)\, dy_2\, dz_2}{\pi\left[z_2^2 + y_2^2 + (L+x_0)^2\right]^2} \quad . \tag{B-10}$$

APPENDIX C

TYPICAL INTEGRATIONS

The integrations performed on the geometric view factors given in Equations (B-5), (B-9), and (B-10) necessary to derive Equations (4-44) and (4-45) are indicated here. These results were obtained from standard integral tables.

In Equation (B-5), integration with respect to z_1 from $-\infty$ to $+\infty$ will yield

$$\int_{-\infty}^{+\infty} \frac{dz_1}{\left[z_1^2 + H^2 + (x_1-x_0)^2\right]^2} = \frac{\pi}{2\left[H^2 + (x_1-x_0)^2\right]^{3/2}}. \qquad \text{(C-1)}$$

In Equation (B-9), integration with respect to y_3 from 0 to H and z_3 from $-\infty$ to $+\infty$ yields for use in Equation (4-44)

$$\int_{-\infty}^{+\infty}\int_{0}^{H} \frac{y_3(L-x_0)\, dy_3\, dz_3}{\pi\left[z_3^2 + y_3^2 + (L-x_0)^2\right]^2} = \frac{1}{2}\left[1 - \frac{(L-x_0)}{\left[H^2 + (L-x_0)^2\right]^{1/2}}\right]. \qquad \text{(C-2)}$$

Integration of Equation (B-10) with respect to the same limits gives

$$\int_{-\infty}^{+\infty}\int_{0}^{H} \frac{y_2(L+x_0)\, dy_2\, dz_2}{\pi\left[z_2^2 + y_2^2 + (L+x_0)^2\right]^2} = \frac{1}{2}\left[1 - \frac{(L+x_0)}{\left[H^2 + (L+x_0)^2\right]^{1/2}}\right]. \qquad \text{(C-3)}$$

Equations (C-2) and (C-3) must also be integrated with respect to x_o from -L to +L for use in Equation (4-45). Doing so on Equation (C-2) gives

$$\frac{1}{2}\int_{-L}^{L}\left[1-\frac{(L-x_o)}{\left[H^2+(L-x_o)\right]^{1/2}}\right]dx_o=\frac{2L}{H}+1-\left[4\left(\frac{L}{H}\right)^2+1\right]^{1/2}. \qquad (C\text{-}4)$$

Integration of Equation (C-3) over the same limits gives the same results as in Equation (C-4).

APPENDIX D

DERIVATION OF NUMERICAL INTEGRALS

In this appendix, the details of substituting T(x,1) into Equation (4-45) for $T_1(x_1)$ are given.

The temperature T(x,1) evaluated from Equation (4-22) gives

$$T(x,1) = T_0 + (T_{LH}-T_0)\left(\frac{x_1}{L}\right)^{-\gamma} \quad . \tag{D-1}$$

In Equation (4-45), T(x,1) is raised to the fourth power. Hence,

$$[T(x,1)]^4 = T_0^{\,4} + 4\,T_0^{\,3}\,(T_{LH}-T_0)\left(\frac{x_1}{L}\right)^{-\gamma} + 6\,T_0^{\,2}\,(T_{LH}-T_0)^2\left(\frac{x_1}{L}\right)^{-2\gamma} + 4\,T_0(T_{LH}-T_0)^3\left(\frac{x_1}{L}\right)^{-3\gamma} + (T_{LH}-T_0)^4\left(\frac{x_1}{L}\right)^{-4\gamma} \quad . \tag{D-2}$$

Substituting Equation (D-2) into Equation (4-45) yields five double integrals of the type

$$I_5 = \int_{-L}^{L}\int_{-L}^{L} \frac{T_0^{\,4}\,dx_1\,dx_0}{\left[(x_1-x_0)^2 + H^2\right]^{3/2}} \quad , \tag{D-3}$$

and

$$I_n = \int_{-L}^{L}\int_{-L}^{L} \frac{\left(\frac{x_1}{L}\right)^{-n\gamma} dx_1\,dx_0}{\left[(x_1-x_0)^2 + H^2\right]^{3/2}} \quad , \tag{D-4}$$

where n = 1, 2, 3, or 4.

Equation (D-3) may be integrated using standard integral tables to give

$$I_5 = \frac{2}{H}\left(T_0^4\sqrt{4\left(\frac{L}{H}\right)^2+1} - 2\,T_0^4\right). \qquad \text{(D-5)}$$

Equation (D-4) may be integrated with respect to x_0 to give

$$I_n = \frac{1}{H^2}\int_{-L}^{L}\left\{\frac{-(x_1-L)}{\left[(x_1-L)^2+H^2\right]^{1/2}} + \frac{(x_1+L)}{\left[(x_1+L)^2+H^2\right]^{1/2}}\right\}\left(\frac{x_1}{L}\right)^{-n\gamma} dx_1 . \qquad \text{(D-6)}$$

Equation (D-6) is evaluated from -L to +L. It can be shown that the portion from -L to 0 is equivalent to the portion from 0 to +L. Hence, Equation (D-6) may be rewritten as

$$I_n = \frac{2}{H^2}\int_{0}^{L}\left\{\frac{-(x_1-L)}{\left[(x_1-L)^2+H^2\right]^{1/2}} + \frac{(x_1+L)}{\left[(x_1+L)^2+H^2\right]^{1/2}}\right\}\left(\frac{x_1}{L}\right)^{-n\gamma} dx_1 . \qquad \text{(D-7)}$$

Equation (D-7) may be put in dimensionless form by defining

$$X_1 = \frac{x_1}{L} \qquad \text{(D-8)}$$

and noting that at $x_1 = 0$, $X_1 = 0$, and then $x_1 = L$, $X_1 = 1$. The result is

$$I_n = \frac{2}{H}\left(\frac{L}{H}\right)^2 \int_0^1 \left\{ \frac{-X_1^{1-n\gamma}}{\left[\left(\frac{L}{H}\right)^2 (X_1-1)^2 + 1\right]^{1/2}} + \frac{X_1^{1-n\gamma}}{\left[\left(\frac{L}{H}\right)^2 (X_1+1)^2 + 1\right]^{1/2}} \right.$$

$$\left. + \frac{X_1^{-n\gamma}}{\left[\left(\frac{L}{H}\right)^2 (X_1-1)^2 + 1\right]^{1/2}} + \frac{X_1^{-n\gamma}}{\left[\left(\frac{L}{H}\right)^2 (X_1+1)^2 + 1\right]^{1/2}} \right\} dX_1 \quad . \tag{D-9}$$

The term, γ, which arises in the energy solution of Chapter III is always positive. Hence, the last two terms in Equation (D-9) are discontinuous at $X_1 = 0$. The first two terms will also be discontinuous at $X_1 = 0$, when $n\gamma > 1$, but this situation will not occur for most typical freeze-drying applications. The last two terms may be transformed so that they too will result in convergent integrals at the lower limit for most freeze-drying applications. The transformation which accomplishes this is

$$X_2 = (X_1)^{\frac{1}{2}} \quad . \tag{D-10}$$

The same limits of integration apply. The final result is

$$I_n = \frac{2}{H}\left(\frac{L}{H}\right)^2 \int_0^1 \left\{ \frac{-X_1^{1-n\gamma}}{\left[\left(\frac{L}{H}\right)^2 (X_1-1)^2 + 1\right]^{1/2}} + \frac{X_1^{1-n\gamma}}{\left[\left(\frac{L}{H}\right)^2 (X_1+1)^2 + 1\right]^{1/2}} \right.$$

$$\left. + \frac{2\,X_1^{1-2n\gamma}}{\left[\left(\frac{L}{H}\right)^2 (X_1-1)^2 + 1\right]^{1/2}} + \frac{2\,X_1^{1-2n\gamma}}{\left[\left(\frac{L}{H}\right)^2 (X_1+1)^2 + 1\right]^{1/2}} \right\} dX_1 \quad . \tag{D-11}$$

The last two terms in Equation (D-11) have been transformed according to Equation (D-10). Then in order to keep the notation consistent, the transformation

$$X_1 = X_2 \tag{D-12}$$

is used to give the final form shown in Equation (D-11).

For each value of n in Equation (D-11), there results four integrals. That is, I_1 consists of four integrals, I_2 four integrals, and so forth. Hence, there are sixteen integrals in all, and they must be numerically evaluated. The trapezoidal rule for numerical integration was used in this work. It was found that at least two hundred steps were necessary to produce good convergence. As a check, the Gauss-Legendre quadrature formula for numerical integration was used in some of the early computations.

The final form of the double integration in Equation (4-45) is indicated in Equation (4-46). The H contained in front of the integral in Equation (4-45) cancels with the H in Equation (D-5) and Equation (D-11).

APPENDIX E

HEAT TRANSFER COEFFICIENTS

Details of the derivation of heat transfer coefficients are given. Heat transfer to the porous wall from the adjacent fluid layer is given by Equation (4-29).

$$q_c = - \frac{k(T_m - T_0)}{H} (1-\gamma)\left(\frac{3}{3+RPr}\right)\left(\frac{x}{L}\right)^{-\gamma} \quad . \tag{E-1}$$

The local convection heat transfer coefficient is defined as

$$q_c = h_c(T_m - T_0) \quad . \tag{E-2}$$

Hence, setting the right sides of Equations (E-1) and (E-2) equal to each other gives

$$h_c = \frac{k}{H}(1-\gamma)\left(\frac{3}{3+RPr}\right)\left(\frac{x}{L}\right)^{-\gamma} \quad . \tag{E-3}$$

Equation (E-3) may be rewritten in terms of the Nusselt number defined by

$$Nu = \frac{h_c k}{H} \quad . \tag{E-4}$$

Hence,

$$Nu = (1-\gamma)\left(\frac{3}{3+RPr}\right)\left(\frac{x}{L}\right)^{-\gamma} \quad . \tag{E-5}$$

The average Nusselt number is given by

$$\overline{Nu} = \frac{1}{2L} \int_{-L}^{L} Nu \, dx \quad . \tag{E-6}$$

Substituting Equation (E-5) into Equation (E-6) gives

$$\overline{Nu} = \frac{1}{2L} \int_{-L}^{0} (1-\gamma)\left(\frac{3}{3+RPr}\right)\left(-\frac{x}{L}\right)^{-\gamma} dx + \frac{1}{2L} \int_{0}^{L} (1-\gamma)\left(\frac{3}{3+RPr}\right)\left(\frac{x}{L}\right)^{-\gamma} dx \, . \tag{E-7}$$

It is necessary to divide the region of integration as shown above because the energy solution from -L to 0 has a minus (-) sign in front of x, whereas from 0 to L it does not. The indicated integrations are easily performed and the result is

$$\overline{Nu} = \frac{3}{3 + RPr} \quad . \tag{E-8}$$

In an analogous manner, a local radiation heat transfer coefficient may be defined as

$$q_r = h_r(T_m - T_0) \quad , \tag{E-9}$$

and a corresponding average radiation heat transfer coefficient

$$\overline{h}_r = \frac{1}{2L} \int_{-L}^{L} h_r \, dx \quad , \tag{E-10}$$

or, in terms of q_r

$$\bar{h}_r = \frac{1}{2L}\left(\frac{1}{T_m - T_0}\right)\int_{-L}^{L} q_r \, dx \quad . \tag{E-11}$$

The integral in Equation (E-11) has already been evaluated and is composed of the radiation terms on the left side of Equation (4-45). Since H was divided through Equation (4-45), it is necessary to include an H in the numerator of the right side of Equation (E-11). Hence,

$$\bar{h}_r = \frac{H}{2L}\left(\frac{1}{T_m - T_0}\right)\int_{-L}^{L} q_r \, dx \quad . \tag{E-12}$$

Numerical values of $\bar{h}_r$ are obtained after Equation (4-45) has been solved for the unknown temperature and the magnitude of the radiation contribution to heat transfer has been established.

Finally, an overall heat transfer coefficient between the heater and the frozen region may be defined as

$$q = \bar{U}(T_m - T_d) \quad . \tag{E-13}$$

Since

$$q = (\bar{h}_c + \bar{h}_r)(T_m - T_0) \tag{E-14}$$

and

$$q = \frac{k_d}{X_d}(T_0 - T_d) \quad , \tag{E-15}$$

where k_d is the thermal conductivity of the dried layer and X_d is the dried layer thickness. Eliminating T_0 between Equations (E-14) and (E-15) gives

$$q = \frac{1}{\frac{1}{\bar{h}_c + \bar{h}_r} + \frac{X_d}{k_d}} (T_m - T_0) \quad . \tag{E-16}$$

Hence, comparison of Equations (E-13) and (E-16) shows that

$$\bar{U} = \frac{1}{\frac{1}{\bar{h}_{cr}} + \frac{X_d}{k_d}} \tag{E-17}$$

where

$$\bar{h}_{cr} = \bar{h}_c + \bar{h}_r \quad , \tag{E-18}$$

which is the combined surface heat transfer coefficient.

APPENDIX F

INTERFACE POSITION AND DRYING TIME EQUATIONS

The thickness of the dried layer of a sample may be determined from a simple energy balance at the interface between the dried and frozen regions. The heat conducted across the dried layer to the interface is given by

$$q_d = k_d \frac{(T_o - T_d)}{X_d} \quad . \tag{F-1}$$

If no heat is supplied through the frozen region, the heat conducted across the dry layer is just equal to that required to sublimate the ice and raise the temperature of the water-vapor from T_d to T_o. This is represented by

$$q_d = N_w \Delta H + N_w c_p (T_o - T_d) \quad . \tag{F-2}$$

Setting the right sides of Equations (F-1) and (F-2) equal and solving for X_d gives

$$X_d = \frac{k_d (T_o - T_d)}{N_w [\Delta H + c_p (T_o - T_d)]} \quad . \tag{F-3}$$

The flow rate or drying rate may be calculated using

$$N_w = \rho_o v_o \quad , \tag{F-4}$$

and v_o is calculated from the injection Reynolds number R.

Dyer, et al. (5) show that, for the case of no back face heating, that is, all heat for sublimation is conducted across the dried layer, the time to dry to a depth X_d is given by

$$\tau = \frac{\rho_f \, \delta \, X_d^2}{2\left[\frac{k_d(T_o - T_d)}{\Delta H + c_p(T_o - T_d)}\right]} \quad , \qquad \text{(F-5)}$$

where ρ_f is the density of the frozen region and δ is the porosity of the dried layer.

APPENDIX G

SEMI-POROUS CHANNEL VELOCITY DISTRIBUTIONS

Comparison is made of the polynomial and perturbation solutions for the velocity profile in a semi-porous channel.

The shear stress at the walls is given by

$$\tau_w = \mu \left(\frac{\partial u}{\partial y} \right)_w \quad . \tag{G-1}$$

Hence, from Equation (6-2) the derivative $f'(\xi)$ evaluated at each wall is a measure of the shear stress. This quantity is also necessary as a basis for comparison with the perturbation solution. At each wall then

$$f'(0) = \frac{24 - \beta_1}{R + 6} \tag{G-2}$$

and

$$f'(1) = \frac{24 - \beta_1}{R + 6} + \frac{6 \beta_1 + 24 R}{R + 6} + \frac{-6 \beta_1 - 36 R - 72}{R + 6} \quad . \tag{G-3}$$

Donoughe (16) presents similar expressions for calculating the wall shear stresses from the perturbation solutions.

The velocity profiles from the polynomial and perturbation solutions are compared in Tables 2, 3, and 4. The quantities $f'(0)$ and $f'(1)$ from both solutions are compared in Table 5.

Table 2. Comparison of Integral Momentum and Perturbation Solutions for Velocity Profiles, R = 0.1, 0.5

	R = 0.1		R = 0.5	
ξ	Eq. (6-2)	Donoughe (16)	Eq. (6-2)	Donoughe (16)
0.0	0.0	0.0	0.0	0.0
0.05	0.282	0.283	0.273	0.274
0.10	0.536	0.536	0.520	0.522
0.20	0.954	0.955	0.933	0.936
0.30	1.255	1.256	1.237	1.240
0.40	1.437	1.438	1.427	1.429
0.50	1.500	1.500	1.500	1.501
0.60	1.442	1.443	1.453	1.452
0.70	1.265	1.264	1.283	1.281
0.80	0.966	0.965	0.987	0.983
0.90	0.544	0.543	0.560	0.557
0.95	0.288	0.287	0.297	0.295
1.00	0.0	0.0	0.0	0.0

Table 3. Comparison of Integral Momentum and Perturbation Solutions for Velocity Profiles, R = 1.0, 2.0

	R = 1.0		R = 2.0	
ξ	Eq. (6-2)	Donoughe (16)	Eq. (6-2)	Donoughe (16)
0.0	0.0	0.0	0.0	0.0
0.05	0.263	0.264	0.247	0.247
0.10	0.503	0.505	0.475	0.476
0.20	0.911	0.914	0.874	0.874
0.30	1.217	1.220	1.185	1.183
0.40	1.415	1.417	1.397	1.395
0.50	1.500	1.500	1.500	1.498
0.60	1.465	1.463	1.483	1.482
0.70	1.303	1.301	1.335	1.337
0.80	1.009	1.006	1.046	1.049
0.90	0.577	0.574	0.605	0.606
0.95	0.307	0.305	0.323	0.324
1.00	0.0	0.0	0.0	0.0

Table 4. Comparison of Integral Momentum and Perturbation Solutions for Velocity Profiles, R = 3.0, 4.0

	R = 3.0		R = 4.0	
ξ	Eq. (6-2)	Donoughe (16)	Eq. (6-2)	Donoughe (16)
0.0	0.0	0.0	0.0	0.0
0.05	0.234	0.233	0.224	0.221
0.10	0.454	0.451	0.437	0.431
0.20	0.845	0.839	0.823	0.810
0.30	1.160	1.150	1.140	1.121
0.40	1.383	1.372	1.371	1.351
0.50	1.500	1.493	1.500	1.487
0.60	1.497	1.498	1.509	1.509
0.70	1.360	1.369	1.380	1.397
0.80	1.075	1.089	1.097	1.125
0.90	0.626	0.637	0.643	0.667
0.95	0.336	0.343	0.346	0.360
1.00	0.0	0.0	0.0	0.0

Table 5. Comparison of Integral Momentum and Perturbation Solution Wall Friction and Pressure-Change Relations

	$f''(0)$		$\hat{f}'(1)$	
R	Eq. (G-2)	Donoughe (16)	Eq. (G-3)	Donoughe (16)
0.1	5.941	5.946	6.059	6.046
0.5	5.723	5.742	6.277	6.228
1.0	5.486	5.509	6.514	6.454
2.0	5.102	5.109	6.898	6.901
3.0	4.805	4.781	7.195	7.336
4.0	4.568	4.508	7.432	7.756

APPENDIX H

MASS CONCENTRATION DISTRIBUTIONS

In this section some typical water-vapor mass concentration profiles with respect to the ξ-direction are given. They are presented here in tabular form to illustrate the very small variations in mass concentration which occur across a semi-porous channel. The profiles tabulated here are at the same conditions as for some of those illustrated in Figures 12 and 13 where the x-direction profiles are shown.

The data presented here are calculated using Equation (5-38) for a chamber concentration, ω_c equal to 0.6 lbm H_2O/lbm mixture and a Schmidt number, Sc equal to 0.4.

Table 6. Mass Concentration Profiles in the Dimensionless ξ-direction for L/H = 10 and R = 0.1

ξ	$\omega(0,\xi)$	$\omega(0.5,\xi)$	$\omega(1.0,\xi)$
0.0	0.947	0.912	0.605
0.1	0.947	0.912	0.604
0.2	0.946	0.911	0.603
0.3	0.946	0.911	0.601
0.4	0.946	0.911	0.600
0.5	0.946	0.911	0.599
0.6	0.946	0.911	0.598
0.7	0.946	0.910	0.598
0.8	0.946	0.910	0.598
0.9	0.946	0.910	0.598
1.0	0.946	0.910	0.598

Table 7. Mass Concentration Profiles in the Dimensionless ξ-direction for L/H = 10 and R = 0.5

ξ	$\omega(0,\xi)$	$\omega(0.5,\xi)$	$\omega(1.0,\xi)$
0.0	1.000	1.000	0.627
0.1	1.000	1.000	0.619
0.2	1.000	1.000	0.612
0.3	1.000	1.000	0.605
0.4	1.000	1.000	0.600
0.5	1.000	1.000	0.596
0.6	1.000	1.000	0.592
0.7	1.000	1.000	0.590
0.8	1.000	1.000	0.589
0.9	1.000	1.000	0.588
1.0	1.000	1.000	0.588

Table 8. Mass Concentration Profiles in the Dimensionless ξ-direction for L/H = 36 and R = 0.02

ξ	$\omega(0,\xi)$	$\omega(0.5,\xi)$	$\omega(1.0,\xi)$
0.0	0.998	0.992	0.601
0.1	0.998	0.992	0.601
0.2	0.998	0.992	0.601
0.3	0.998	0.992	0.600
0.4	0.998	0.992	0.600
0.5	0.998	0.992	0.600
0.6	0.998	0.992	0.600
0.7	0.998	0.992	0.600
0.8	0.998	0.992	0.600
0.9	0.998	0.992	0.600
1.0	0.998	0.992	0.600

APPENDIX I

PROPERTY DATA USED IN THE THEORETICAL CALCULATIONS

The following equations and data were used for numerical calculations for freeze-drying:

	Reference Number
1. Latent heat of sublimation of frozen beef	
$\Delta H = 1488$ Btu/lbm	(59)
2. Latent heat of sublimation of pure ice	
$\Delta H = 1220$ Btu/lbm	(61)
3. Thermal conductivity of freeze-dried beef at one torr	
$k_d = 0.0503$ Btu/hr ft $^{\circ}$F	(62)
4. Thermal conductivity of freeze-dried Haddock at 0.08 torr	
$k_d = 0.013$ Btu/hr ft $^{\circ}$F	(54)
5. Density of water-vapor	
$\rho_o = \frac{p_c}{R_g T_o}$ lbm/ft^3	(64)

where p_c is in lbf/ft^2 and T is in $^{\circ}$R.

6. Absolute viscosity of water-vapor

$$\mu = \frac{0.659\ T^{3/2} \times 10^{-6}}{623.0 + T} \text{ lbm/ft sec} \qquad (63)$$

where T is in $^{\circ}R$.

7. Constant pressure specific heat of water-vapor

$$c_p = 0.445 \text{ Btu/lbm } ^{\circ}R \qquad (61)$$

8. Emissivity of freeze-dried beef

$$\epsilon = 0.75 \qquad (58)$$

9. Stefan-Boltzmann constant

$$\sigma = 0.173 \times 10^{-8} \text{ Btu/hr ft}^2 (^{\circ}F)^4 \qquad (41)$$

10. Gas constant for water-vapor

$$R_g = 85.8 \text{ ft lbf/lbm } ^{\circ}R \qquad (64)$$

11. Density of frozen beef, approximated by the density of ice

$$\rho_f = 62.4 \text{ lbm/ft}^3 \qquad (61)$$

12. Porosity of freeze-dried beef

$$\delta = 0.70 \qquad (1)$$

13. Thermal conducitivity of water-vapor

$$k = 0.012 \text{ Btu/hr ft } ^{\circ}F \qquad (41)$$

14. Prandtl number of water-vapor

$$Pr = 1.0 \tag{41}$$

15. Schmidt number of water-vapor

$$Sc = 0.4 \tag{41}$$

LITERATURE CITED

1. Harper, J. C. and A. L. Tappel, Advances in Food Research, Vol. VII, Academic Press, New York, 1957, pp. 171-234.

2. Hardin, T. C., Heat and Mass Transfer Mechanisms in Freeze-Drying, Ph.D. Thesis, Georgia Institute of Technology, Atlanta, Georgia, 1965.

3. Bannister, J. D., Heat and Mass Transfer Mechanisms in Sublimation Drying, M.S. Thesis, Northwestern University, 1961.

4. Koumoutsos, N. G. and J. E. Sunderland, "Freeze Dehydration," Technika Chronika, Athens, Greece, 1963.

5. Dyer, D. F. and J. E. Sunderland, "Heat and Mass Transfer Mechanisms in Sublimation Dehydration," Paper 67-WA/HT-22, presented at the ASME Winter Annual Meeting, November, 1967.

6. Burke, R. F. and R. V. Decareau, Advances in Food Research, Vol. XIII, Academic Press, New York, 1964, pp. 1-88.

7. Hill, J. E., Sublimation Dehydration in the Continuous Transition and Free Molecular Regimes, Ph.D. Thesis, Georgia Institute of Technology, Atlanta, Georgia, 1967.

8. Lambert, J. B., Heat and Mass Transfer in Freeze-Drying, Ph.D. Thesis, University of Wisconsin, 1956.

9. Kan, B. and F. deWinter, "The Acceleration of the Freeze-Drying Process Through Improved Heat Transfer," Paper presented at Institute Food Technology Mtg., Portland, Oregon, 1966.

10. Peck, R. E. and R. A. Moraine, "Engineering Studies on the Freeze-Drying of Foods," Quartermaster Contract Report (DA 19-129-QM-1366), 1959.

11. Berman, A. S., "Laminar Flow in Channels with Porous Walls," Journal of Applied Physics, Vol. 24, No. 9, 1953, pp. 1232-1235.

12. Berman, A. S., "Laminar Flow in an Annulus with Porous Walls," Journal of Applied Physics, Vol. 29, No. 1, 1958, pp. 71-75.

13. Sellers, J. R., "Laminar Flow in Channels with Porous Walls at High Suction Reynolds Numbers," Journal of Applied Physics, Vol. 26, No. 4, 1955, pp. 489-490.

14. Yuan, S. W., "Further Investigation of Laminar Flow in Channels with Porous Walls," Journal of Applied Physics, Vol. 27, No. 3, 1956, pp. 267-269.

15. Berman, A. S., "Concerning Laminar Flow in Channels with Porous Walls," Journal of Applied Physics, Vol. 27, No. 12, 1956, pp. 1557-1558.

16. Donoughe, P. L., "Analysis of Laminar Incompressible Flow in Semi-Porous Channels," NACA, TN 3759, August, 1956, 25 pp.

17. Eckert, E. R. G., Donoughe, P. L., and B. J. Moore, "Velocity and Friction Characteristics of Laminar Viscous Boundary-Layer and Channel Flow Over Surfaces with Ejection or Suction," NACA, TN 4102, December, 1957, 57 pp.

18. White, F. M., Jr., Barfield, B. F., and M. J. Goglia, "Laminar Flow in a Uniformly Porous Channel," Journal of Applied Mechanics, Vol. 25, 1958, pp. 613-617.

19. White, F. M., Jr., Laminar Flow in Porous Ducts, Ph.D. Thesis, Georgia Institute of Technology, Atlanta, Georgia, 1959.

20. Terrill, R. M., "Laminar Flow in a Uniformly Porous Channel," The Aeronautical Quarterly, Vol. 15, No. 3, 1964, pp. 299-310.

21. Terrill, R. M., "Laminar Flow in a Uniformly Porous Channel with Large Injection," The Aeronautical Quarterly, Vol. 16, No. 4, 1965, pp. 323-332.

22. Terrill, R. M. and G. M. Shrestha, "Laminar Flow Through Parallel and Uniformly Porous Walls of Different Permeability," ZAMP, Vol. 16, No. 4, 1965, pp. 470-482.

23. Knight, B. K., Jr. and B. B. McInteer, Laminar Incompressible Flow in Channels with Porous Walls, LA-DC-5309, Contract W-7405-ENG-36, 1956, 23 pp.

24. Horton, T. E. and S. W. Yuan, "Laminar Flow in the Entrance Region of a Porous Wall Channel," Applied Scientific Research, Vol. 14, Sect. A, No. 4, 1964-1965, pp. 223-249.

25. Yuan, S. W. and A. B. Finkelstein, "Laminar Pipe Flow with Injection and Suction Through a Porous Wall," Transactions ASME, Vol. 78, No. 4, 1956, pp. 719-724.

26. Yuan, S. W. and A. B. Finkelstein, "Heat Transfer in Laminar Pipe Flow with Uniform Coolant Injection," Jet Propulsion, Vol. 28, No. 3, 1958, pp. 178-181.

27. Weissberg, A. L., "Laminar Flow in the Entrance Region of a Porous Pipe," The Physics of Fluids, Vol. 2, No. 5, 1959, pp. 510-516.

28. Hornbeck, R. W., Rouleau, W. T., and Fletcher Osterle, "Laminar Entry Problem in Porous Tubes," The Physics of Fluids, Vol. 6, No. 11, 1963, pp. 1649-1954.

29. White, F. M., Jr., "Laminar Flow in a Uniformly Porous Tube," Trans. ASME, Vol. 84 E, No. 1, 1962, pp. 201-204.

30. Terrill, R. M., "Heat Transfer in Laminar Flow Between Parallel Porous Plates," International Journal Heat Mass Transfer, Vol. 8, 1965, pp. 1491-1497.

31. Carter, L. J. and W. N. Gill, "Asymtotic Solution for Combined Free and Forced Convection in Vertical and Horizontal Conduits with Uniform Suction and Blowing," A.I.Ch.E. Journal, Vol. 10, No. 3, 1964, pp. 330-339.

32. Lee, S. M. and W. N. Gill, "Heat Transfer in Laminar and Turbulent Flows Between Parallel Plates with Transverse Flow," A.I.Ch.E. Journal, Vol. 10, No. 6, 1964, pp. 896-901.

33. Inman, R. M., "Heat Transfer for Laminar Flow in an Annulus with Porous Walls," Journal of Aero/Space Sciences, Vol. 26, No. 8, 1959, pp. 532-533.

34. Keshock, E. G. and R. Siegel, "Combined Radiation and Convection in an Asymmetrically Heated Parallel Plate Flow Channel," Trans. ASME, Vol. 84 C, No. 3, pp. 341-350.

35. Mercer, W. E. III, Convection and Radiation Heat Transfer in the Entrance Region Between Parallel Plates, M.S. Thesis, Air Force Institute of Technology, W.P.A.F.B., 1965.

36. Seban, R. A., "Heat Transfer to a Fluid Flowing Turbulently Between Parallel Walls with Asymmetric Wall Temperatures," Trans. ASME, Vol. 72, 1950, pp. 789-795.

37. Mouradian, E. M. and J. E. Sunderland, "The Velocity and Temperature Distributions in a Liquid Film," Part I, Applied Scientific Research, Vol. 14, Sect. A, 1965, pp. 431-452.

38. Mouradian, E. M. and J. E. Sunderland, "The Velocity and Temperature Distributions in a Liquid Film," Part II, Applied Scientific Research, Vol. 14, Sect. A, 1965, pp. 453-470.

39. Eckert, E. R. G., Schneider, P. J., Hayday, A. A., and R. M. Larson, "Mass-Transfer Cooling of a Laminar Boundary Layer by Injection of a Light-Weight Foreign Gas," Jet Propulsion, Vol. 28, No. 1, 1958, pp. 34-39.

40. Bird, R. B., Stewart, W. E., and E. N. Lightfoot, Transport Phenomena, John Wiley & Sons, Inc., New York, 1960, pp. 608-619.

41. Eckert, E. R. G. and R. M. Drake, Jr., Heat and Mass Transfer, McGraw-Hill, New York, 1959, pp. 456-469.

42. Jakob, M., Heat Transfer, Vol. 11, John Wiley & Sons, Inc., New York, 1957, pp. 394-415.

43. Cess, R. D. and E. C. Shaffer, "Summary of Laminar Heat Transfer Between Parallel Plates with Unsymmetrical Wall Temperatures," Journal of the Aero/Space Sciences, Vol. 26, No. 8, 1959, p. 538.

44. Lundberg, D. D. and J. A. Miller, Laminar Convection Heat Transfer in Entrance Region Between Parallel Flat Plates, Naval P. G. School, Monterey, California, TR-54, AD-619031, 1965.

45. McCuen, P. A., Kays, W. M., and W. C. Reynolds, Heat Transfer with Laminar and Turbulent Flow Between Parallel Planes with Constant and Variable Wall Temperature and Heat Flux, Stanford University, Thermosciences Division, California, Rept. AHT-3, 1962.

46. Smithies, W. R. and T. S. Blakley, "Design of Freeze-Drying Equipment for the Dehydration of Foodstuffs," Food Technology, Vol. 13, No. 11, 1959, pp. 610-614.

47. Fisher, F. R., editor, Freeze-Drying of Foods, National Academy of Sciences-National Research Council, Quartermaster Food and Container Institute for the Armed Forces, 1961.

48. Cotsen, S. and Smith, D. B., editors, Freeze-Drying of Foodstuffs, Columbine Press, Manchester, England, 1963.

49. Sparrow, E. M. and R. D. Cess, Radiation Heat Transfer, Brooks/Cole, Belmont, California, 1966.

50. Marduchow, N. I., "On Laminar Flow Through a Channel or Tube with Injection: Applications of the Method of Averages," Quarterly of Applied Mathematics, Vol. 14, No. 4, 1957, pp. 361-368.

51. Zamzow, W. H. and W. R. Marshall, Jr., "Freeze-Drying with Radiant Energy," Chemical Engineering Progress, Vol. 24, No. 1, 1952, pp. 21-32.

52. Abelow, I. M. and E. W. Flosdorf, "Freeze-Drying," Chemical Engineering Progress, Vol. 53, No. 12, 1957, pp. 597-600.

53. Lusk, G., Karel, M., and S. A. Goldblith, "Effect of Some Processing Parameters on the Rates of Freeze-Drying of Shrimp," Food Technology, Vol. 19, No. 4, 1965, pp. 620-622.

54. Lusk, G., Karel, M., and S. A. Goldblith, "Thermal Conductivity of of Some Freeze-Dried Fish," Food Technology, Vol. 18, No. 10, 1964, pp. 1625-1628.

55. Smith, D. K., Similar Solutions for Internal Flows with Suction or Injection at the Wall, Ph.D. Thesis, North Carolina State University, Raleigh, North Carolina, 1965.

56. Ishizawa, S. and E. Hori, "The Flow of a Viscous Fluid Through a Porous Wall Into a Narrow Gap," Bulletin of JSME, Vol. 9, No. 36, 1966, pp. 719-730.

57. Knudsen, J. G. and D. L. Katz, Fluid Dynamics and Heat Transfer, McGraw-Hill, New York, 1958.

58. Sevcik, V. J. and J. E. Sunderland, "Emissivity of Beef," Food Technology, Vol. 16, No. 9, pp. 124-126.

59. Dyer, D. F., Carpenter, D. K., and J. E. Sunderland, "Equilibrium Vapor Pressure of Frozen Bovine Muscle," Journal of Food Science, Vol. 31, No. 2, 1966, pp. 196-201.

60. Hill, J. E. and J. E. Sunderland, "Equilibrium Vapor Pressure and Latent Heat of Sublimation for Frozen Meats," Food Technology, Vol. 21, No. 9, 1967, pp. 112-114.

61. Keenan, J. H. and F. G. Keyes, Thermodynamic Properties of Steam, John Wiley & Sons, Inc., New York, 1936.

62. Massey, W. M., Jr. and J. E. Sunderland, "Measurement of Thermal Conductivity During Freeze-Drying of Beef," Food Technology, Vol. 21, No. 3 A, 1967, pp. 90A.

63. Reid, R. C. and T. K. Sherwood, The Properties of Gases and Liquids, McGraw-Hill, New York, 1958.

64. Lay, J. E., Thermodynamics, Charles E. Merrill, 1963.

VITA

William M. Massey, Jr. was born in Nashville, Tennessee on March 10, 1941. His parents moved to Buffalo, New York one year later, where he began his education in the New York public schools. He also lived in Martinsville, Virginia and Chattanooga, Tennessee, where he attended the McCallie Preparatory School for four years and was graduated in May, 1959.

He began his college career in September, 1959 at the Georgia Institute of Technology. He attended school under the co-operative plan and worked for the E. I. duPont de Nemours and Company in Chattanooga, Tennessee. In 1964, he received a B. S. degree in Mechanical Engineering Co-operative Plan. He spent the summer of 1964 with the DuPont Company in Waynesboro, Virginia and returned to Georgia Tech in the fall of 1964 to begin his graduate study. He received a M. S. degree in Mechanical Engineering in June, 1966, and continued on in his work there for the Ph.D.

Mr. Massey was married in June, 1963 to the former Nita Elaine Richardson and they have two children, Michelle and Gregory.